

Electronic Thesis and Dissertation Repository

---

9-16-2016 12:00 AM

## Fabrication and Cross-linking of L-Aspartic Acid Functionalized Poly(ester amide)-based Tissue Engineering Scaffolds

Shuyu Liu

*The University of Western Ontario*

Supervisor

Dr. Kibret Mequanint

*The University of Western Ontario* Joint Supervisor

Dr. Elizabeth Gillies

*The University of Western Ontario*

Graduate Program in Chemical and Biochemical Engineering

A thesis submitted in partial fulfillment of the requirements for the degree in Master of Engineering Science

© Shuyu Liu 2016

Follow this and additional works at: <https://ir.lib.uwo.ca/etd>



Part of the [Biochemical and Biomolecular Engineering Commons](#)

---

### Recommended Citation

Liu, Shuyu, "Fabrication and Cross-linking of L-Aspartic Acid Functionalized Poly(ester amide)-based Tissue Engineering Scaffolds" (2016). *Electronic Thesis and Dissertation Repository*. 4141.

<https://ir.lib.uwo.ca/etd/4141>

This Dissertation/Thesis is brought to you for free and open access by Scholarship@Western. It has been accepted for inclusion in Electronic Thesis and Dissertation Repository by an authorized administrator of Scholarship@Western. For more information, please contact [wlsadmin@uwo.ca](mailto:wlsadmin@uwo.ca).

## Abstract

Scaffold fabrication is essential in tissue engineering. Amino acid based poly(ester amide)s (PEAs) have been investigated as scaffold materials due to their non-toxic degradation byproducts, and easily tunable mechanical and biological properties. However, L-aspartic acid functionalized PEAs showed poor morphological stability when immersed in buffer. This work focuses on the further functionalization of L-aspartic acid based PEAs, scaffold fabrication and cross-linking of the scaffold to improve morphological stability. Photo-cross-linkable and thermally cross-linkable PEAs were synthesized successfully and characterized. Two scaffold fabrication methods were applied: 1) electrospinning was applied to photo-cross-linkable PEAs, followed by UV treatment to cross-link electrospun scaffolds; 2) solvent casting/particulate leaching was applied to thermally cross-linkable PEAs with *in situ* thermal cross-linking. The cross-linking degree was demonstrated with morphological change by immersing the cross-linked scaffold in phosphate-buffered saline. Photo-cross-linking turned out to be insufficient to produce scaffolds that were able to survive in aqueous environment, while *in situ* thermal cross-linking provided highly-cross-linked scaffold. The existence and use of residual carboxylic groups on scaffolds prepared by both electrospinning was proven by model protein conjugation. Confocal microscopy imaging showed stronger fluorescence on conjugated samples than adsorbed samples.

## Keywords

Poly(ester amide)s, electrospinning, solvent casting/particulate leaching, photo-cross-linking, thermal cross-linking, model compound conjugation

## **Acknowledgements**

I would like to acknowledge the guidance from my supervisors Drs. Kibret Mequanint and Elizabeth Gillies. I really appreciated their continuous encouragement when I had difficulties with my research and felt frustrated. They helped me keep my confidence throughout the two years. I would also like to thank the Natural Sciences and Engineering Research Council (NSERC) of Canada for financial aid.

I would also like to acknowledge the helpful discussions from lab members from both research groups. I would also like to thank Somiraa Said for her help with electrospinning and feedback with my results. I also want to thank our laboratory technician, Aneta Borecki, for helping with GPC samples. I would like to thank all of my group mates for their encouragement and support. Last but not least, I wish to thank my parents for their continuous love and support.

# Table of Contents

Acknowledgements.....	ii
List of Tables .....	vii
List of Figures.....	viii
List of Schemes.....	xi
List of Abbreviations .....	xiii
1 Scope and Thesis Outline.....	1
1.1 Scope.....	1
1.2 Thesis Outline .....	2
2 Literature Review.....	3
2.1 Tissue Engineering.....	3
2.1.1 Natural Polymers for Tissue Engineering Scaffold .....	5
2.1.2 Synthetic Polymers for Tissue Engineering Scaffold .....	7
2.2 Tissue Engineering Scaffold Fabrication Strategies .....	8
2.2.1 Electrospinning .....	8
2.2.2 Solvent Casting/Particulate Leaching (SCPL).....	11
2.2.3 Gas Foaming .....	13
2.2.4 Freeze Drying.....	14
2.4.5 Cross-linking in Tissue Engineering Scaffold Fabrication.....	15
2.3 Poly(ester amides) (PEAs).....	18
2.3.1 PEA Synthesis.....	19
2.3.2 PEA Functionalization .....	21

2.3.3	Biodegradability of PEAs .....	23
2.3.4	Biocompatibility of PEAs .....	25
2.4	Objectives and Rationale for This Thesis .....	26
Chapter 3 .....		28
3	Materials and Methods .....	28
3.1	Materials .....	28
3.2	Material Characterization .....	28
3.2.1	Nuclear Magnetic Resonance Spectroscopy (NMR) .....	28
3.2.2	Fourier-Transform Infrared Spectroscopy (FTIR) .....	28
3.2.3	Gel Permeation Chromatography (GPC) .....	28
3.3	Monomer Synthesis .....	29
3.3.1	Synthesis Procedure for Monomers 1 .....	29
3.3.1	Synthesis Procedure for Monomers 2 .....	29
3.3.3	Synthesis of Monomer 3 .....	30
3.4	PEA Nomenclature .....	30
3.5	Polymer Synthesis .....	31
3.5.1	Synthesis Procedure for the Interfacial Polymerization to Prepare Poly(ester amide)s, 8-Phe-4-Asp(O- <i>t</i> -Bu)-4 .....	31
3.5.2	Synthesis Procedure for the Interfacial Polymerization to Prepare Poly(ester amide)s, 8-Phe-8-Asp(O- <i>t</i> -Bu)-4 .....	31
3.5.3	General Deprotection Procedure .....	32
3.5.4	General Synthesis Procedure of Cinnamate-functionalized PEAs .....	32
3.5.5	Synthesis of Methacrylate-functionalized 8-Phe-8-Asp(OH)-4 .....	34
3.6	Synthesis of Functionalized Rhodamine Dyes .....	35

3.6.1	Rhodamine B Base, 8.....	35
3.6.2	Rhodamine B Piperazine Amide, 9.....	35
3.6.3	Rhodamine B Primary Amide, 10.....	36
3.7	Scaffold Fabrication.....	37
3.7.1	Electrospinning of Cinnamate-functionalized PEAs .....	37
3.7.2	Post-Electrospinning Photo-cross-linking .....	37
3.7.3	<i>In Situ</i> Cross-linking and Solvent Casting of Methacrylate-functionalized 8-Phe-8-Asp(OH)-4 .....	38
3.8	Conjugation of Model Compounds onto Functionalized PEA Scaffolds .....	38
3.8.1	General Procedure for the Conjugation of Rhodamine a Dye to a Carboxylic Acid-Functionalized PEA .....	38
3.8.2	Conjugation of BSA, Tetramethylrhodamine Conjugate to Cinnamate-functionalized PEA Scaffolds .....	38
3.9	Scaffold Characterization.....	39
3.9.1	Confocal Microscopy.....	39
3.9.2	Scanning Electron Microscopy (SEM).....	39
	Chapter 4.....	40
4	Results and Discussion .....	40
4.1	Monomer Synthesis .....	40
4.2	L-Aspartic Acid Functionalized Poly(ester amide)s Synthesis and Characterization .....	41
4.3	Design of Photo-cross-linkable Cinnamate-functionalized PEAs .....	45
4.3.1	Cinnamate-functionalized PEA Synthesis and Characterization.....	47
4.3.2	Electrospinning of PEAs.....	52
4.4	Model Compound conjugation .....	61

4.4.1	Rhodamine Dye Derivative Synthesis .....	61
4.4.2	Rhodamine Dye as Model Compound.....	62
4.4.3	BSA Tetramethylrhodamine conjugate as Model Compound .....	65
4.5	Design of a Thermally Cross-linkable Methacrylate-functionalized PEA .....	66
4.5.1	Methacrylate-functionalized PEA Synthesis and Characterization .....	69
4.5.2	<i>In Situ</i> Thermal Cross-linking.....	72
	Chapter 5.....	75
5	Conclusions and Future Directions.....	75
5.1	Conclusions.....	75
5.2	Future Directions .....	76
	References.....	77
	Appendices Permission to Reuse Copyrighted Material .....	89
	Curriculum Vitae .....	91

## List of Tables

Table 4.1 Molecular weight of PEAs.....	45
Table 4.2 Molecular weight of cinnamate PEAs .....	52



## List of Figures

Figure 2.1: A diagrammatic representation of the <i>in vitro</i> tissue engineering process, where a cell-seeded scaffold is matured <i>in vitro</i> in a bioreactor prior to implantation into the patient.....	4
Figure 2.2: Example chemical structures of polysaccharides (amylose and chitosan).....	7
Figure 2.3: Chemical structures of PLA, PGA, PLA-PEG and poly(anhydride)s.....	8
Figure 2.4: Example of eletrospinning fibers prepared from poly(ester amide)s. Scale bars represent 50 $\mu\text{m}$ , 10 $\mu\text{m}$ and 5 $\mu\text{m}$ , respectively.....	8
Figure 2.5: Electrospinning apparatus.....	9
Figure 2.6: Example of solvent casting/particulate leaching scaffold prepared from polyurethane. Scale bar represents 500 $\mu\text{m}$ .....	12
Figure 2.7: Example of gas foaming scaffold prepared from poly (D,L-lactic acid). Scale bar represent 100 $\mu\text{m}$ .....	14
Figure 2.8: Example of a freeze dried scaffold prepared from a 2 wt% chitosan solution in 0.2 M acetic acid. Scale bar represent 200 $\mu\text{m}$ .....	15
Figure 2.9: <i>In situ</i> photocross-linking apparatus.....	18
Figure: 4.1 $^1\text{H}$ NMR spectrum of 8-Phe-4-Asp(OH)-4 functional PEAs, (DMSO- $\text{d}_6$ , 600MHz).....	43
Figure 4.2: $^1\text{H}$ NMR spectrum of 8-Phe-8-Asp(OH)-4 functional PEAs, (DMSO- $\text{d}_6$ , 600MHz).....	44
Figure 4.3: Overlaid GPC (RI detection) traces of 8-Phe-4-Asp(O- <i>t</i> -Bu)-4 and 8-Phe-8-Asp(O- <i>t</i> -Bu)-4.....	45
Figure 4.4: $^1\text{H}$ NMR spectrum of cinnamate-functionalized 8-Phe-4-Asp(OH)-4 (DMSO- $\text{d}_6$ , 600MHz).....	49
Figure 4.5: $^1\text{H}$ NMR spectrum of cinnamate-functionalized 8-Phe-8-Asp(OH)-4, (DMSO- $\text{d}_6$ , 600MHz).....	50
Figure 4.6: FTIR spectrum of cinnamate-functionalized 8-Phe-8-Asp(OH)-4.....	51

Figure 4.7: Overlaid GPC (RI detection) traces of cinnamate 8-Phe-4-Asp(OH)-4 and cinnamate 8-Phe-8-Asp(OH)-4.....	52
Figure 4.8: Phase contrast micrographs and SEM images of electrospun 8-Phe-4-Asp(OH)-4 mats at various concentrations. (A), (E) and (I) show electrospun fibers on glass slides. ....	54
Figure 4.9: Electrospinning of 8-Phe-8-Asp(OH)-4 with 100% CHCl <sub>3</sub> .....	56
Figure 4.10: Electrospun mats: (A) original 8-Phe-8-Asp(OH)-4 fibers, (B) 8-Phe-8-Asp(OH)-4 fibers after immersion in PBS for 1 day, (C) original 8-Phe-4-Asp(OH)-4 fibers, (B) 8-Phe-4-Asp(OH)-4 fibers after immersion in PBS for 1 day.....	57
Figure 4.11: Electrospun cinnamate 8-Phe-4-Asp(OH)-4 functional PEAs, (A, C, E, G) before and (B, D, F, H) after UV treatment. Red circles highlight the damaged fibers after UV treatment.....	59
Figure 4.12: Electrospun mats: (A) original cinnamate-functionalized 8-Phe-8-Asp(OH)-4 cross-linked fibers, (B) cinnamate-functionalized 8-Phe-8-Asp(OH)-4 cross-linked fiber after immersion in PBS for 6 days, (C) original cinnamate-functionalized 8-Phe-4-Asp(OH)-4 cross-linked fibers, (D) cinnamate-functionalized 8-Phe-4-Asp(OH)-4 cross-linked fiber after immersion in PBS for 1 day.....	60
Figure 4.13: Calibration curves for (A) rhodamine piperazine amine, 9, at 565 nm; (B) rhodamine primary amine, 10, at 564.5 nm.....	63
Figure 4.14: Confocal microscopy images of (A) Rhodamine primary amide conjugated PEA electrospun mats, (B) rhodamine adsorbed PEA electrospun mats.....	65
Figure 4.15: Fluorescence images of 8-Phe-8-Asp(OH)-4 electrospun mats. (A) BSA tetramethylrhodamine conjugate conjugated to the surface of 8-Phe-8-Asp(OH)-4. (B) and BSA tetramethylrhodamine conjugate adsorbed to surface of 8-Phe-8-Asp(OH)-4 .	66
Figure 4.16: Solvent casting apparatus.....	67
Figure 4.17: Uncross-linked 8-Phe-8-Asp(OH)-4 scaffold fabricated by SCPL (A) before salt is leached out (B) after salt is leached out.....	68
Figure 4.18: <sup>1</sup> H NMR spectrum of methacrylate 8-Phe-8-Asp(OH)-4 functional PEAs, (600 MHz, DMSO-d <sub>6</sub> ) .....	71

Figure 4.19: Overlaid GPC (RI detection) traces of Methacrylate 8-Phe-8-Asp(OH)-4 and 8-Phe-8-Asp(OH)-4. .... 71

Figure 4.20: Cross-linked 8-Phe-8-Asp(OH)-4 solvent casting scaffold (A) scaffold before immersion in PBS and (B) scaffold after immersion in PBS for 5 days. .... 74

Figure 4.21: Overlaid FTIR of cross-linked methacrylate 8-Phe-8-Asp(OH)-4 solvent casting scaffold and uncross-linked methacrylate 8-Phe-8-Asp(OH)-4 ..... 74

## List of Schemes

Scheme 2.1: Procedure of enhanced SCPL with centrifugation. ....	12
Scheme 2.2: Schematic cross-linking reactions. 1) Glutaraldehyde covalently bonds to amino groups; 2) 1-Ethyl-3-diaminopropyl-carbodiimide (EDC) and N-hydroxysuccinimide (NHS) catalyses covalent bindings between carboxylic groups and amino groups; 3) Genipin reacts in a similar manner as glutaraldehyde. <sup>61</sup> .....	17
Scheme 2.3: Structure of amino acid derived PEAs .....	19
Scheme 2.4: Synthesis of di- <i>p</i> -toluenesulfonic acid salts of bis( $\alpha$ -amino acid $\alpha$ , $\omega$ -alkylene diester, 1) .....	20
Scheme 2.5: Synthesis of di- <i>p</i> -nitrophenyl ester dicarboxylic acids, 2 .....	20
Scheme 2.6: Synthesis of PEAs, 3, via solution polycondensation of di- <i>p</i> -toluenesulfonic acid salt, 1 and di- <i>p</i> -nitrophenyl ester, 2 .....	20
Scheme 2.7: Synthesis of PEAs, 2, via interfacial polycondensation of di- <i>p</i> -toluenesulfonic acid salt, 1 and diacid chloride. ....	21
Scheme 2.8: Structure of fumaryl chloride and 2-butene-1,4-diol .....	21
Scheme 2.9: Structure of 2-nitro-1,3- benzenedimethanol .....	22
Scheme 2.10: Structure of L-lysine, L-aspartic acid and L-serine .....	22
Scheme 4.1: Synthesis of di- <i>p</i> -toluenesulfonic acid salt monomers 1 and 2 .....	41
Scheme 4.2: Synthesis of bis-L-aspartic acid- $\beta$ -( <i>tert</i> -butyl ester) diester 3 .....	41
Scheme 4.3: Synthesis of L-aspartic acid functionalized PEAs. ....	42
Scheme 4.4: Trans-cis photoisomerization of the cinnamoyl moiety .....	46
Scheme 4.5: (a) Head-to-head and (b) Head-to-tail photodimerization of the cinnamoyl moiety. ....	46
Scheme 4.6: Synthesis of cinnamate-functionalized PEAs. ....	48
Scheme 4.7: Mechanism of EDC/DMAP-mediated esterification of a carboxylic acid... ..	48
Scheme 4.8: Syntheses of rhodamine B piperazine amine .....	62

Scheme 4.9: Syntheses of rhodamine B primary amine .....	62
Scheme 4.10: Conjugation of model compound to 8-Phe-8-Asp(OH)-4 using EDC/sulfo-NHS peptide coupling. ....	64
Scheme 4.11: Synthesis of methacrylate-functionalized PEAs .....	69
Scheme 4.12: Free radical polymerization mechanism. ....	72

## List of Abbreviations

2-D	Two-dimensional
3-D	Three-dimensional
AIBN	Azobisisobutyronitrile
Asp	L-aspartic acid
Boc	t-Butyloxycarbonyl
bFGF	Basic fibroblast growth factor
BSA	Bovine serum albumin
<i>D</i>	Polydispersity index
DCC	<i>N,N</i> -dicyclohexylcarbodiimide
DCM	Dichloromethane
DCU	Dicyclohexylurea
DIPEA	<i>N,N</i> -Diisopropylethylamine
DMAP	4-(Dimethylamino)pyridine
DMF	<i>N,N</i> -Dimethylformamide
DMSO	Dimethyl sulfoxide
DMSO-d <sub>6</sub>	Deuterated DMSO
DPTS	4-(Dimethylamino)pyridinium 4-toluenesulfonate
ECM	Extracellular matrix
EDC	<i>N</i> -(3-dimethylaminopropyl)- <i>N'</i> -ethylcarbodiimide
EtOAc	Ethyl acetate
FN	Fibronectin
FTIR	Fourier transform infrared
GPC	Gel permeation chromatography

GTA	Glutaraldehyde
MeOH	Methanol
MES	4-morpholineethanesulfonic acid
MgSO <sub>4</sub>	Magnesium sulfate
M <sub>n</sub>	Number average molecular weight
M <sub>w</sub>	Weight average molecular weight
MWCO	Molecular weight cut-off
NaHCO <sub>3</sub>	Sodium bicarbonate
NHS	<i>N</i> -hydroxysuccinimide
NMR	Nuclear magnetic resonance
PBS	Phosphate-buffered saline
PCL	Poly(caprolactone)
PEA	Poly(ester amide)
PEG	Poly(ethylene glycol)
PGA	Poly(glycolic acid)
Phe	L-phenylalanine
PLA	Poly(lactic acid)
PMMA	Poly(methyl methacrylate)
SCPL	Solvent casting/particulate leaching
SEM	Scanning electron microscopy
TE	Tissue Engineering
TEMPO	2,2,6,6-tetramethylpiperidine-1-oxy
TFA	Trifluoroacetic acid
TGF-β	Transforming growth factor-β

T <sub>g</sub>	Glass transition temperature
UV	Ultraviolet
wt%	Weight percent



# Chapter 1

## 1 Scope and Thesis Outline

### 1.1 Scope

Tissue engineering and regenerative medicine have developed actively in recent years as an alternative choice for the replacement of diseased or injured tissue.<sup>1</sup> This approach involves the seeding of cells on a scaffold, where the scaffold provides support for cell attachment, proliferation and differentiation until the cells form their own extracellular matrix (ECM). To meet these requirements, the material chosen to fabricate the scaffold needs to have proper biodegradability, biocompatibility, and mechanical properties.<sup>2</sup> A wide variety of polymers have been investigated. Natural polymers, such as alginate<sup>3</sup>, chitosan<sup>4</sup>, collagen and elastin<sup>5</sup>, are widely used in biomedical applications because of their potential favorable cell-material interaction. However, they have shortcomings such as uncontrollable degradation rates and weak mechanical properties.<sup>6,7</sup> On the other hand, synthetic polymers have easily tunable mechanical and biodegradation properties and good batch-to-batch reproducibility.<sup>8</sup> Despite the advantages of each category of material, issues such as poor morphological stability limit the application of some materials. Cross-linking was previously reported in tissue engineering scaffold fabrication as a solution to deal with poor mechanical properties and scaffold morphological stability.<sup>9,10</sup>

Poly(ester amide)s (PEAs) are a family of synthetic polymers that have been investigated in the biomedical field. PEAs are promising because of their easily tunable properties and non-toxic degradation products. A family of aspartic acid incorporated L-phenylalanine based PEA was synthesized in our lab.<sup>11</sup> Despite the encouraging cell attachment, spreading and metabolic activity data on 2-dimensional (2-D) PEA films, the 3-D electrospun scaffold was not stable in aqueous conditions. Fiber fusion led to the loss of the scaffold morphology.<sup>12</sup>

In this work, both photo-cross-linking and thermal cross-linking were combined into scaffold fabrication methods to improve aspartic acid derived PEA scaffold dimensional and morphological stability in aqueous solution.

## **1.2 Thesis Outline**

This thesis contains five chapters. Chapter 2 provides a literature review of tissue engineering, natural and synthetic materials, tissue engineering scaffold fabrication, the synthesis of PEAs, biodegradation and biocompatibility of PEAs, and cross-linking methods in tissue engineering scaffold fabrication. The rationale and objectives of this work are also included. Chapter 3 contains the materials and methods for the synthesis of functionalized poly(ester amide) material, as well as the experimental conditions for characterization, cross-linking and scaffold fabrication methods. Chapter 4 presents and discusses all research findings of this work. Lastly, Chapter 5 provides the conclusions of the findings in this study and future directions for this project.

## Chapter 2

### 2 Literature Review

#### 2.1 Tissue Engineering

Mechanically and biologically competent replacement organs and tissues are in high demand due to limited donated organs and tissues. In the United States alone, a patient is added on the transplant waiting list every 10 minutes, and 21 people die every day while waiting for transplantation. Thus, tissue engineering (TE), as an alternative solution to organ and tissue transplantation, has been developed dramatically in recent years and has been used in a variety of applications including skin<sup>13</sup>, bone<sup>14</sup>, cartilage<sup>4</sup>, nerves<sup>15</sup>, liver<sup>16</sup>, and vascular grafts<sup>5</sup>. A good example of a commercialized tissue engineering product is artificial skin.

During a meeting sponsored by the National Science Foundation (NFS) in 1988, "tissue engineering" was defined as the application of the principles and methods of engineering and the life sciences toward the fundamental understanding of structure/function relationships in normal and pathological mammalian tissues and the development of biological substitutes to restore, maintain, or improve functions.<sup>17</sup> Implied from this definition, the aim of tissue engineering is to create an autologous implant.

The main elements of an engineered tissue are the cells and the scaffolds. When cells are seeded onto a scaffold, they are able to form the foundation of the desired tissue. Scaffolds serve as a temporary template and/or growth factor delivery device. In this system, growth factors are loaded on the scaffold and cells harvested from the body are encouraged to spread and differentiate into desired tissue within the matrices.<sup>18</sup> The overall tenet of tissue engineering involves harvesting cells from patients, seeding the cells onto appropriate scaffolds, stimulating their growth and proliferation, and

transplanting the construct back to patients (Figure 2.1). It is not surprising, therefore, that scaffold design and fabrication are essential.

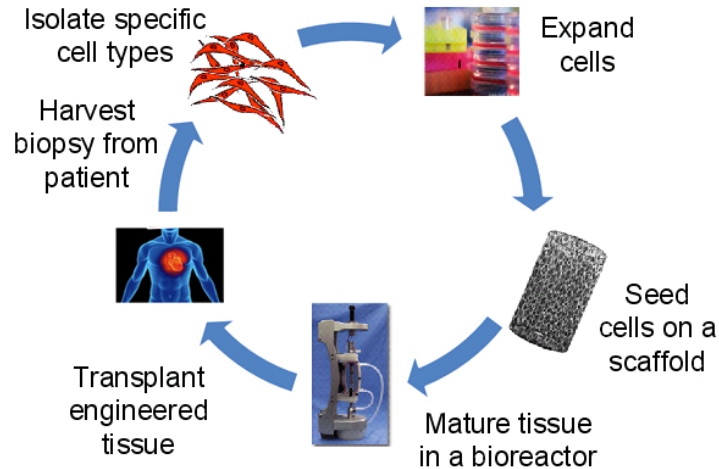


**Figure 2.1: A diagrammatic representation of the *in vitro* tissue engineering process, where a cell-seeded scaffold is matured *in vitro* in a bioreactor prior to implantation into the patient.**

An ideal engineered scaffold should mimic the extracellular matrix (ECM), which provides not only a mechanical support to cells within connective tissues, but also plays an important role in defining cellular behavior as a dynamic, mobile, and flexible component.<sup>19</sup> The ECM performs its functions mainly by two mechanisms.<sup>20</sup> First, it serves as a temporary reservoir for biomolecules such as growth factors, cytohormones and enzymes. Second, the ECM proteins interact with cell receptors directly to regulate cell adhesion and migration. Thus, tissue engineering scaffolds should meet some or all of the following requirements: 1) promote cell attachment and extracellular matrix deposition; 2) allow transport of nutrients, gases and waste, ensuring cell proliferation and differentiation; 3) exhibit appropriate chemical and mechanical properties to minimize inflammation *in vivo*; (4) degrade in a controllable rate producing degradation products that are non-toxic.<sup>21-23</sup>

Depending on applications, tissue engineering scaffolds need to meet different specific requirements. Providing adequate mechanical support is an essential scaffold requirement. For hard tissues, the mechanical modulus ranges from 10 to 1500 MPa, while for soft tissues, the mechanical modulus ranges from 0.4 to 350 MPa. If the scaffold cannot provide a mechanical modulus in the above range, then any nascent tissue formation will probably also fail due to excessive deformation.<sup>24</sup> In vascular tissue engineering, for example, the burst pressure of mammalian artery is 3200 mmHg, which means the scaffolds should be able to load at least the same stress. In bone tissue engineering, the scaffold mechanical properties are different. For example, the compressive modulus of human lumbar is around 88 MPa, and ideally the scaffold should meet the same requirement.<sup>25</sup>

### **2.1.1 Natural Polymers for Tissue Engineering Scaffold**

Because of the bioactive properties of natural polymers and the potential advantage of the inherent favorable cell attachment properties, natural polymers have long been used to fabricate tissue engineering scaffolds.<sup>26</sup> Among natural polymers, protein-based polymers<sup>5</sup> including collagen, elastin and silk fibroin and polysaccharides (chitosan, hyaluronic acid, alginate, agarose) are the most widely investigated.

Protein-based polymers have the advantage that they mimic many features of the natural ECM. Therefore, they have functions such as promoting cell growth and directing cell migration. However, the main drawbacks of protein-based polymers are weak mechanical properties and poor batch-to-batch reproducibility.<sup>26</sup>

Collagen has been widely investigated as a biomaterial for tissue engineering scaffolds because it is the major component of the ECM and has been demonstrated to have excellent biocompatibility and biodegradability. To obtain collagen-based biomaterials, mainly two techniques are used: 1) decellularize a collagen matrix preserving the original

tissue shape and ECM structure; 2) extraction, purification and polymerization of collagen and its diverse components to form a functional scaffold.<sup>27</sup>

Gelatin is another natural polymer derived from the acid or alkaline processing of collagen. This processing yields gelatin with different isoelectric points. When positively charged and negatively charged proteins are mixed together, a polyion complex forms<sup>26</sup>. Thus, gelatin has the potential to form complexes with charged bioactive molecules. This advantage of gelatin makes it a good candidate for controlled release applications. Basic fibroblast growth factor (bFGF)<sup>28</sup>, transforming growth factor beta (TGF- $\beta$ 1)<sup>29</sup> and fibronectin have been reported to be successfully complexed with gelatin. Also, gelatin is easy to process, so that it is manufactured into different shapes such as hydrogels and sponges. Gelatin microspheres are the most widely-used carrier that can be incorporated into a second scaffold such as a hydrogel.

Polysaccharides are a class of biopolymers composed of simple sugar monomers. They can be obtained from several sources. For example, dextran can be obtained from microbial sources, chitosan can be obtained from crustaceans, and starch can be obtained from vegetal sources. Polysaccharides tend to have good hemocompatibility because of their chemical similarities with heparin.<sup>26</sup> In addition, they are non-toxic, show interaction with living cells, and generally have low cost compared to collagen.<sup>26,30</sup> Polysaccharides have been reported as tissue engineering scaffold materials as well as carriers. Chitosan, for example, was fabricated alone using freeze drying and electrospinning into porous scaffold or mixed with other materials (e.g. gelatin<sup>31</sup>, alginate<sup>32</sup>, poly(vinyl alcohol)<sup>33</sup>), then fabricated as composite material. Starch-based biodegradable polymers have been proposed to have great potential in drug release systems and tissue engineering scaffolds.<sup>34</sup> Figure 2.2 gives examples of polysaccharide chemical structures.

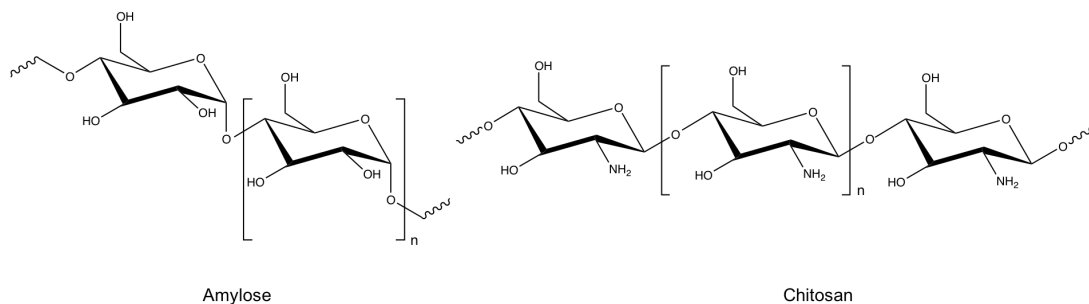


**Figure 2.2: Example chemical structures of polysaccharides (amylose and chitosan)**

### 2.1.2 Synthetic Polymers for Tissue Engineering Scaffold

Biodegradable synthetic polymers are an alternative for fabricating tissue engineering scaffolds. They offer a wide range of advantages over natural polymers including: 1) easy tailoring of mechanical properties and degradation rates to fit in various applications; 2) fabrication in different shapes and morphologies beneficial to cell growth; 3) incorporation of chemical functional groups conducive to cell growth; 4) capacity to be manufactured on a large scale reproducibly.<sup>8</sup>

Poly( $\alpha$ -hydroxy acids) such as polyglycolide (PGA), polylactide (PLA) and their copolymers are the most widely used synthetic polymers in tissue engineering applications and have been approved by the food and drug administration (FDA) for medical use.<sup>8</sup> The major advantage of PGA is that its degradation product is glycolic acid which is a natural metabolite. The hydrolysis of PLA produces lactic acid which also enters the tricarboxylic acid cycle and can be metabolized by the body. However, major drawbacks of poly( $\alpha$ -hydroxy acids) include: 1) hydrophobicity of the polymers; 2) a bulk degradation mechanism resulting in an accelerated rate at later stages, with an increasing accumulation of acidic degradation products. If surrounding tissue is not able to metabolize degradation products at a sufficient rate, inflammatory reactions will take place.<sup>35</sup>

To overcome the limitations of poly( $\alpha$ -hydroxy acids), other biodegradable synthetic polymers have been developed. For example, poly(lactic acid-co-ethylene glycol) is an alternative to increase hydrophilicity.<sup>36</sup> Poly(anhydride)s were developed to address the

problem of acidic degradation product accumulation and they degrade by surface erosion and their degradation rate can be predicted.<sup>37</sup> Figure 2.3 shows the structures of PLA, PGA, PLA-PEG and poly(anhydride)s

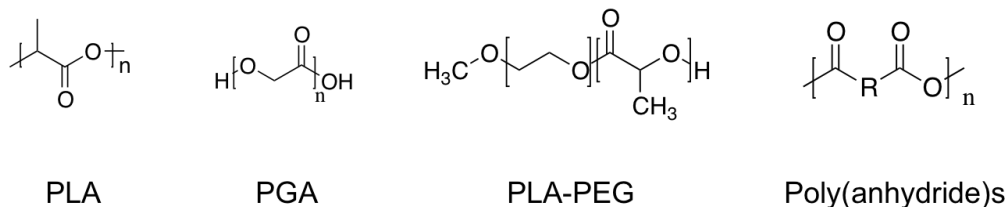


**Figure 2.3: Chemical structures of PLA, PGA, PLA-PEG and poly(anhydride)s.**

## 2.2 Tissue Engineering Scaffold Fabrication Strategies

### 2.2.1 Electrospinning

Electrospinning was first developed in 1902 by Cooley and Morton and has been widely used to fabricate tissue engineering scaffolds in the past decades. It is of interest because of its simple setup and flexibility. It can also be applied to various materials. Electrospinning produces sub-micrometer diameter fibers that form a porous matrix with a large surface to volume ratio, allowing efficient cell infiltration and nutrient transport. An example of electrospun fibers is shown in Figure 2.4.

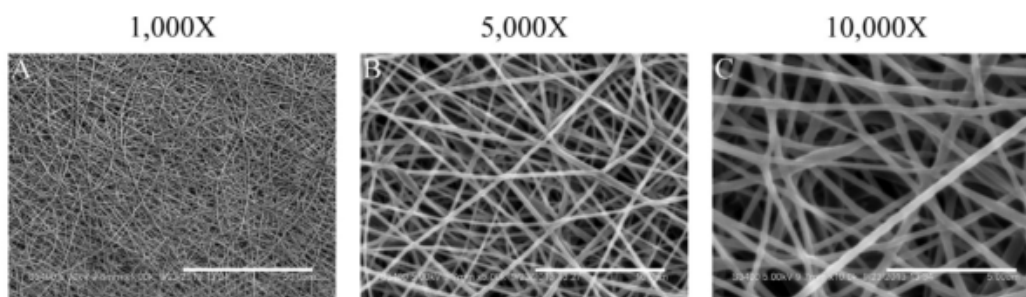


**Figure 2.4: Example of eletrospinning fibers prepared from poly(ester amide)s. Scale bars represent 50 µm, 10 µm and 5 µm, respectively.<sup>12</sup> Reproduced with permission from the reference. Copyright © 2014 Acta Materialia Inc. Published by Elsevier Ltd.**



An electrospinning apparatus consists of a high voltage power supply, a syringe pump, and a collector (Figure 2.5). High voltage is applied to create an electrostatic field between the needle tip and the collector. By forcing the polymer solution out of the syringe at a certain flow rate, a solution droplet forms at the needle tip due to surface tension. Once the electrostatic force overcomes surface tension, a jet initiates and travels to the collector. While travelling, solvent evaporates and electrospun fibers form. The morphology of the electrospun fibers is influenced by many parameters.

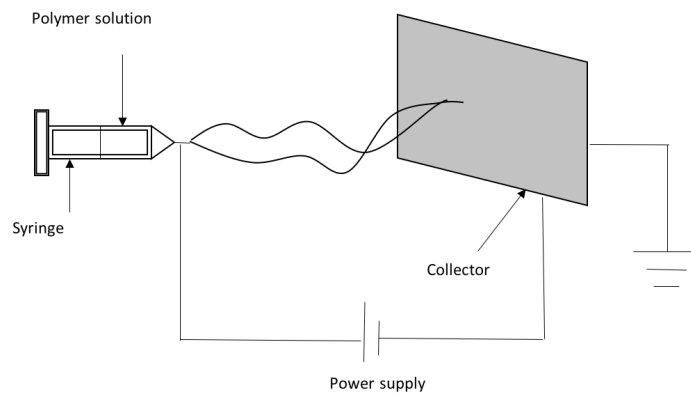


**Figure 2.5: Electrospinning apparatus.**

### **Viscosity/solution concentration**

Viscosity/solution concentration has been demonstrated in many studies to be a major factor in electrospinning. When the viscosity is too low, beads form instead of fibers. In the worst case, an electrospayed product is formed. When the viscosity is too high that reaches above a certain point, fiber formation is not possible due to the droplet drying out at the needle tip before the jet could be initiated, thus preventing electrospinning. Even within the viscosity range that fibers can be formed, their morphology varies at different viscosities.

Electrospinning of poly(ethylene glycol) and poly(D,L-lactic acid)<sup>38,39</sup> showed that at concentrations under 4 wt% and 20 wt% for PEG and PLA, respectively, the fibers had irregular morphologies and a wide range of diameters. With increasing concentration, the fiber morphology became more regular. On average, the fiber diameter becomes larger and more uniform with increasing viscosity.

### **Polymer molecular weight**

The impact of polymer molecular weight has been investigated in previous studies. Gupta et al.<sup>40</sup> electrospun a series of poly(methyl methacrylate)s (PMMA) with molecular weights ranging from 12470 to 365700 g/mol. Electrospinning conditions were kept identical over this molecular weight range. With increasing molecular weight, the number of beads and droplets was reduced, which may be attributed to chain entanglements. In another work,<sup>41</sup> poly(vinyl alcohol) with molecular weights ranging from 9000 to 186000 g/mol was electrospun. They found that for each molecular weight, there was a minimal concentration for fibrous structure formation. With increasing of molecular weight and concentration, fiber diameter increased.

### **Dielectric constant**

Dielectric constant is a quantity measuring the ability of a substance to store electrical energy in an electric field. A few studies have been performed to demonstrate the role dielectric constant plays in electrospun fiber morphology. To test the influence of dielectric constant of solvents, it is required that the chosen solvents differ significantly in dielectric constant but have similar other physical properties such as viscosity. For example, PCL was electrospun in acetic acid and formic acid. When the dielectric constant of the solvent was below 19 at 20 °C, either micrometer fibers were obtained or the solution was electrospayed.<sup>42</sup>

### **Flow rate**

It has been shown that smaller diameter fibers were obtained with lower flow rate. When electrospinning poly(D,L-lactic acid) and the flow rate reaches 75  $\mu\text{L}/\text{min}$ , beads started to form because the delivery rate of the solution jet to the capillary tip exceeded the rate at which the solution was removed from the tip by the electric forces.<sup>39</sup>

In addition to the parameters mentioned above, the distance between the needle tip<sup>43,44</sup> and collector as well as the spinning voltage<sup>45,46</sup> impact electrospun fiber diameter and morphology.

### **2.2.2 Solvent Casting/Particulate Leaching (SCPL)**

Solvent casting/particulate leaching is another commonly used method of scaffold fabrication. This procedure involves the dissolution of a biodegradable polymer in volatile solvents and casting the solution into a mold packed with porogens (usually a salt, e.g. NaCl)<sup>47</sup> or mixing porogens with polymer solution before casting into a mold<sup>48</sup>. Then the solvent is evaporated and porogens are leached out. Ideally, the porogen should not be soluble in the polymer solution and the solvent used to leach out the porogen should not affect the morphology of the polymer scaffold. This method is preferable because the pore size and porosity can be easily controlled by selecting proper particle size and the amount of porogens used. Scaffold mechanical properties and degradation time can also be varied by adjusting the polymer solution concentration.<sup>49</sup> However, in SCPL method, it is difficult to control the pore morphology and a dense surface skin layer on the scaffold is often observed in SCPL method.<sup>23</sup> Furthermore, as the porogens are encased by polymer solution and thus polymer following solvent evaporation, leaching out porogens can sometimes be difficult. Figure 2.6 shows an example structure of SCPL scaffold.

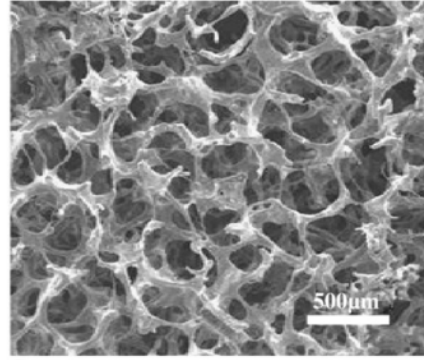
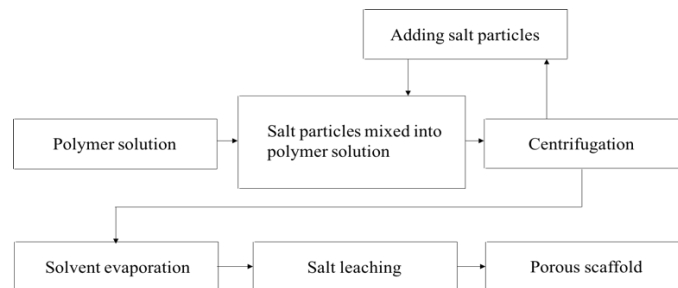


**Figure 2.6: Example of solvent casting/particulate leaching scaffold prepared from polyurethane. Scale bar represents 500  $\mu\text{m}$ .<sup>48</sup> Reproduced with permission from the reference. Copyright © 2009 Elsevier B.V.**

Research has been conducted to optimize the inner structure of the scaffolds. Salt fusion<sup>50</sup> is one of the methods combined with SCPL to increase the interconnectivity of the scaffolds. NaCl crystals were incubated in 95% humidity, which resulted in crystal fusion, creating enhanced interconnectivity. Increased interconnectivity may be useful in a wide range of biomedical applications that require cell-cell interactions. As the density of the polymer solution and porogen are often different, the distribution of pores inside the scaffold is non-uniform. An enhanced SCPL method was investigated, which was combined with centrifugation to solve this problem.<sup>48</sup> Porogens were densely packed after centrifugation so that the interconnectivity was improved. The procedure of the enhanced SCPL method is shown in scheme 2.1.



**Scheme 2.1: Procedure of enhanced SCPL with centrifugation.**

Some studies combined SCPL with gas foaming to fabricate scaffolds with enhanced pore interconnectivity. In one study<sup>51</sup>,  $\text{NH}_4\text{HCO}_3$  was used as a gas foaming agent as well

as porogen. The polymer solution was mixed with  $\text{NH}_4\text{HCO}_3$ , then cast into a mold. After the solvent evaporated completely or partially, the scaffolds were immersed in hot water allowing the evolution of ammonia and carbon dioxide. This resulted in increased porosity and enhanced pore interconnectivity within the scaffold. In addition, the skin layer was not found on either side of the scaffold. In another study, researchers optimized SCPL into a solvent merging/particulate leaching method<sup>52</sup>. Instead of mixing polymer solution with porogens, polymer and porogens were mixed in the solid state and packed into a mold. Under negative pressure, organic solvent flowed through the mold dissolving the polymer, then a non-solvent was introduced to solidify the polymer matrix, and lastly, a large amount of water was introduced to leach out the porogen. This procedure resulted in a 3-D scaffold with high porosity and interconnectivity. Without the process of solvent evaporation of the polymer/porogen composite, this procedure is simpler and more rapid than conventional SCPL.

### **2.2.3 Gas Foaming**

The gas foaming procedure usually depends on three principles: 1) saturation of the polymer with a gaseous penetrant (physical blowing agents) at high pressure; 2) quenching of the polymer/gas mixture into a super-saturated stage either by reduced pressure or increased temperature; 3) nucleation and growth of gas cells dispersed throughout the polymer matrix.<sup>53</sup> Organic solvents are not necessary in gas foaming, avoiding possible cytotoxicity from residual solvents.<sup>54</sup> Inert gases such as  $\text{N}_2$  and  $\text{CO}_2$  are often used as agents for their advantages of low cost, environmental acceptability and low human toxicity. The morphology of the resulting scaffold is influenced by pressure, vending rates and processing temperature.<sup>55</sup> However, gas foaming always results in closed pores within the scaffold.<sup>22</sup> An example of gas foaming scaffold is shown in Figure 2.7.

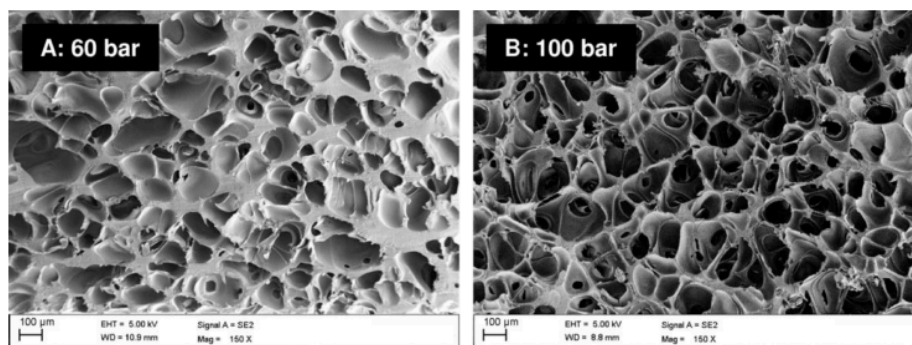


**Figure 2.7: Example of gas foaming scaffold prepared from poly (D,L-lactic acid). Scale bar represent 100  $\mu\text{m}$ .<sup>55</sup> Reproduced with permission from reference. Copyright © 2011 Wiley Periodicals, Inc.**

#### **2.2.4 Freeze Drying**

The process of freeze drying involves freezing a suspension of the material and water, which leads to a structure of ice crystals surrounded by the material. By subsequent sublimation of the ice under high vacuum, a porous scaffold is formed. The pore volume fraction can be controlled by the amount of precipitate in the suspension, and the pore structure on the scaffold results from the structure of the ice crystal. Thus, the pore structure can be controlled by adjusting the freezing process. The cooling rate and freezing temperature are the two main factors that have been studied. Rapid, uncontrolled freezing leads to scaffold heterogeneity.<sup>56</sup> Also it was shown that with a decrease in the freezing temperature, the mean pore diameter decreases.<sup>57</sup> However, the pore structure of the scaffold is not easy to control and it is difficult to obtain open and large pores. An example of freeze drying scaffold is shown in Figure 2.8.

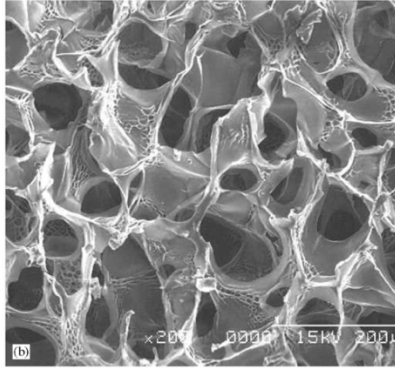


**Figure 2.8: Example of a freeze dried scaffold prepared from a 2 wt% chitosan solution in 0.2 M acetic acid. Scale bar represent 200  $\mu\text{m}$ .<sup>58</sup> Reproduced with permission from the reference. Copyright © 1999 Elsevier Science Ltd.**

#### **2.4.5 Cross-linking in Tissue Engineering Scaffold Fabrication**

In tissue engineering scaffold fabrication, cross-linking can be used to provide scaffolds with optimized properties. Cross-linked scaffolds have shown improved morphological stability<sup>59</sup>, slower degradation rate<sup>6</sup>, better mechanical strength and flexibility.<sup>10</sup>

Electrospinning is an efficient technique to produce 3-D porous scaffolds that mimic natural ECM for cell growth, proliferation and differentiation. However, some materials, including natural materials such as gelatin<sup>10</sup>, synthetic materials such as poly(vinyl alcohol)<sup>9,59</sup> exhibit poor morphological stability in aqueous solution after electrospinning. When immersed in buffer, electrospun fibrous mats swell and collapse to films. Thus, cross-linking was introduced as an approach to preserve the 3-D morphology in place.

Glutaraldehyde<sup>6,7</sup> and diisocyanates, as well as genipin<sup>10,60</sup>, carbodiimides<sup>61</sup>, and acyl azide<sup>62</sup> have been used as chemical cross-linking agents. Cross-linking mechanisms are shown in Scheme 2.2. Glutaraldehyde (GTA) is the most successful chemical agent used to treat collagenous tissue. GTA-based cross-linking employs inexpensive and readily-available reagents and requires relatively short reaction times. Researchers have

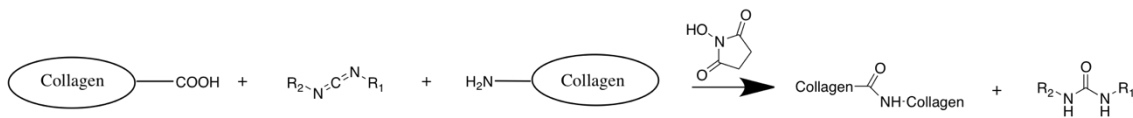
demonstrated that GTA cross-linking can be done in the vapor phase by simply subjecting gelatin electrospun fibers to saturated GTA vapor at room temperature<sup>7</sup>. However, cytotoxicity of GTA limited its application in biomedical fields. Therefore, genipin, an alternative cross-linking agent to GTA, has been successfully applied to collagenous tissue and gelatin and it has resulted in better biocompatibility as well as less cytotoxicity. In addition, it was found that compared to GTA cross-linked scaffolds, genipin cross-linked scaffolds showed enhanced mechanical properties<sup>6</sup>. Another method was set up to cross-link gelatin films by immersing them in genipin solution<sup>10</sup>. The cross-linked films showed increased thermal stability and mechanical properties. However, this method couldn't be successfully applied to gelatin electrospun mats, as once the mats were immersed in aqueous solution, the morphologies of the mats changed immediately. To preserve the fiber morphology after immersion in aqueous solution, Panzavolta et al. designed a series of experiments involving the electropinning of mixtures of gelatin and genipin.<sup>60</sup> SEM images showed that there weren't significant differences between the morphologies of electrospun fibers from only gelatin solution and those from genipin and gelatin mixtures. Although the latter provided better water-resistance, the fiber morphology was still affected.



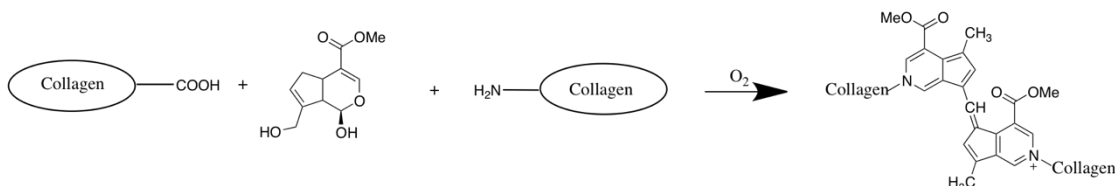
1) Glutaraldehyde



2) Carbodiimide



3) Genipin



**Scheme 2.2: Schematic cross-linking reactions. 1) Glutaraldehyde covalently bonds to amino groups; 2) 1-Ethyl-3-diaminopropyl-carbodiimide (EDC) and N-hydroxysuccinimide (NHS) catalyses covalent bindings between carboxylic groups and amino groups; 3) Genipin reacts in a similar manner as glutaraldehyde.<sup>63</sup>**

All of the above examples involved post-electrospinning treatment - electrospinning followed by cross-linking. The problem with this method is that one of the goals of cross-linking is to help maintain the fiber morphology in buffer. However, the cross-linking step usually requires immersing the electrospun mat in solution. In this case, the fiber morphology would have already changed before scaffolds are cross-linked. Also, this process prolongs and complicates the production process. To address the above issues, research has been conducted with the aim of combining the fiber fabrication and cross-linking into one step. Cinnamate-modified polymers have been demonstrated to undergo cross-linking upon UV irradiation. Therefore, researchers managed to functionalize poly(methyl methacrylate-co-2-hydroxyethyl acrylate) with cinnamate chloride.<sup>64</sup> The fibers were subjected to UV radiation while traveling to the collector as shown in Figure 2.9. Another group used a similar *in situ* polymerization and

cross-linking during electrospinning to obtain cross-linked poly(2-hydroxyethyl methacrylate) nanofibers.<sup>65</sup>

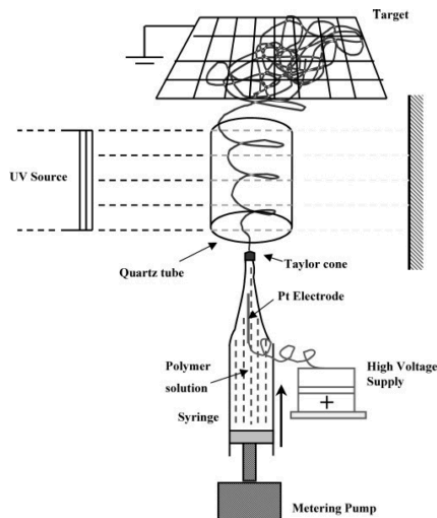


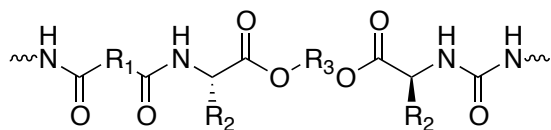
**Figure 2.9: *In situ* photo-cross-linking apparatus.**<sup>64</sup> Produced with permission from the reference. Copyright © 2004, American Chemical Society.

The incorporation of a UV light-induced cross-linking procedure is efficient. However, this method requires a special setup and is limited to photocurable materials. Tang et al. reported an *in situ* cross-linking based on a common electrospinning setup by adding glutaraldehyde and hydrochloric acid into the electrospinning PVA solution right before processing.<sup>9</sup> The resulting fibers showed insolubility after soaking in water.

### 2.3 Poly(ester amides) (PEAs)

Poly(ester amide)s (PEAs) (Scheme 2.3) composed of diols, dicarboxylic acids and amino acids are a family of synthetic materials that is promising in biomedical applications. They are of great interest because of their easily tunable properties, non-toxic degradation products and their ability degraded both hydrolytically and enzymatically.<sup>66</sup> PEAs have ester (-COO-) and amide (-NHCO-) bonds on polymer backbone. Ester bonds are hydrolysable in the absence or presence of enzymes. Amide

bonds provide relatively good thermal and mechanical properties because of strong intermolecular hydrogen bonding interactions and can be degraded enzymatically.<sup>67</sup>

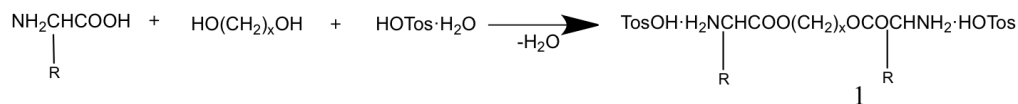


**Scheme 2.3: Structure of amino acid derived PEAs**

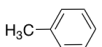
### 2.3.1 PEA Synthesis

For the synthesis of PEAs, polycondensation is usually applied to react diamide-diol, diester-diamine, ester-diamine or diamide-diester monomers with dicarboxylic acid derivatives or diols. Solution polymerization<sup>68,69</sup> and interfacial polymerization<sup>12,66</sup> have both been reported.

Solution polymerization has been applied to synthesize L-lysine (Lys)<sup>70</sup>, L-phenylalanine(Phe)<sup>71</sup>, L-valine (Val)<sup>72</sup>, L-leucine (Leu)<sup>72</sup> and L-aspartic acid (Asp)<sup>11</sup> derived PEAs successfully. Katsarava et al. have established a general solution polymerization procedure for PEAs involving: 1) preparation of di-*p*-toluenesulfonic acid salts of bis ( $\alpha$ -amino acid)  $\alpha$ ,  $\omega$ -alkylene diesters (Scheme 2.4); 2) preparation of di-*p*-nitrophenyl esters of dicarboxylic acids (Scheme 2.5); 3) condensation of these two components to obtain the PEAs (Scheme 2.6).<sup>72</sup>



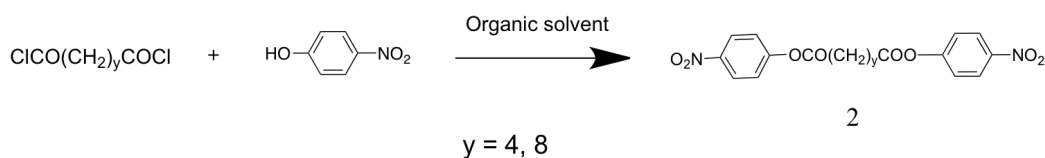
R = CH(CH<sub>3</sub>)<sub>2</sub>, (Val); CH<sub>2</sub>CH(CH<sub>3</sub>)<sub>2</sub>, (Leu); CH(CH<sub>3</sub>)CH<sub>2</sub>CH<sub>3</sub>, (Ile)

(CH<sub>2</sub>)<sub>3</sub>CH<sub>3</sub>, (Nle); , (Phe); (CH<sub>3</sub>)<sub>2</sub>SCH<sub>3</sub>, (Met)

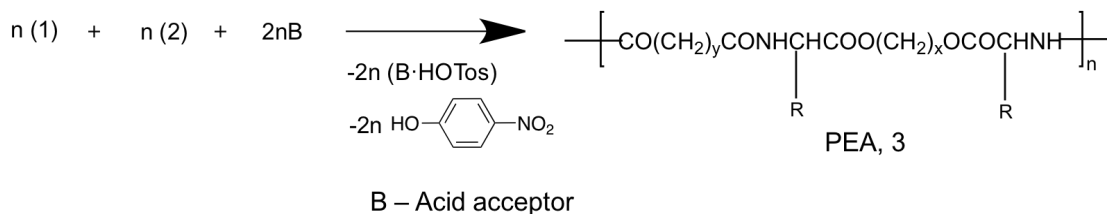
TosOH = *p*-Toluenesulfonic acid

x = 3, 4, 6 (number of methylene groups in diol residue)

**Scheme 2.4: Synthesis of di-*p*-toluenesulfonic acid salts of bis( $\alpha$ -amino acid  $\alpha$ ,  $\omega$ -alkylene diester, 1)**



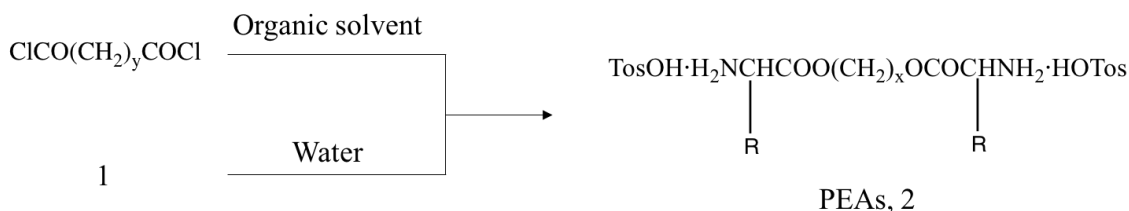
**Scheme 2.5: Synthesis of di-*p*-nitrophenyl ester dicarboxylic acids, 2**



**Scheme 2.6: Synthesis of PEAs, 3, via solution polycondensation of di-*p*-toluenesulfonic acid salt, 1 and di-*p*-nitrophenyl ester, 2**

Interfacial polymerization usually involves dissolution of a diacid chloride in organic solvent, dissolution of a diamine in water, and a reaction of the two solutions.<sup>67</sup> The first step of interfacial polymerization is the same as solution polymerization as shown in Scheme 2.4. Scheme 2.7 shows the second procedure of interfacial polymerization. Interfacial polymerization can be conducted at room temperature. The high rate of polymerization prevents other side reactions. Compared to solution polymerization, interfacial polymerization has less restrictions on purity and stoichiometry.<sup>66</sup> A previous

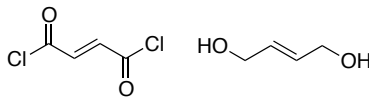
study done by our group compared PEAs derived from L-alanine, L-phenylalanine and L-lysine by interfacial polymerization and solution polymerization.<sup>73</sup> PEAs prepared by interfacial polymerization had higher molecular weight than their counterparts prepared by solution polymerization.



**Scheme 2.7: Synthesis of PEAs, 2, via interfacial polycondensation of di-*p*-toluenesulfonic acid salt, 1 and diacid chloride.**

### 2.3.2 PEA Functionalization

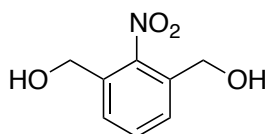
With the aim of exploiting PEAs for a wide range of applications such as drug<sup>74</sup> and gene delivery<sup>75</sup> as well as tissue engineering<sup>76</sup>, the functionality of PEAs has been further expanded through the introduction of different functional groups. For example, the structure of the diol and dicarboxylic acid components could be varied to achieve PEAs with different properties. Guo et al. synthesized a family of unsaturated PEAs (UPEAs) that have carbon-carbon double bonds on the polymer backbone, using fumaryl chloride and 2-butene-1,4-diol<sup>69</sup> (Scheme 2.8).



**Scheme 2.8: Structure of fumaryl chloride and 2-butene-1,4-diol**

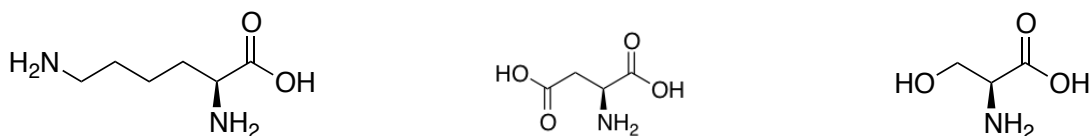
The carbon-carbon double bond in the polymer backbone allowed easy photo-cross-linking. In their follow-up study, those UPEAs were photo-cross-linked with poly(ethylene glycol) diacrylate to form biodegradable hydrogels for drug release applications.<sup>77</sup> In addition, UPEAs have potential application in controllable

biodegradability and the carbon-carbon double bond can be used to load bioactive molecules. In another study,<sup>78</sup> photodegradable *o*-nitrobenzyl moieties were incorporated in PEA backbones to give photodegradable properties. 2-Nitro-1,3-benzenedimethanol (Scheme 2.9) was condensed with L-phenylalanine to provide a diester, which was then polymerized with sebacoyl chloride so that the photodegradable moieties were distributed throughout the polymer backbone.



**Scheme 2.9: Structure of 2-nitro-1,3- benzenedimethanol**

Another widely-used method to add functionality to PEAs has involved the incorporation of amino acids or amino acid derivatives with pendant functional groups. L-lysine<sup>11,70</sup>, L-aspartic acid<sup>12,79</sup>, and L-serine<sup>68</sup> (Scheme 2.10) have been incorporated into PEAs.



**Scheme 2.10: Structure of L-lysine, L-aspartic acid and L-serine**

Deng et al. synthesized PEAs with pendant amine groups by using a L-lysine derivative as one monomer in solution polymerization, followed by a deprotection process.<sup>70</sup> The utility of amine groups was confirmed by conjugating a fluorescent dye. Thus, these amine groups can be potentially conjugated with bioactive molecules and expand the application of PEAs in biomedical and pharmaceutical fields. Compared to L-lysine, the incorporation of L-aspartic acid is complementary, because it allows conjugation of bioactive molecules with reactive amines. Furthermore, the incorporation of Asp results in a negative charge presented to cells at neutral pH, while the pendent amine groups are cationically charged.

For Asp-derived PEAs, they were synthesized successfully by ring-opening polymerization using tin 2-ethylhexanoate at 155 °C.<sup>79</sup> However, the resulting molecular weight was low, which is not desirable for biomedical applications because high molecular weight is required to ensure that materials are able to be fabricated into scaffolds and possess sufficient mechanical properties and dimensional stability. A homogenous solution polycondensation was developed.<sup>11</sup> The PEAs were synthesized at a temperature around 60-70 °C with 48 h reaction time. Compared to ring-opening polymerization, higher molecular weight was obtained. Knight et al. further developed an interfacial polymerization for Asp-derived PEAs synthesis.<sup>12</sup> This method was conducted at room temperature and yielded PEAs with high molecular weight within a shorter reaction time and the activation of the pendant carboxylic groups was confirmed by converting to NHS esters using carbonyl diimidazole followed by N-hydroxysuccinimide. Then the reactivity of the NHS ester was demonstrated by a reaction with benzylamine.<sup>12</sup>

In addition, a family of PEAs with pendant hydroxyl groups were also developed by Deng et al.<sup>68</sup> An L-Serine derivative was introduced into PEA backbone with the pendant alcohol protected as a benzyl ether. The hydroxyl groups were deprotected using a Pd/C-catalyzed hydrogenation reaction. Those hydroxyl groups were further converted to acrylate groups for photo-gelation.

### **2.3.3 Biodegradability of PEAs**

Biodegradation rate is an important parameter for biomaterials and it has been extensively explored for some polymers. For tissue engineering scaffolds, an appropriate biodegradation rate means the scaffold should degrade at a rate slow enough to provide enough support before cells secrete and form their own ECM, but yet sufficiently rapid that will be degraded *in vivo* after the new ECM is formed.

The biodegradation rate of PEAs can be influenced by factors such as the different building blocks used in the PEA synthesis, the enzymes used in the degradation study, and the method of introducing enzymes into the systems. PEAs derived from amino acids have the potential of enhanced biodegradability. In this case, the enzymatic degradation of PEAs is highly specific for the amino acids incorporated in PEA backbone.  $\alpha$ -Chymotrypsin is known to have high specificity for aromatic amino acids in proteins, so that the incorporation of L-phenylalanine in PEA backbone will enhance its biodegradation in the presence of  $\alpha$ -chymotrypsin. According to another study,<sup>80</sup> increased hydrophobicity caused by longer methylene groups in diester portion also led to higher  $\alpha$ -chymotrypsin affinity and accelerated degradation. As most of the amino acids in nature are L-form and proteases are highly specific for L-amino acids, it is reasonable to anticipate that the D/L amino acid ratio will have an impact on amino acid based PEA biodegradability. Fan et al. synthesized a series of PEAs containing Phe with different D/L ratio then subjected them to  $\alpha$ -chymotrypsin degradation. The result suggested that degradation rate strongly depended on D/L ratio.<sup>81</sup> Tsitlanadze et al. also tested the influence of different enzymes ways to introduce enzymes into system to PEA degradation.<sup>80</sup> They added enzyme powder into the polymer solution then cast the solutions into films to obtain enzyme-impregnated PEA films. These PEAs were self-degradable and could be potentially used in biomedical applications where enzyme release is desired.

Two methods are available for measuring the degradation rate of PEAs – a gravimetric method (weight loss)<sup>80</sup> and potentiometric titration.<sup>82</sup> The gravimetric method is most commonly used in measuring the biodegradation rates of polymers. However, it has limitations at the early stages of biodegradation. The situation is always complicated by water adsorption, especially for high water affinity materials. The rationale of potentiometric is that hydrolyzing the materials will give carboxylic acid groups. Based



on the amount of NaOH required to neutralize the acid, the biodegradation rate can be determined. Nevertheless, to acquire a complete understanding of PEA degradation, weight loss is an essential parameter, particularly in the late stage of degradation and for biomaterials that degrade slowly.

### **2.3.4 Biocompatibility of PEAs**

PEA biocompatibility has been tested with various cells including human coronary artery smooth muscle cells<sup>73</sup>, bovine aortic endothelial cells,<sup>68,70</sup> and fibroblasts<sup>68</sup>. Biodegradable PEAs provided sufficient support for cell attachment, migration and proliferation. PEA electrospun fibers were even found to support cell growth in serum-depleted conditions.<sup>83</sup>

PEA biocompatibility is affected by material surface properties such as hydrophobicity/hydrophilicity and surface charge. Deng et al. conducted a cell culture study on a family of PEAs derived from serine that provided pendant hydroxyl groups.<sup>68</sup> With an increasing serine ratio, hydrophobicity of the PEAs decreases. Fibroblasts and bovine aortic endothelial cells were seeded onto PEA films. Cell morphology and proliferation data suggested that in order to achieve sufficient cell adhesion, the contact angle of the PEAs needed to be higher than 60°. In another study done by the same group,<sup>84</sup> cell attachment was compared among positively charged (Lys-functionalized), negatively charged (Asp-functionalized) and neutral (non-functionalized) PEAs. All the PEAs supported endothelial cell adhesion and growth, while the positively charged PEAs showed the best result.

To improve cell attachment and proliferation on PEAs, bioactive molecules were conjugated to provide pendent groups for further modification. The release of bioactive molecules from PEAs was expected to induce cell proliferation and differentiation. Chu and coworkers<sup>85</sup> have coupled 4-amino TEMPO with the –COOH provided by L-lysine

segment on PEAs. 4-Amino TEMPO served as the source of NO· which is known for a huge host of biological functions. TGF-β1 was conjugated successfully by a 1-ethyl-3-(3-dimethylaminopropyl)carbodiimide (EDC)/sulfo-N-hydroxysuccinimide (sulfo-NHS) conjugation strategy on Asp-derived PEAs by our group<sup>12</sup>.

## 2.4 Objectives and Rationale for This Thesis

As shown in the literature review above, PEAs have been investigated for biomedical applications because of their desirable properties. To expand the functionality of PEAs and fulfill the criteria for specific applications, different built-in functional groups have been incorporated into either PEA backbones or as pendant functional groups. A family of L-aspartic acid derived PEAs were developed in our group. Cell studies on these PEA 2-D films showed that cell proliferation was maintained throughout 7-day culture and the incorporation of L-aspartic acid provides pendant carboxylic groups allowing conjugation of TGF-β1. However, the 3-D electrospun PEA scaffolds fused during post-electrospinning processing, which is not desirable. As previously reported<sup>10,64,86,87</sup>, cross-linking was widely-used to improve scaffold dimensional and morphological stability after or during scaffold fabrication. Post scaffold fabrication cross-linking doesn't require a special set-up but the morphology may have already changed before cross-linking is complete. *In situ* scaffold fabrication cross-linking is more efficient and prevents morphological change before the fabrication process is complete but may require a special setup. Based on the different set-up of each scaffold fabrication methods, i.e. electrospinning and solvent casting particulate leaching in this work, photo-cross-linking and thermal cross-linking were applied to 3-D scaffolds in order to improve their morphological stability.

In view of the rationale above, the objectives of this work were to:

- Synthesize and characterize photo-cross-linkable PEAs prepared by reacting pendant carboxylic groups with hydroxyethyl cinnamate.

- Perform post-electrospinning cross-linking of photo-cross-linkable PEAs
- Synthesize and characterize thermally-cross-linkable PEAs by reacting pendant carboxylic groups with hydroxyethyl methacrylate.
- Perform *in situ* thermal cross-linking of thermally-cross-linkable PEAs 3-D scaffold via solvent casting particulate leaching.

## Chapter 3

### 3 Materials and Methods

#### 3.1 Materials

Solvents were purchased from Caledon Labs (Georgetown, ON). All other chemicals were purchased from Sigma Aldrich (Milwaukee, WI). Unless noted otherwise, all chemicals were used as received. Dichloromethane (DCM) was distilled from  $\text{CaH}_2$ .

#### 3.2 Material Characterization

##### 3.2.1 Nuclear Magnetic Resonance Spectroscopy (NMR)

$^1\text{H}$  (600 MHz) nuclear magnetic resonance (NMR) spectra were obtained on a Varian Inova 600 spectrometer (Varian Canada Inc., Mississauga, ON). Chemical shifts are reported in parts per million (ppm) and are calibrated against residual solvent signals of chloroform ( $\text{CDCl}_3$ ,  $\delta$  7.27 ppm) or dimethyl sulfoxide (DMSO,  $\delta$  2.50 ppm).

##### 3.2.2 Fourier-Transform Infrared Spectroscopy (FTIR)

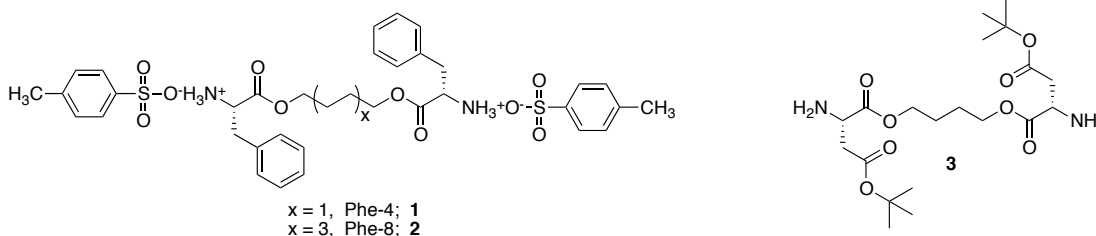
Infrared spectroscopy was performed on a Bruker Vector 22 Spectrometer from Bruker Optics (Bruker Corporation, Billerica, MA) equipped with a MIRacle Attenuated Total Reflectance (ATR) diamond crystal plate sample cell (PIKE Technologies, Madison, WI). The samples were run as solid films in air for 32 scans with a resolution of  $4\text{ cm}^{-1}$  over the scan range of  $600\text{ cm}^{-1}$  to  $3200\text{ cm}^{-1}$ . Spectra were collected and processed in Opus 6.5 FTIR software (Bruker Optics) and reported in wavenumbers ( $\text{cm}^{-1}$ ).

##### 3.2.3 Gel Permeation Chromatography (GPC)

Gel permeation chromatography data were obtained using a Waters 2695 Separations Module equipped with a Waters 2414 Refractive Index Detector (Waters Limited, Mississauga, ON) and two PLgel  $5\text{ }\mu\text{m}$  mixed-D ( $300\text{ mm} \times 7.5\text{ mm}$ ) columns connected in series (Varian Canada Inc., Mississauga, ON). Samples ( $5\text{ mg/mL}$ ) dissolved in the

eluent, which comprised of 10 mM LiBr and 1 % (v/v) NEt<sub>3</sub> in DMF at 85°C were injected (100 μL) at a flow rate of 1 mL/min and calibrated against polystyrene standards. Molecular weights are reported in grams/mole (g/mol).

### 3.3 Monomer Synthesis



#### 3.3.1 Synthesis Procedure for Monomers 1

A suspension of L-phenylalanine (10.9 g, 66 mmol, 2.2 equiv.), *p*-toluenesulfonic acid·H<sub>2</sub>O (*p*TsOH·H<sub>2</sub>O) (12.4 g, 72 mmol, 2.4 equiv.) in toluene (100 mL) was refluxed at 120 °C with stirring in a flask equipped with a Dean-Stark trap to remove the water produced. To this solution 1,4-butanediol (2.70 g, 30 mmol, 1.0 equiv.) was added and the resulting mixture was heated at reflux for 48 h. The resulting material was filtered and recrystallized from boiling water to provide monomer **1** or **2**. Yield: Phe-4, **1**: 8.2 g, 71%; Phe-8, **2**: 11.4 g 80%. Spectral data agreed with those previously reported.<sup>73</sup>

#### 3.3.1 Synthesis Procedure for Monomers 2

A suspension of L-phenylalanine (10.9 g, 66 mmol, 2.2 equiv.), *p*-toluenesulfonic acid·H<sub>2</sub>O (*p*TsOH·H<sub>2</sub>O) (12.4 g, 72 mmol, 2.4 equiv.) in toluene (100 mL) was refluxed at 120 °C with stirring in a flask equipped with a Dean-Stark trap to remove the water produced. To this solution 1,8-butanediol (4.39 g, 30 mmol, 1.0 equiv.) was added and the resulting mixture was heated at reflux for 48 h. The resulting material was filtered and

recrystallized from boiling water to provide monomer **1** or **2**. Yield: Phe-4, **1**: 8.2 g, 71%; Phe-8, **2**: 11.4 g 80%. Spectral data agreed with those previously reported.<sup>73</sup>

### 3.3.3 Synthesis of Monomer **3**

*N*- $\alpha$ -carboxybenzyl-L-aspartic acid- $\beta$ -*t*-butyl ester hydrate (0.51 g, 1.5 mmol, 3 equiv.) was dissolved in 4 mL of dichloromethane. 1,4-Butanediol (0.045 g, 0.5 mmol, 1 equiv.), *N,N'*-dicyclohexylcarbodiimide (DCC) (0.31 g, 1.5 mmol, 3 equiv.), 4-(dimethylamino)pyridine (DMAP) (0.012 g, 0.1 mmol, 0.2 equiv.), and 4-(dimethylamino)pyridinium *p*-toluenesulfonate (DPTS) (0.029 g, 0.1 mmol, 0.2 equiv.) were added to the solution. The mixture was stirred for 2 h at room temperature. The reaction mixture was then filtered through celite to remove the dicyclohexylurea (DCU). The solvent was removed *in vacuo*. The product was purified by column chromatography using 70:30 hexane:ethyl acetate. The resulting product was dissolved in anhydrous ethanol. Pd/C catalyst was added to the solution. The mixture was stirred for 2 h under a hydrogen atmosphere. The reaction mixture was filtered through celite and the solvent was removed under reduced pressure producing bis-L-aspartic acid- $\beta$ -(*tert*-butyl ester) diester **3**. Yield: 0.2 g, 47%. Spectral data agreed with those previously reported.<sup>11</sup>

### 3.4 PEA Nomenclature

The polymers are named by the methylene groups from the diacid, the three letter amino acid designation, and by the number of methylene groups in the diol at last. For example, 8-Phe-4-Asp(O-*t*-Bu) stands for the incorporation of the aspartic acid monomer as a co-monomer at a mole ratio of 10% relative to the di-*p*-toluenesulfonic acid salt monomer. For example, PEAs derived from sebacoyl chloride (8), L-phenylalanine (phe) and 1,8-octanediol (8), functionalized with L-aspartic acid (Asp), denoted as 8-Phe-8-Asp(OH)-4.

## 3.5 Polymer Synthesis

### 3.5.1 Synthesis Procedure for the Interfacial Polymerization to Prepare Poly(ester amide)s, 8-Phe-4-Asp(O-*t*-Bu)-4

Sodium carbonate (0.59 g, 5.6 mmol, 2.0 equiv.) and the di-*p*-toluenesulfonic acid salt monomer **1** (2.5 mmol, 0.9 equiv.) were dissolved in deionized water (35 mL). Bis-L-aspartic acid  $\beta$ -(*t*-butyl ester) diester **3**, (0.12 g, 0.28 mmol, 0.1 equiv.) was dissolved in DCM (15 mL), then the organic solution was added to the aqueous solution. The reaction mixture was stirred for 30 min. Sebacoyl chloride (0.6 mL, 2.78 mmol, 1.0 equiv.) was diluted in anhydrous DCM (10 mL), then was added in to the two-phase solution dropwise over 20 min. The reaction was run for overnight. When the reaction was completed, the solvent was removed *in vacuo*. Then, the resulting PEA was dissolved in DCM and filtered to remove the insoluble salts. The filtrate was dialyzed against dimethylformamide (DMF) for 6 h twice. Spectral data for the polymers agreed with those previously reported.<sup>12</sup> GPC: 8-Phe-4-Asp(O-*t*-Bu)-4:  $M_n$ = 31.9 kg/mol,  $M_w$ = 58.9 kg/mol,  $D$  = 1.85.

### 3.5.2 Synthesis Procedure for the Interfacial Polymerization to Prepare Poly(ester amide)s, 8-Phe-8-Asp(O-*t*-Bu)-4

Sodium carbonate (0.59 g, 5.6 mmol, 2.0 equiv.) and the di-*p*-toluenesulfonic acid salt monomer **2** (2.5 mmol, 0.9 equiv.) were dissolved in deionized water (35 mL). Bis-L-aspartic acid  $\beta$ -(*t*-butyl ester) diester **3**, (0.12 g, 0.28 mmol, 0.1 equiv.) was dissolved in DCM (15 mL), then the organic solution was added to the aqueous solution. The reaction mixture was stirred for 30 min. Sebacoyl chloride (0.6 mL, 2.78 mmol, 1.0 equiv.) was diluted in anhydrous DCM (10 mL), then was added in to the two-phase solution dropwise over 20 min. The reaction was run for overnight. When the reaction was completed, the solvent was removed *in vacuo*. Then, the resulting PEA was dissolved in DCM and filtered to remove the insoluble salts. The filtrate was dialyzed

against dimethylformamide (DMF) for 6 h twice. Spectral data for the polymers agreed with those previously reported.<sup>12</sup> GPC: 8-Phe-8-Asp(O-*t*-Bu)-4:  $M_n = 42.4$  kg/mol,  $M_w = 74.1$  kg/mol,  $D = 1.62$ .

### 3.5.3 General Deprotection Procedure

Each *t*-Bu-protected functional PEAs (8-Phe-4-Asp(O-*t*-Bu)-4 or 8-Phe-8-Asp(O-*t*-Bu)-4) (0.1–0.2 g) was dissolved in 1:1 trifluoroacetic acid (TFA): CH<sub>2</sub>Cl<sub>2</sub> (2 mL) and reacted for 2 h. The solvents were subsequently removed *in vacuo*. The product was dried *in vacuo*, yielding the functional PEA with pendant carboxylic acid groups (8-Phe-4-Asp(OH)-4 and 8-Phe-8-Asp(OH)-4). Spectral data for the polymers agreed with those previously reported.<sup>12</sup>

### 3.5.4 General Synthesis Procedure of Cinnamate-functionalized PEAs

#### 3.5.4.1 Synthesis of Hydroxyethyl Cinnamate, 7

Cinnamic acid (0.5 g, 3.37 mmol, 1 equiv.) was dissolved in ethylene glycol (4.19 g, 67.5 mmol, 20 equiv.). *p*TsOH·H<sub>2</sub>O (0.064 g, 0.337 mmol, 0.1 equiv.) was added to the solution. The mixture was then heated at 100 °C and stirred overnight. Upon the completion of the reaction the solution was light green in color. It was then diluted with ethyl acetate, and the mixture was extracted with H<sub>2</sub>O 3 times, dilute NaHCO<sub>3</sub> 3 times and brine. The organic phase was collected, dried with MgSO<sub>4</sub>, and then filtered. The solvent was removed *in vacuo*. The crude product was purified by column chromatography using 70:30 hexane:ethyl acetate. Yield: 0.170 g, 26%. Spectral data agreed with those previously reported.<sup>88</sup>

#### 3.5.4.2 Synthesis Procedure for the Reaction of Hydroxyethyl Cinnamate 7 with 8-Phe-4-Asp(OH)-4

8-Phe-4-Asp(OH)-4 (0.1 g) and *N*-(3-dimethylaminopropyl)-*N'*-ethylcarbodiimide hydrochloride (EDC·HCl) (0.076 g, 0.396 mmol) were dissolved in anhydrous DMF (2 mL) and stirred for 15 min. Then, hydroxyethyl cinnamate (0.019 g, 0.099 mmol) and



DMAP (0.02 g, 0.165 mmol) were added to the solution. The reaction was run for 4 h under 45 °C. The solution was then diluted with ethyl acetate, washed with saturated NH<sub>4</sub>Cl, dilute NaHCO<sub>3</sub>, and brine. The organic phase was kept and the solvent was removed *in vacuo*. The crude product was dissolved in DMF and was dialyzed against DMF for 12 h using a membrane with a molecular weight cut-off (MWCO) of 25 kg/mol.

#### 3.5.4.3 Synthesis Procedure for the Reaction of Hydroxyethyl Cinnamate 7 with 8-Phe-8-Asp(OH)-4

8-Phe-8-Asp(OH)-4 (0.1 g) and *N*-(3-dimethylaminopropyl)-*N'*-ethylcarbodiimide hydrochloride (EDC·HCl) (0.076 g, 0.396 mmol) were dissolved in anhydrous DMF (2 mL) and stirred for 15 min. Then, hydroxyethyl cinnamate (0.019 g, 0.099 mmol) and DMAP (0.02 g, 0.165 mmol) were added to the solution. The reaction was run for 4 h under 45 °C. The solution was then diluted with ethyl acetate, washed with saturated NH<sub>4</sub>Cl, dilute NaHCO<sub>3</sub>, and brine. The organic phase was kept and the solvent was removed *in vacuo*. The crude product was dissolved in DMF and was dialyzed against DMF for 12 h using a membrane with a molecular weight cut-off (MWCO) of 25 kg/mol.

#### 3.5.4.4 Cinnamate 8-Phe-4-Asp(OH)-4

This polymer was prepared by the general synthesis procedure described above (section 3.5.3.2). Yield: 0.076 g, 61%. <sup>1</sup>H NMR (600 MHz, DMSO-d<sub>6</sub>): δ 8.20 (d, 1.8H, J = 8.19, -C(O)-NH-C<sub>α</sub>H-CH<sub>2</sub>-Ph), 7.71-7.64 (m, 1H, aromatic ring on cinnamoyl moiety), 7.41-7.36 (m, 0.8H, - aromatic ring on cinnamoyl moiety), 7.27-7.13 (m, 9H, -CH<sub>2</sub>-Ph), 4.55-4.50 (m, 0.3H, -C<sub>α</sub>H-CH<sub>2</sub>-C(O)OH), 4.50-4.37 (m, 1.7H, -C<sub>α</sub>H-CH<sub>2</sub>-Ph), 4.07-3.86 (m, 4H, -C(O)O-CH<sub>2</sub>-), 3.02-2.78 (m, 3.3H, -C<sub>α</sub>H-CH<sub>2</sub>-Ph), 2.72-2.49 (m, 0.7H, -C<sub>α</sub>H-CH<sub>2</sub>-C(O)OH), 2.18-1.94 (m, 4H, -CH<sub>2</sub>-C(O)-NH-C<sub>α</sub>H-CH<sub>2</sub>-C(O)OH, -CH<sub>2</sub>-C(O)-NH-C<sub>α</sub>H-CH<sub>2</sub>-Ph), 1.61-1.31 (m, 8H, -C(O)O-CH<sub>2</sub>-CH<sub>2</sub>-, -CH<sub>2</sub>-CH<sub>2</sub>-C(O)-NH-), 1.26-0.99 (m, 8H, -(CH<sub>2</sub>)<sub>4</sub>-CH<sub>2</sub>-CH<sub>2</sub>-C(O)-NH-). GPC: M<sub>n</sub> = 14.2 kg/mol, M<sub>w</sub> = 27.7 kg/mol, Đ = 1.95.

#### 3.5.4.5 Cinnamate 8-Phe-8-Asp(OH)-4

This polymer was prepared by the general synthesis procedure described above (section 3.5.4.2). Yield: 0.073 g, 56%.  $^1\text{H}$  NMR (600 MHz, DMSO- $d_6$ ):  $\delta$  8.17 (d, 1.8H,  $J = 7.6$ , -C(O)-NH-  $C_\alpha\text{H-CH}_2\text{-Ph}$ ), 7.7-7.6 (m, 1H, aromatic ring from cinnamoyl moiety), 7.42-7.34 (m, 0.8H, - aromatic ring from cinnamoyl moiety), 7.26-7.10 (m, 9H, -CH<sub>2</sub>-Ph), 4.60-4.52 (m, 0.2H, - $C_\alpha\text{H-CH}_2\text{-C(O)OH}$ ), 4.44-4.34 (m, 1.8H, - $C_\alpha\text{H-CH}_2\text{-Ph}$ ), 4.00-3.86 (m, 4H, -C(O)O-CH<sub>2</sub>-), 3.00-2.78 (m, 3.6H, - $C_\alpha\text{H-CH}_2\text{-Ph}$ ), 2.05-1.94 (m, 4H, -CH<sub>2</sub>-C(O)-NH- $C_\alpha\text{H-CH}_2\text{-C(O)OH}$ , -CH<sub>2</sub>- C(O)-NH- $C_\alpha\text{H-CH}_2\text{-Ph}$ ), 1.51-1.25 (m, 8H, -C(O)O-CH<sub>2</sub>-CH<sub>2</sub>-, -CH<sub>2</sub>-CH<sub>2</sub>-C(O)-NH-), 1.24-0.99 (m, 15.8H, -C(O)O-CH<sub>2</sub>-CH<sub>2</sub>-(CH<sub>2</sub>)<sub>4</sub>-, -(CH<sub>2</sub>)<sub>4</sub>-CH<sub>2</sub>-CH<sub>2</sub>-C(O)-NH-). FTIR: 3292 (N-H stretch, amide), 3060 (C-H stretch, aromatic), 2929 (C-H stretch, aliphatic), 2853 (C-H stretch, aliphatic), 1734 (C=O stretch, ester), 1644 (C=O stretch, amide), 1534 (C=C stretch, aromatic), 1452 (C=C stretch, aromatic), 1176 (C-O stretch, ester), 985 (*trans* C=C stretch, alkene). GPC:  $M_n = 23.9$  kg/mol,  $M_w = 43.0$  kg/mol,  $D = 1.79$ .

#### 3.5.5 Synthesis of Methacrylate-functionalized 8-Phe-8-Asp(OH)-4

8-Phe-8-Asp(OH)-4 (0.1 g) and EDC·HCl (0.076 g, 0.396 mmol) were dissolved in anhydrous DMF (2 mL) and stirred for 15 min. Then, hydroxyethyl methacrylate (0.019 g, 0.099 mmol) and DMAP (0.02 g, 0.165 mmol) were added to the solution. The reaction was run for 4 h at 45 °C. The solution was then diluted with ethyl acetate and washed with saturated NH<sub>4</sub>Cl, dilute NaHCO<sub>3</sub>, and then brine. The organic phase was kept and the solvent was removed *in vacuo*. The crude product was dissolved in DMF and was dialyzed against DMF for 6 h twice with a membrane having a molecular weight cut-off of 25 kg/mol. Yield: 0.048 g, 41%.  $^1\text{H}$  NMR (600 MHz, DMSO- $d_6$ ):  $\delta$  8.17 (d, 2.0H,  $J = 7.6$ , -C(O)-NH-  $C_\alpha\text{H-CH}_2\text{-Ph}$ ), 7.26-7.10 (m, 9H, -CH<sub>2</sub>-Ph), 5.97 (0.03H, -CH=CH<sub>2</sub>), 5.62 (t, 0.03H, -CH=CH<sub>2</sub>), 4.60-4.52 (m, 0.2H, - $C_\alpha\text{H-CH}_2\text{-C(O)OH}$ ), 4.44-4.34 (m, 1.8H, - $C_\alpha\text{H-CH}_2\text{-Ph}$ ), 4.00-3.86 (m, 4H, -C(O)O-CH<sub>2</sub>-), 3.00-2.78 (m, 3.6H, - $C_\alpha\text{H-CH}_2\text{-Ph}$ ),

2.05-1.94 (m, 4H,  $-CH_2-C(O)-NH-C_6H-CH_2-C(O)OH$ ,  $-CH_2-C(O)-NH-C_6H-CH_2-Ph$ ), 1.81 (0.12H,  $CH_2=C(CH_3)-C(O)$ ) 1.51-1.25 (m, 8H,  $-C(O)O-CH_2-CH_2-$ ,  $-CH_2-CH_2-C(O)-NH-$ ), 1.24-0.99 (m, 15.8H,  $-C(O)O-CH_2-CH_2-(CH_2)_4-$ ,  $-(CH_2)_4-CH_2-CH_2-C(O)-NH-$ ). FTIR: 3304 (N-H stretch, amide), 3050 (C-H stretch, aromatic), 2927 (C-H stretch, aliphatic), 2850 (C-H stretch, aliphatic), 1734 (C=O stretch, ester), 1600 (C=O stretch, amide), 1540 (C=C stretch, aromatic), 1452 (C=C stretch, aromatic), 1180 (C-O stretch, ester), 798 (C-H out of plane bending, alkene). GPC:  $M_n=17.9$  kg/mol,  $M_w=38.6$  kg/mol,  $D=2.14$ .

### 3.6 Synthesis of Functionalized Rhodamine Dyes

#### 3.6.1 Rhodamine B Base, **8**

Rhodamine B (0.5 g, 1.0 mmol) was dissolved and partitioned between aqueous 1M NaOH (50 mL) and ethyl acetate (50 mL). After isolation of the organic layer, the aqueous layer was extracted with two additional portions of ethyl acetate. The combined organic layers were then washed with NaOH and brine. The resulting organic solution was dried over  $Na_2SO_4$ , filtered, and concentrated under vacuum to afford the product. Yield = 0.39 g, 84%. Spectral data agreed with those previously reported.<sup>89</sup>

#### 3.6.2 Rhodamine B Piperazine Amide, **9**

The reaction was performed under an atmosphere of  $N_2$  with flame-dried glassware.  $CH_2Cl_2$  was distilled from  $CaH_2$ . A 2.0 M solution of trimethylaluminum in toluene (0.46 mL, 0.90 mmol) was added dropwise to a solution of piperazine (0.16 g, 1.8 mmol) in 2 mL  $CH_2Cl_2$  at room temperature. The resulting mixture was stirred for 1 h and a white precipitate was observed. A solution of rhodamine base B, **8** (0.20 g, 0.45 mmol) in 1 mL  $CH_2Cl_2$  was then added dropwise and the reaction mixture was stirred at reflux for 24 h. 0.1 M HCl was then added dropwise until gas evolution ceased. The resulting mixture was filtered and the residual solids were washed with  $CH_2Cl_2$  and 4:1  $CH_2Cl_2/MeOH$  solution. The filtrate was combined and concentrated then dissolved in  $CH_2Cl_2$ , filtered to

remove insoluble and concentrated again. The glassy solid was partitioned between dilute NaHCO<sub>3</sub> and ethyl acetate. The aqueous solution was washed with ethyl acetate 3 times. The retained aqueous layer was saturated with NaCl, acidified with 1 M HCl, and then extracted with 2:1 isopropanol/CH<sub>2</sub>Cl<sub>2</sub> multiple times until a faint pink color persisted. Organic layer was dried with MgSO<sub>4</sub>, filtered and concentrated. The glassy purple solid was dissolved in minimum methanol, then precipitated by adding a big volume of ethyl ether into the solution dropwise. The product was collected by filtration. Yield = 0.13 g, 59%. Spectral data agreed with those previously reported.<sup>89</sup>

### 3.6.3 Rhodamine B Primary Amide, 10

#### 3.6.3.1 Synthesis of *tert*-butyl (3-bromopropyl)carbamate, 11

3-Bromopropylamine (1.00 g, 4.57 mmol) and di-*tert*-butyl dicarbonate (1.25 g, 5.71 mmol) were dissolved in 10 mL CH<sub>2</sub>Cl<sub>2</sub>. The flask was cooled in ice bath, then triethylamine (0.63 mL, 4.57 mmol) was added. After the reaction was run overnight at room temperature, the reaction solution was diluted with CH<sub>2</sub>Cl<sub>2</sub> and extracted with brine. The organic layer was dried with MgSO<sub>4</sub>, filtered and concentrated to obtain the crude product, that was subsequently purified by silica gel chromatography using 9:1 hexane/ethyl acetate as the eluent. Yield = 86%. Spectral data agreed with those previously reported.<sup>90</sup>

#### 3.6.3.2 Synthesis of Protected Rhodamine B Primary Amide, 12

Rhodamine B piperazine amide, **9** (0.20 g, 0.38 mmol) and *tert*-butyl (3-bromopropyl)carbamate (0.11 g, 0.48 mmol) were dissolved in DMF. *N,N*-Diisopropylethylamine (DIPEA) (0.18 g, 1.41 mmol) was added to the solution. The reaction was stirred at room temperature overnight. The solution was then diluted with saturated NaHCO<sub>3</sub> solution, then extracted with ethyl acetate. The aqueous layer was collected and washed with 1:3 isopropanol/CH<sub>2</sub>Cl<sub>2</sub>. Organic layer was dried with MgSO<sub>4</sub>, filtered, and dried under vacuum. Yield = 0.1 g, 39%. <sup>1</sup>H NMR (600 MHz, CDCl<sub>3</sub>): δ 7.71-7.67 (m, 1.1H), δ 7.60-7.53 (m, 0.5H), δ 6.99-6.92 (m, 0.3H), δ 6.72 (s, 1.0H), δ

4.32 (t,  $J = 7.14$  Hz 0.5H),  $\delta$  3.76-3.51 (m, 5.1H),  $\delta$  1.60 (s, 9.2H),  $\delta$  1.42 (s, 2.1H),  $\delta$  1.34 (t,  $J = 7.14$  Hz 5.72H),  $\delta$  1.23 (t,  $J = 5.42$  Hz, 1.0H),

### **3.6.3.3 Deprotection of the Boc-protected Amine-functionalized Rhodamine**

#### **Derivative 12.**

The protected derivative **12** (0.10 g, 0.15 mmol) was dissolved in 1:1 trifluoroacetic acid/ $\text{CH}_2\text{Cl}_2$  and stirred for 2 h. The solvent was then removed *in vacuo*. Yield = 0.06 g, 75%.  $^1\text{H}$  NMR (600 MHz,  $\text{CDCl}_3$ ):  $\delta$  7.76-7.72 (m, 2.6H),  $\delta$  7.57-7.51 (m, 1H),  $\delta$  7.35-7.29 (m, 1.29H),  $\delta$  6.94-6.87 (m, 1.8H),  $\delta$  6.75-6.72 (m, 1.6H),  $\delta$  6.15 (m, 1.0H),  $\delta$  4.34 (t,  $J = 5.34$  Hz, 1.9H),  $\delta$  3.80-3.43 (br, m, 20H),  $\delta$  3.41-3.27 (m, 7.9H),  $\delta$  2.05-1.99 (m, 1.7H),  $\delta$  1.42-1.23 (m, 12H)

## **3.7 Scaffold Fabrication**

### **3.7.1 Electrospinning of Cinnamate-functionalized PEAs**

Electrospinning was used to develop 3-D fibers of cinnamate-functionalized PEA materials. PEA solutions, at range 8 wt% to 16 wt% concentration, were prepared in a co-solvent mixture of chloroform ( $\text{CHCl}_3$ ): dimethylformamide (DMF) at a ratio of 9:1. The polymer solution (0.5 mL) was transferred to a 0.5 cc glass syringe (Becton, Dickinson and Co., Franklin Lakes, NJ) equipped with a blunt-tip stainless steel needle (22 gauge). High voltage (20 kV), supplied by a high voltage DC power supply (Gamma high voltage, Ormond Beach, FL), was applied to the needle. The flow rate was maintained at 0.1 mL/h with a syringe pump (KD Scientific, Holliston, MA). The fibers were collected on aluminum foil on a rotating mandrel (1500 rpm) placed at 8 cm from the needle tip.

### **3.7.2 Post-Electrospinning Photo-cross-linking**

3-D PEA electrospun mats were placed under medium pressure mercury lamp (Hanovia S9 PC 451050/805221), around 20 cm to the bulb, which was contained in a quartz water jacket, for 0.5 h, 1 h, and 2 h for cross-linking.

### **3.7.3 *In Situ* Cross-linking and Solvent Casting of Methacrylate-functionalized 8-Phe-8-Asp(OH)-4**

Ground and sieved NH<sub>4</sub>Cl particles (180-220 μm), serving as a porogen, were packed into a cylindrical infiltration chamber. The polymer and Azobisisobutyronitrile (AIBN) (20 wt.%) solution (0.5 g/mL PEA dissolved in dimethylformamide) was subsequently poured over the porogen bed. Following infiltration, the chamber was put in N<sub>2</sub> environment and heated up to 75 °C to allow thermal cross-linking for 30 h. Then the solvent was allowed to evaporate in a fume hood for one day at room temperature. The porogen was then leached by immersing the scaffold in deionized water for 24 h at room temperature.

## **3.8 Conjugation of Model Compounds onto Functionalized PEA Scaffolds**

### **3.8.1 General Procedure for the Conjugation of Rhodamine a Dye to a Carboxylic Acid-Functionalized PEA**

8-Phe-8-Asp(OH)-4 (0.1 g) and EDC·HCl (0.076 g, 0.396 mmol) were dissolved in anhydrous DMF (2 mL) and stirred for 15min. Then, rhodamine B amide **16** or **17** (0.099 mmol) and DMAP (0.02 g, 0.165 mmol) were added. The reaction was run for 4 h at 45 °C. The solution was then diluted with ethyl acetate and washed with saturated NH<sub>4</sub>Cl, dilute NaHCO<sub>3</sub>, and brine. The organic phase was kept and the solvent was removed *in vacuo*. The crude product was dissolved in DMF and was dialyzed against DMF until no further color was found in the dialysate. The absorbance of dialysate at 565 nm was monitored by UV-vis spectroscopy to determine the degree of conjugation.

### **3.8.2 Conjugation of BSA, Tetramethylrhodamine Conjugate to Cinnamate-functionalized PEA Scaffolds**

BSA, tetramethylrhodamine conjugate was conjugated to the surface of cinnamate 8-Phe-4-Asp(OH)-4 electrospun mats as a model compound. The electrospun mat (0.5

mm square) was immersed for 15 min in 4-morpholineethanesulfonic acid (MES) buffer (0.1 M, pH 5.0, 4 mL) containing *N*-(3-dimethylaminopropyl)-*N*'ethylcarbodiimide (EDC, 2 mM) and *N*-hydroxysulfosuccinimide sodium salt (sulfo-NHS, 5mM) to activate the pendant carboxylic acid groups of the cinnamate 8-Phe-4-Asp(OH)-4. After 15 min, the MES buffer was removed and replaced by phosphate-buffered saline (PBS) (10 mM, PH 8.5, 4 mL). Then the BSA, tetramethylrhodamine conjugate was added to reach a final concentration of 1.5 mg/mL and allowed to react for 2 h. The conjugated mats were washed three times with PBS (pH 7.4) and then deionized water for 5 min each. A sample that was subjected to the same conditions but without EDC coupling agent and sulfo-NHS served as a control.

### **3.9 Scaffold Characterization**

#### **3.9.1 Confocal Microscopy**

Model compound **9**, **10**, and BSA conjugated or adsorbed scaffold samples were mounted on slides in SHUR/Mount™ (TBS<sup>®</sup>, NC, USA) and imaged with a Zeiss LSM 510 DUO Vario confocal microscope (Zeiss, Canada), rhodamine excitation used a 1 mW 543 nm HeNe laser, signal was captured with an LP 560 nm Emission filter. The fluorescence of the samples was tested.

#### **3.9.2 Scanning Electron Microscopy (SEM)**

The electrospun fiber mats and solvent casting/particulate leaching scaffold were visualized using scanning electron microscopy (S-2600 or 3400S, Hitachi, Ltd., Tokyo, Japan). The scaffolds were mounted on carbon-taped aluminum stubs and sputtered with gold (Quorum Emitech K550X, Quorum Technologies Ltd, Kent, UK) or a gold-palladium mixture (HummerVI Sputter Coater, Anatech USA, Union City, CA) at a current of 12 mA for 90 or 240 sec, respectively. Secondary electron detection was achieved at voltages between 5 and 20 kV at various magnifications.

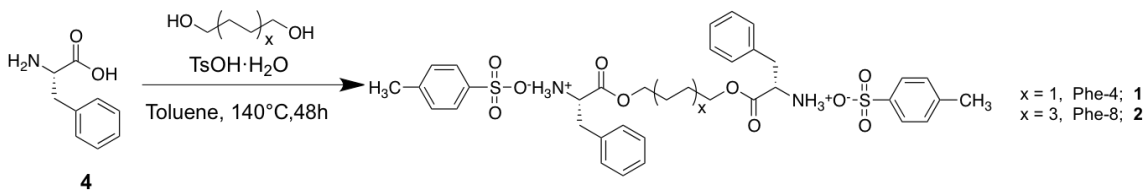
## Chapter 4

### 4 Results and Discussion

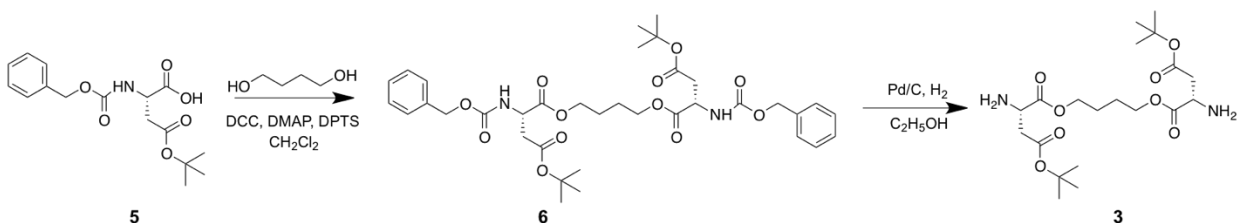
#### 4.1 Monomer Synthesis

In this work, L-phenylalanine (L-Phe) was used in the polymer backbone as its aromatic ring provides rigidity that affords favorable mechanical properties in the resulting polymer, and its di-*p*-toluenesulfonic acid salt monomer was easily purified.<sup>11</sup> L-Aspartic acid (L-Asp) monomer was also used to generate pendant carboxyl groups on the polymer backbone. The carboxyl groups facilitate further modifications including the conjugation of growth factors or small molecules to impart specific functions such as cross-linking. 1,4-Butanediol and 1,8-octanediol were selected as the diol components, again because of the favorable physical properties that we have previously observed.<sup>11,73</sup> Specifically, the use of 1,4-butanediol and 1,8-octanediol and sebecic acid was to impart elasticity and hydrophobicity. As shown in Scheme 4.1, the L-Phe-based monomers **1** and **2** were synthesized by the reaction of L-Phe **4** with the diol in toluene in the presence of *p*-toluenesulfonic acid with removal of the produced water using a Dean-Stark trap as previously reported.<sup>11,69,73</sup> For the preparation of the L-Asp monomer, the commercially available orthogonally protected aspartic acid derivative **5** was first reacted with 1,4-butanediol in the presence of *N,N'*-dicyclohexylcarbodiimide (DCC), 4-(dimethylamino)pyridine (DMAP), and 4-(dimethylamino)pyridinium *p*-toluenesulfonate (DPTS) to provide the diester **6** (Scheme 4.2). The crude product was purified by column chromatography. The carbobenzyloxy (CBZ) protecting group was then removed by Pd/C catalyzed hydrogenation in ethanol to give diester **3**. The *t*-butyl groups on **3** protect the pendant carboxylic group of L-aspartic acid, preventing its reaction during the polymerization. It can be removed from the polymer using 1:1 trifluoroacetic acid (TFA) : dichloromethane.<sup>11</sup>





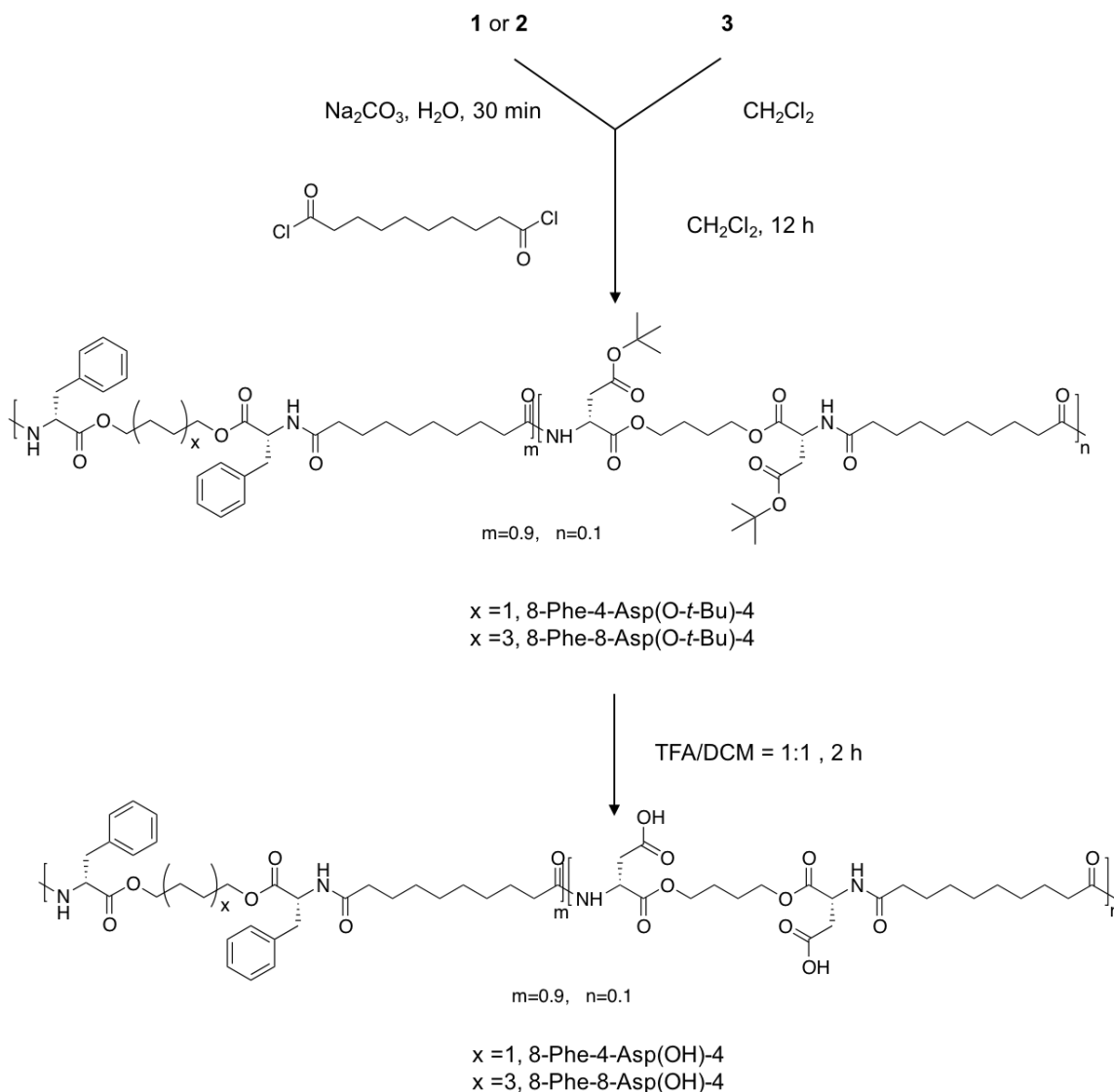
**Scheme 4.1: Synthesis of di-*p*-toluenesulfonic acid salt monomers **1** and **2**.**



**Scheme 4.2: Synthesis of bis-L-aspartic acid- $\beta$ -(*tert*-butyl ester) diester **3**.**

## 4.2 L-Aspartic Acid Functionalized Poly(ester amide)s Synthesis and Characterization

Interfacial polymerization was carried out because it is faster, has less restrictions on purity and stoichiometry, and yields polymers with higher molecular weight.<sup>66,73</sup> The interfacial polymerization synthetic route for functionalized PEAs was previously reported by our group.<sup>12,73</sup> Since the diacid chloride is relatively unstable, it is preferable to add the solution of it in organic solvent to the stirred aqueous diamine solution.<sup>91</sup> As shown in Scheme 4.3, monomer **3** and sebacoyl chloride were dissolved in  $\text{CH}_2\text{Cl}_2$ , then the organic solution was added to a solution of the di-*p*-toluenesulfonic acid salt monomer **1** or **2** in an aqueous  $\text{Na}_2\text{CO}_3$  solution. The reaction mixture was stirred for 12 h.



**Scheme 4.3: Synthesis of L-aspartic acid functionalized PEAs.**

$^1\text{H}$  NMR spectroscopy was used to confirm the polymer structure and the L-Asp content of this specific batch. Figures 4.1 and 4.2 show  $^1\text{H}$  NMR spectra of 8-Phe-4-Asp(OH)-4 and 8-Phe-8-Asp(OH)-4, respectively. Overall, the spectra are consistent with those previously reported for the polymers.<sup>12</sup> In Figure 4.1, two peaks clearly suggest the presence of the aspartic acid. Peaks at 4.50 ppm and 2.53 ppm illustrate the protons on  $\alpha$ - and  $\beta$ -carbons respectively (labeled as **2** and **5** on Figure 4.1 respectively). Based on the

relative integrations of the peaks at 4.50 ppm and 4.42 ppm corresponding to protons  $-C_{\alpha}H-CH_2-Ph$  and  $-C_{\alpha}H-CH_2-C(O)OH$  (labeled as **1** and **2** on Figure 4.1 respectively), the L-aspartic acid functionalized ratio is around 15% for 8-Phe-4-Asp(OH)-4 for this batch. In Figure 4.2, two peaks clearly suggest the presence of aspartic acid, 4.52 ppm and 2.57 ppm illustrates the protons on  $\alpha$ - and  $\beta$ -carbons respectively (labeled as **6** and **8** on Figure 4.2 respectively). Based on the relative integrations of the peaks at 4.52 ppm and 4.42 ppm corresponding to protons  $-C_{\alpha}H-CH_2-Ph$  and  $-C_{\alpha}H-CH_2-C(O)OH$  (labeled as **6** and **7** on Figure 4.2 respectively), the L-aspartic acid functionalized ratio is around 20% for 8-Phe-8-Asp(OH)-4 for this batch. A higher functionalized ratio than starting material was obtained. This may be because monomer **3** and sebacoyl chloride tend to be in organic phase, while monomer **1** and **2** tend to stay in aqueous phase, leading to rate of reaction between monomer **3** and sebacoyl chloride being faster than that between monomers **1** or **2** and sebacoyl chloride.

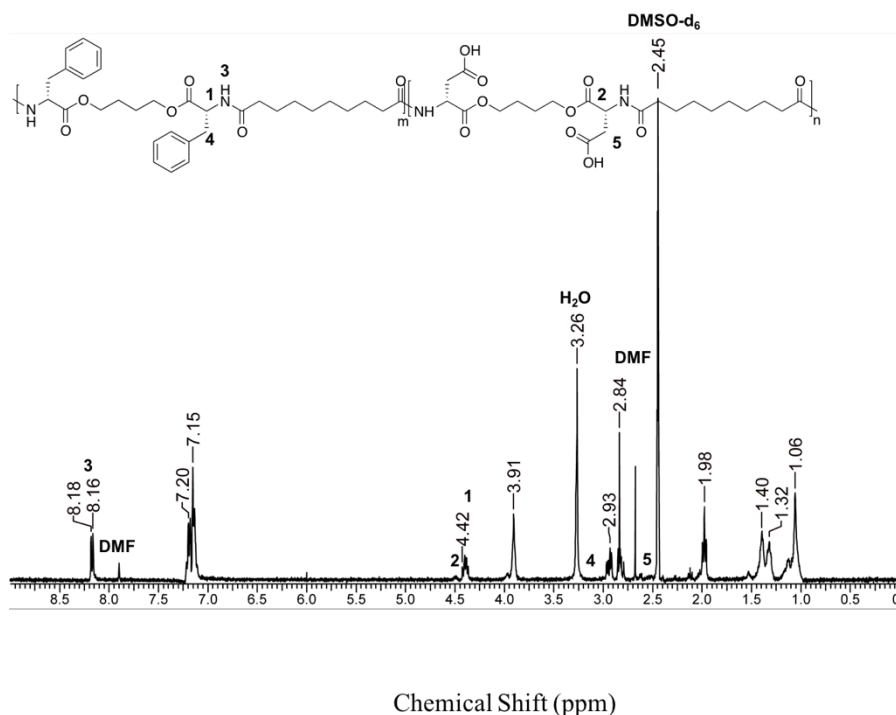


**Figure: 4.1**  $^1H$  NMR spectrum of 8-Phe-4-Asp(OH)-4 functional PEAs, (DMSO- $d_6$ , 600MHz).

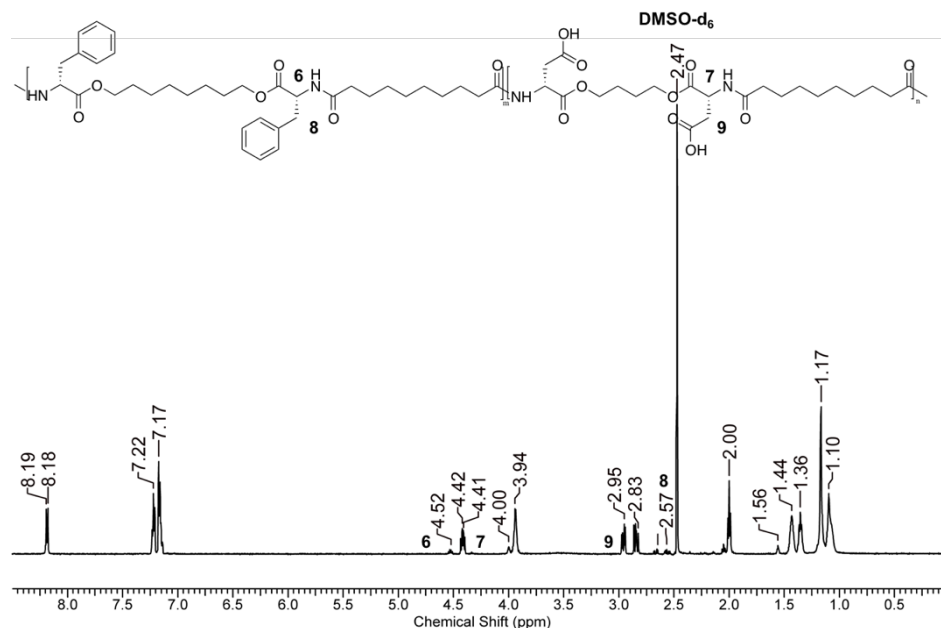


**Figure 4.2:**  $^1\text{H}$  NMR spectrum of 8-Phe-8-Asp(OH)-4 functional PEAs, (DMSO- $\text{d}_6$ , 600MHz).

Gel permeation chromatography (GPC) was used to determine the molecular weight and polydispersity index of the polymer. This is important because molecular weight affects the performance of polymer, and needs to be reasonably high to provide proper mechanical strength. Figure 4.3 presents the overlaid GPC (RI detection) traces of 8-Phe-4-Asp(O-*t*-Bu)-4 and 8-Phe-8-Asp(O-*t*-Bu)-4. Table 4.1 tabulates the molecular weight of PEAs. GPC analysis was performed for the *tert*-butyl group protected PEAs, because the carboxylic groups on the deprotected PEA will interact with the GPC column.<sup>12</sup>

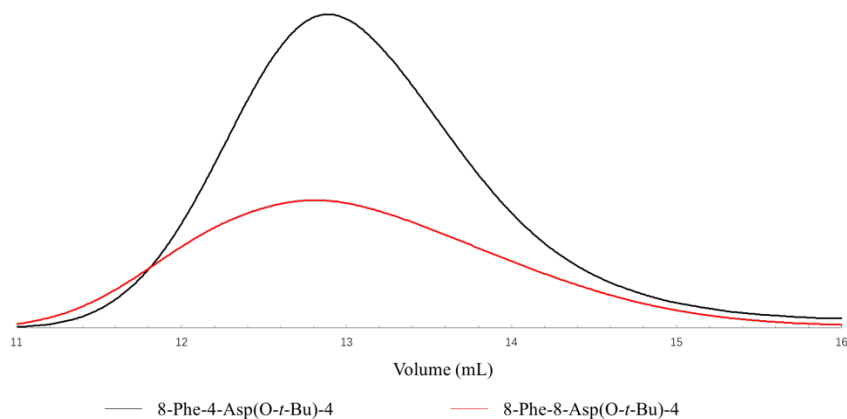


**Figure 4.3: Overlaid GPC (RI detection) traces of 8-Phe-4-Asp(O-*t*-Bu)-4 and 8-Phe-8-Asp(O-*t*-Bu)-4.**

**Table 4.1 Molecular weight of PEAs**

Polymer	$M_n$ (kg/mol)	$M_w$ (kg/mol)	$D$
8-Phe-4-Asp(O- <i>t</i> -Bu)-4	31.9	58.9	1.85
8-Phe-8-Asp(O- <i>t</i> -Bu)-4	42.4	74.1	1.62

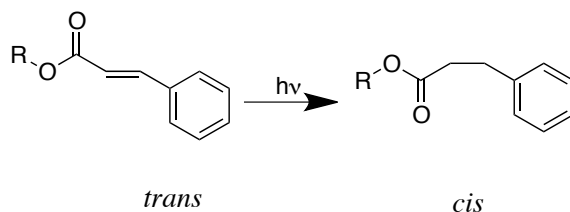
### 4.3 Design of Photo-cross-linkable Cinnamate-functionalized PEAs

As previously reported,<sup>12</sup> L-aspartic acid functionalized PEA electrospun mats showed poor morphological stability in aqueous media. To address this limitation, post-electrospinning photo-cross-linking was proposed. UV cross-linking was chosen because it requires a short reaction time, can be performed using a simple setup and it is easily controlled based on the intensity and duration of the irradiation.<sup>92</sup>

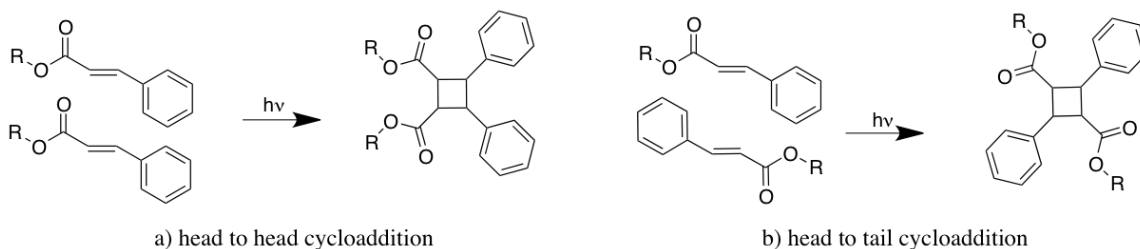
Cinnamic acid and its derivatives exist in plant cell walls as intermediate metabolites in the biosynthetic pathway and undergo photo-reactions.<sup>93</sup> Homopolymers and copolymers

synthesized from cinnamic acid and its derivatives have previously been reported to exhibit good biocompatibility,<sup>93-95</sup> and the low toxicity of cinnamic acid makes it favorable in biomedical applications.<sup>96</sup>

The photochemistry of cinnamates involves two reactions upon ultraviolet-B (UV-B) irradiation without chemical additives such as photo-initiator. The *trans-cis* isomerization is favored at an early stage of irradiation (Scheme 4.4) and then the photodimerization from head-to-head and head-to-tail [ $2\pi + 2\pi$ ] cycloaddition leads to the formation of a cyclobutane ring (Scheme 4.5). This chemistry has desirable characteristics for biomedical applications, as it prevents the addition of unnecessary chemicals that may cause cytotoxicity. Furthermore, the lack of organic solvent makes it suitable for a solid-state reaction, thus preventing potential morphological damage by solvents.



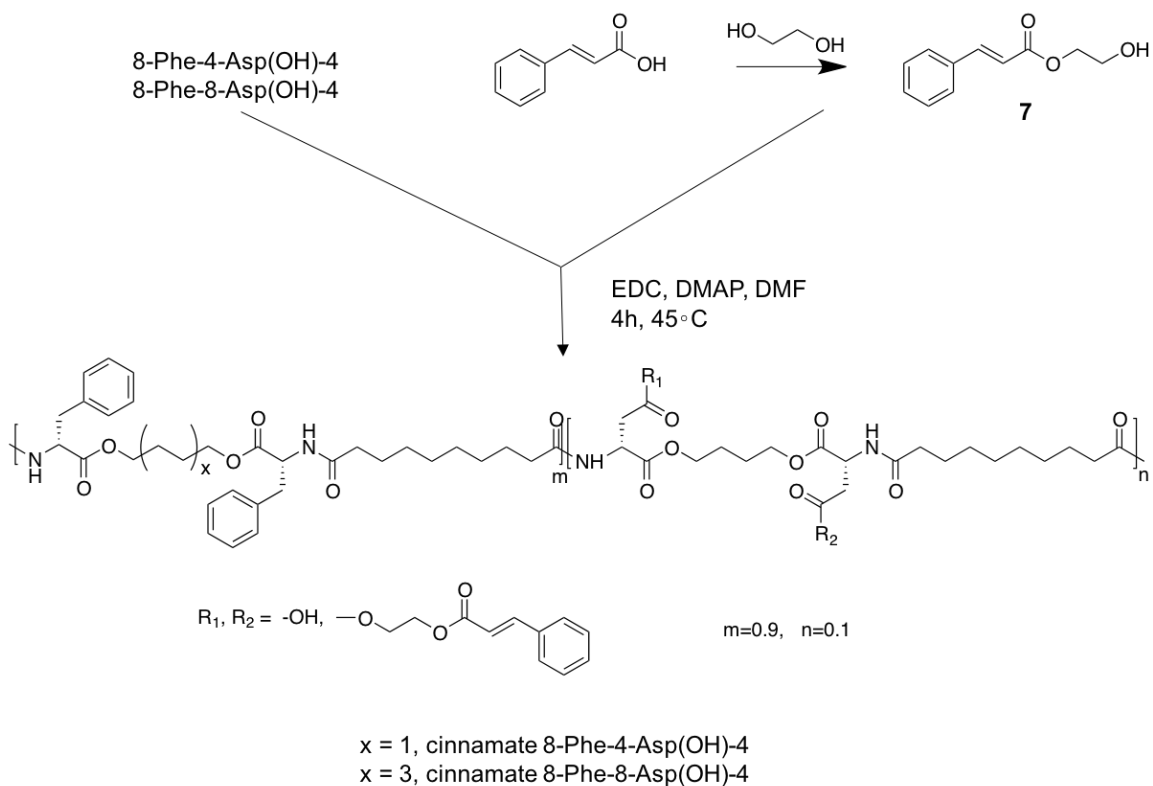
**Scheme 4.4: Trans-cis photoisomerization of the cinnamoyl moiety**



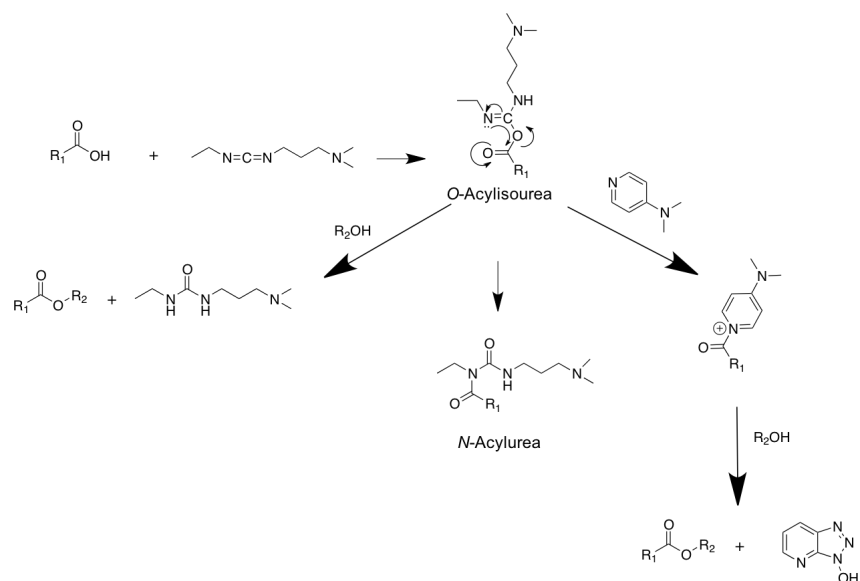
**Scheme 4.5: (a) Head-to-head and (b) Head-to-tail photodimerization of the cinnamoyl moiety.**

### 4.3.1 Cinnamate-functionalized PEA Synthesis and Characterization

With pendant carboxylic groups on L-aspartic acid functionalized PEAs, it is feasible to incorporate photo-cross-linkable functional groups. To incorporate the cinnamoyl moiety onto the PEAs, cinnamic acid and ethylene glycol were reacted in the presence of catalytic of *p*-toluenesulfonic acid to produce hydroxyethyl cinnamate as shown in Scheme 4.6. Ethylene glycol served as the reactant as well as the solvent. Excess ethylene glycol was used to ensure only one hydroxyl group was reacted with cinnamic acid, leaving the other for the reaction with free carboxyl groups on PEAs. The reaction between the pendant carboxylic acid groups on the PEA backbone and hydroxyethyl cinnamate was then conducted using a dehydrative coupling by EDC/DMAP (Scheme 4.6). The mechanism of EDC/DMAP coupling is shown in Scheme 4.7. EDC initially reacts with carboxylic acid, forming *O*-acylisourea. The intermediate then reacts with an alcohol to form an ester. However, it can also go through a rearrangement to form an *N*-acylurea which is a side reaction need to be avoided because it leads to consumption of the carboxylate with no desired ester formation. The addition of DMAP in catalytic amount can prevent the rearrangement by its quick reaction with *O*-acylisourea, forming an acyl pyridinium species incapable of rearrangement.<sup>97</sup> In this work, 1.2 equivalents of EDC per carboxylic acid was used to ensure complete reaction of carboxylic acids on PEAs. The reaction was performed at 45 °C to accelerate the reaction rate.



**Scheme 4.6: Synthesis of cinnamate-functionalized PEAs.**



**Scheme 4.7: Mechanism of EDC/DMAP-mediated esterification of a carboxylic acid.**



Figures 4.4 and 4.5 show  $^1\text{H}$  NMR spectra of cinnamate-functionalized 8-Phe-4-Asp(OH)-4 and 8-Phe-8-Asp(OH)-4 PEAs, respectively. Small peaks at 7.7 ppm and 7.4 ppm correspond to the phenyl group on cinnamoyl moiety, labeled as **10** and **11** in Figure 4.4 and as **13** and **14** in Figure 4.5.

According to the integration of peaks **10** and **11** versus **12** in Figure 4.4 and **13** and **14** versus **15** in Figure 4.5, approximately half of the carboxyl groups were reacted with hydroxyethyl cinnamate. As only 5% molar ratio hydroxyethyl cinnamate was incorporated onto PEA backbone, peaks representing other protons on cinnamoyl moiety might not be obvious.

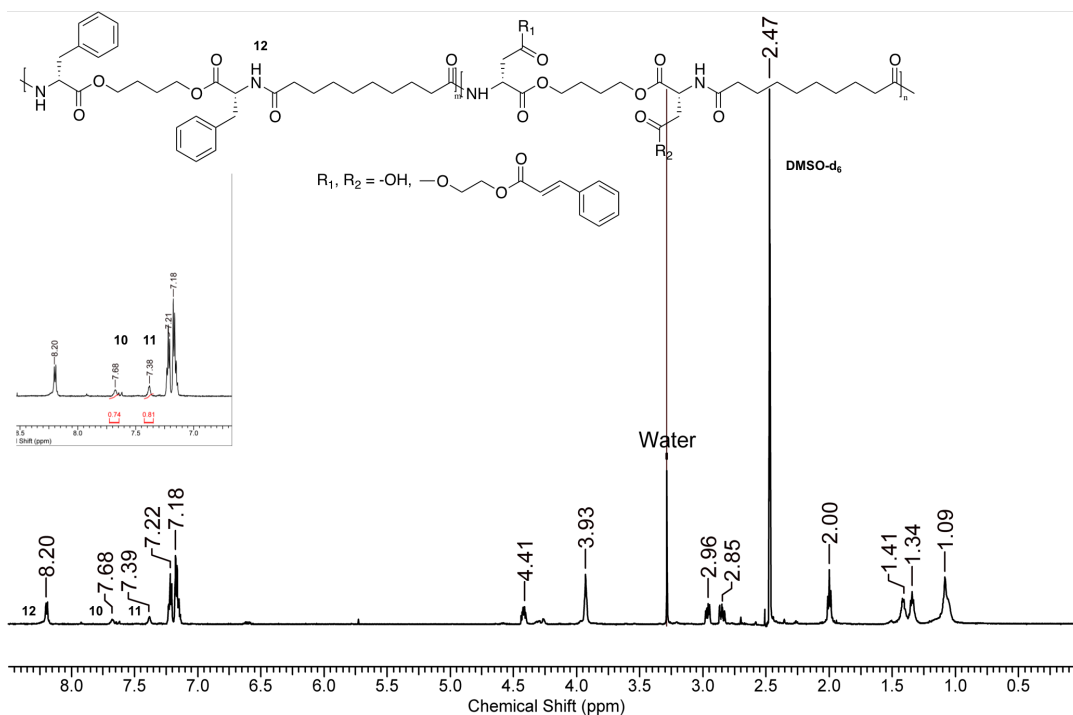


**Figure 4.4:**  $^1\text{H}$  NMR spectrum of cinnamate-functionalized 8-Phe-4-Asp(OH)-4 ( $\text{DMSO-d}_6$ , 600MHz).

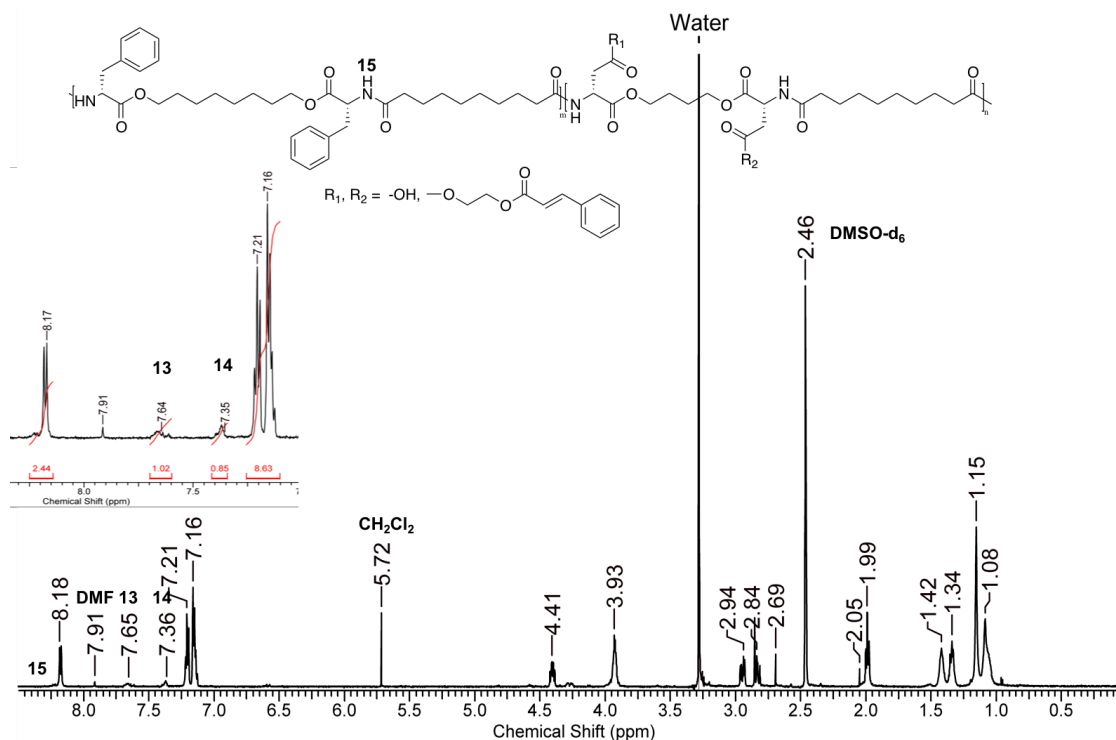


**Figure 4.5:  $^1H$  NMR spectrum of cinnamate-functionalized 8-Phe-8-Asp(OH)-4, (DMSO- $d_6$ , 600MHz)**

The structure of the cinnamate 8-Phe-8-Asp(OH)-4 was also confirmed by FTIR spectroscopy (shown in Figure 4.6). The sharp peak at  $1735\text{ cm}^{-1}$  corresponds to the  $C=O$  ester stretch. Strong absorption around  $1640\text{ cm}^{-1}$  can be assigned to the  $C=O$  stretching on an amide bond. An aromatic  $C=C$  stretch appears around  $1534\text{ cm}^{-1}$ . The peak around  $980\text{ cm}^{-1}$  represents the trans-vinylene C-H deformation on cinnamoyl moiety.<sup>98</sup>

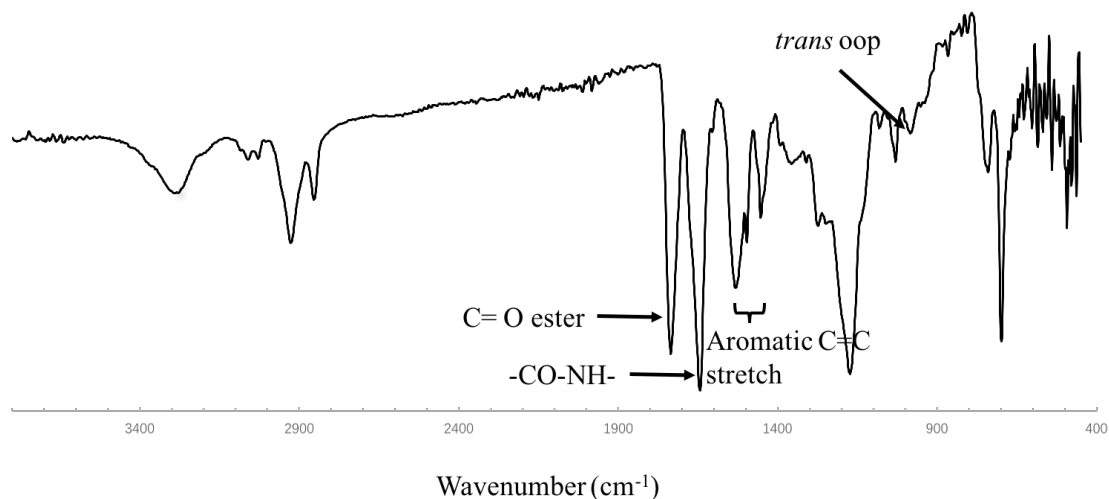


**Figure 4.6: FTIR spectrum of cinnamate-functionalized 8-Phe-8-Asp(OH)-4.**

GPC was used to determine the molecular weights of cinnamate-functionalized 8-Phe-4-Asp(OH)-4 and 8-Phe-8-Asp(OH)-4. Figure 4.7 shows the overlaid GPC (RI detection) traces of cinnamate 8-Phe-4-Asp(OH)-4 PEAs and cinnamate 8-Phe-8-Asp(OH)-4 PEAs. Table 4.2 presented the molecular weight of cinnamate PEAs. Compared to starting polymers, cinnamate-functionalized PEAs have both lower  $M_n$  and  $M_w$ . This can likely be attributed to residual carboxylic acids present on the polymer that result in undesired interactions with the column packing materials. However, full functionalization of the carboxylic acids was not desired as this would render the polymers unable to undergo further reactions as targeted for the scaffolds.

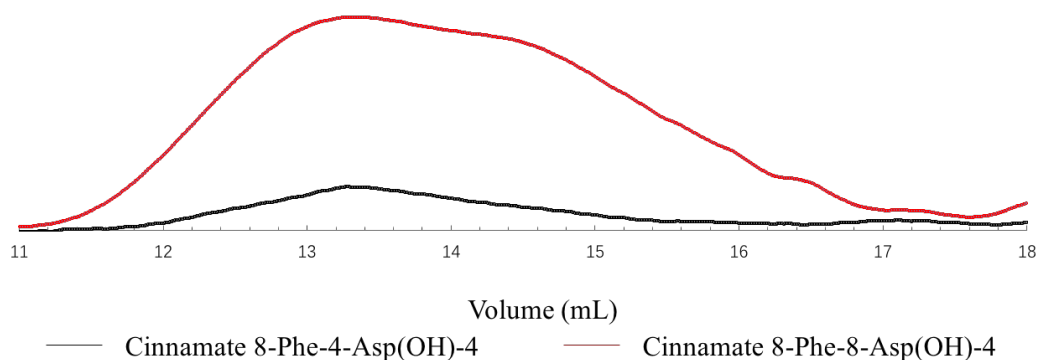


**Figure 4.7: Overlaid GPC (RI detection) traces of cinnamate 8-Phe-4-Asp(OH)-4 and cinnamate 8-Phe-8-Asp(OH)-4**

**Table 4.2 Molecular weight of cinnamate PEAs**

Polymer	$M_n$ (kg/mol)	$M_w$ (kg/mol)	$\bar{D}$
Cinnamate-functionalized 8-Phe-4-Asp(OH)-4	14.2	27.7	1.95
Cinnamate-functionalized 8-Phe-8-Asp(OH)-4	23.9	43.0	1.79

### 4.3.2 Electrospinning of PEAs

Cinnamate-functionalized PEAs were fabricated into 3-D scaffolds by electrospinning. Electrospinning was chosen because of its easy setup and the flexibility of tuning scaffold morphology by changing parameters. The resulting 3-D electrospun structure can be determined by SEM imaging. In this work, before SEM imaging, electrospun fibers were collected on glass slide for 30 seconds, then the morphology was checked by optical

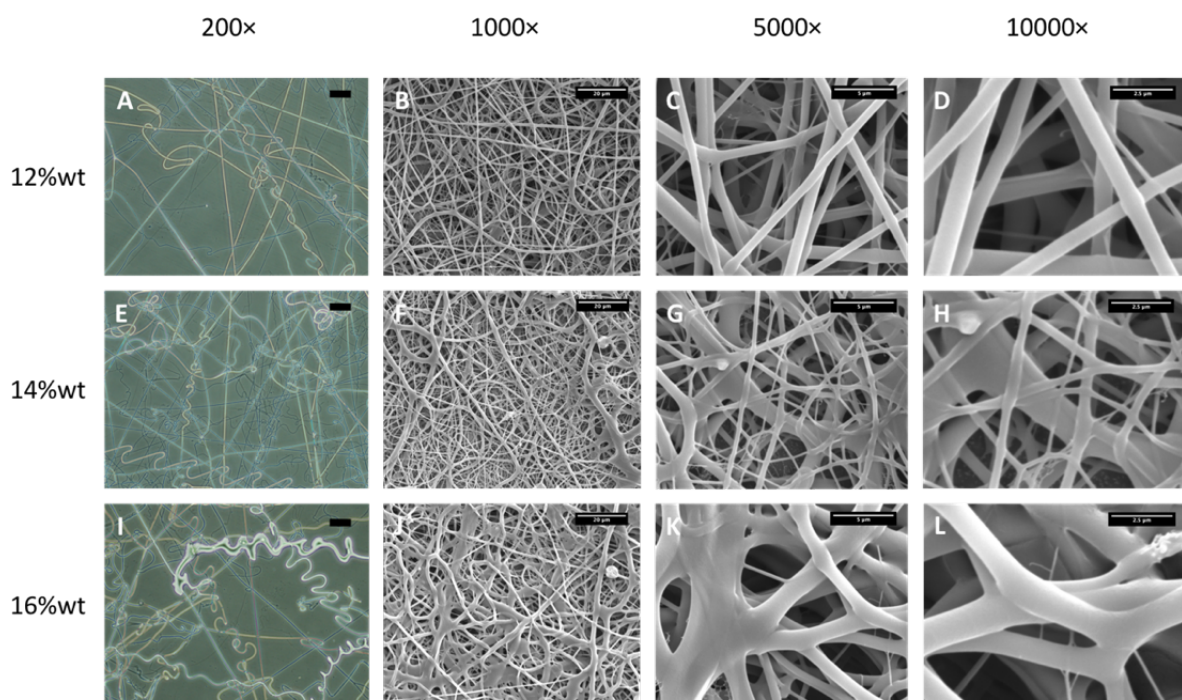
microscope, which was a facile way to observe fiber morphology. As shown in Figure 4.8 (A), (E), (I), phase contrast micrographs of fiber morphology correspond to SEM images of fibers. However, even though optical microscopy suggested the fiber morphology, it only can serve as supplementary information for SEM images for the following reasons: 1) the magnification of the optical microscope is much lower than that of SEM, so the morphology of single fiber cannot be observed; 2) as the electrospun fibers are designed to form multilayers on the collector, the optical microscope was not able to show the 3-D structure of the scaffold. However, checking fiber morphology by optical microscope before SEM imaging is a less time-consuming way to optimize electrospinning parameters.

L-phenylalanine and L-aspartic acid derived PEAs were previously electrospun in our group.<sup>12</sup> The same electrospinning parameters was used as starting point for electrospinning in this work. However, some problems arose: 1) the PEA molecular weight was not exactly the same as what had been previously synthesized; 2) electrospun fibers exhibited a tendency to undergo fusion in the case of 8-Phe-8-Asp(OH)-4 and cinnamate-functionalized 8-Phe-8-Asp(OH)-4. Therefore, variations in polymer solution concentration and solvent were studied in order to obtain good electrospun fibers.

### **Electrospinning of Cinnamate-functionalized 8-Phe-4-Asp(OH)-4**

Polymer molecular weight has been proven to be an essential parameter in electrospinning process.<sup>40,41</sup> At the same polymer concentration, higher molecular weight results in higher viscosity. As molecular weight varies from batch to batch, the polymer concentration was slightly different each time, ranging from 8 wt% to 12 wt% in solvents of 9:1 weight ratio  $\text{CHCl}_3$ :DMF to obtain good electrospun fibers. Cinnamate-functionalized 8-Phe-4-Asp(OH)-4 was electrospun with the same conditions as its 8-Phe-4-Asp(OH)-4 counterpart and produced good electrospun fibers. Figure 4.8

shows a panel of images demonstrating the effect of polymer concentration on fiber morphology. It can be seen that at the concentration of 12 wt%, the fibers are oriented randomly in a criss-crossing grid-like pattern. This structure is desirable because it mimics the physiological structure of extracellular matrix. However, when the polymer concentration increased from 12 wt% to 16 wt%, electrospun fibers became less uniform, and fibers with larger diameter began to form. Concentrations under 12 wt% resulted in bead formation. Based on SEM imaging, the polymer concentration was set as 12 wt% with polymer  $M_n$  around 18 kg/mol and  $M_w$  around 38 kg/mol.



Scale bars represent 100  $\mu\text{m}$ , 20  $\mu\text{m}$ , 5  $\mu\text{m}$ , 2.5  $\mu\text{m}$ , respectively

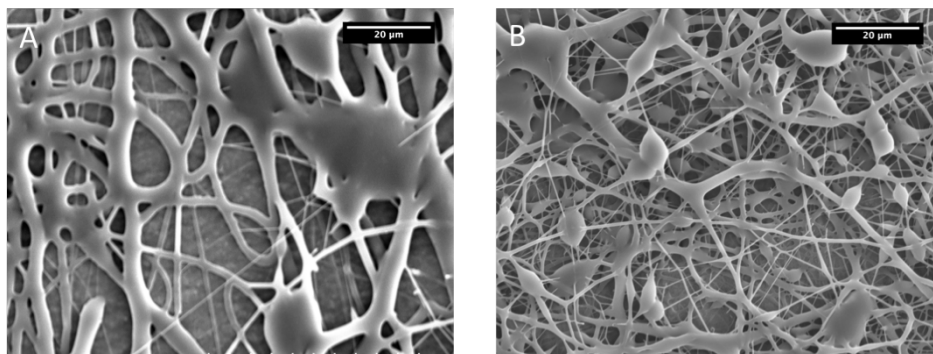
**Figure 4.8:** Phase contrast micrographs and SEM images of electrospun 8-Phe-4-Asp(OH)-4 mats at various concentrations. (A), (E) and (I) show electrospun fibers on glass slides.

#### **Electrospinning of Cinnamate-functionalized 8-Phe-8-Asp(OH)-4**

As described above, electrospun fibers were imaged by optical microscopy first, followed by SEM. In the case of 8-Phe-8-Asp(OH)-4 and cinnamate-functionalized

8-Phe-8-Asp(OH)-4, good fibers were observed by optical microscopy. However, when the electrospinning time was extended to hours and the fiber morphology was imaged by SEM, fiber fusion was observed. One possible reason for fiber fusion may be the effect of residual solvent. During the electrospinning process, the solvent was expected to evaporate while the fibers were deposited to the collector. 9:1 of CHCl<sub>3</sub>:DMF was used as the solvent in these initial attempts in order to effectively dissolve 8-Phe-8-Asp(OH)-4. However, as DMF is not as volatile as CHCl<sub>3</sub>, it was possible that fibers were not completely dry when they reached the collector so that the residual DMF partially dissolved the fibers. Based on this hypothesis, polymers were dissolved in 100% CHCl<sub>3</sub> and electrospun. Figure 4.9 shows the SEM images of fiber morphology electrospun with 100% CHCl<sub>3</sub>. As seen in Figure 4.9, the fibers were less fused but became non-uniform and beads started to form. The bead formation might be due to a decrease in dielectric constant accompanied with the elimination of DMF.<sup>99</sup> Previous research has demonstrated that when dielectric constant became lower than a certain point, beads started to appear.<sup>42</sup>

In Figure 4.9, images (A) and (B) were obtained following the electrospinning of the same batch of polymer with the same electrospinning parameters but separately. The observed morphologies were not consistent. This suggests that the residual solvent on the electrospun mats was not the only reason for morphological instability, which was also implied by the fact that solvent with weight ratio 9:1 of CHCl<sub>3</sub> and DMF produced good fibers for 8-Phe-4-Asp(OH)-4.



Scale bars represent 20  $\mu\text{m}$

**Figure 4.9: Electrospinning of 8-Phe-8-Asp(OH)-4 with 100%  $\text{CHCl}_3$**

Previous research has shown that a low glass transition temperature ( $T_g$ ) could be an issue in electrospinning. Polymers with a  $T_g$  higher than room temperature are relatively easy to electrospin, while rubbery polymers are challenging,<sup>100</sup> because of their flexibility at the temperature above  $T_g$  so that the 3-D structure tends to collapse. 8-Phe-8-Asp(OH)-4 has a  $T_g$  of 26  $^\circ\text{C}$ , which is close to room temperature. The morphologies of the fibers might have not changed right after electrospinning, but the structure may not be stable for long periods of time at room temperature. This explains why non-fused fibers were observed at the initial electrospinning stage. The fact that the polymer becomes more flexible at the temperature higher than  $T_g$  also explains the different fiber morphology obtained with the same electrospinning parameters used in the study (Figure 4.9).

The fiber morphological stability was further tested by immersing electrospun mats in PBS. Figure 4.10 shows SEM images of electrospun mats before and after immersion. It is clear that immersing the fiber mats in PBS further compromised fiber morphology (Figure 4.10B, D). As previously reported,<sup>83</sup> the electrospun fiber structure of non-functionalized PEAs (i.e. 8-Phe-4) have better morphological stability in aqueous media. A possible explanation is that the incorporation of 10% molar ratio aspartic acid monomer introduces hydrophilic carboxylic groups and increases the hydrophilicity of PEAs, so that the morphology of functionalized PEAs is more vulnerable to water. Figure



4.10B and D, and Figure 4.10D show SEM images of 8-Phe-4-Asp(OH)-4 fibers. These fibers exhibit more serious fusions problems than 8-Phe-8-Asp(OH)-4 (Figure 4.10B). This can be explained by comparing the chemical structure of 8-Phe-8-Asp(OH)-4 and 8-Phe-4-Asp(OH)-4. The former PEA has longer carbon chain that was incorporated by 1,8-octanediol, giving a higher hydrophobicity than that of its 8-Phe-4-Asp(OH)-4 counterparts.

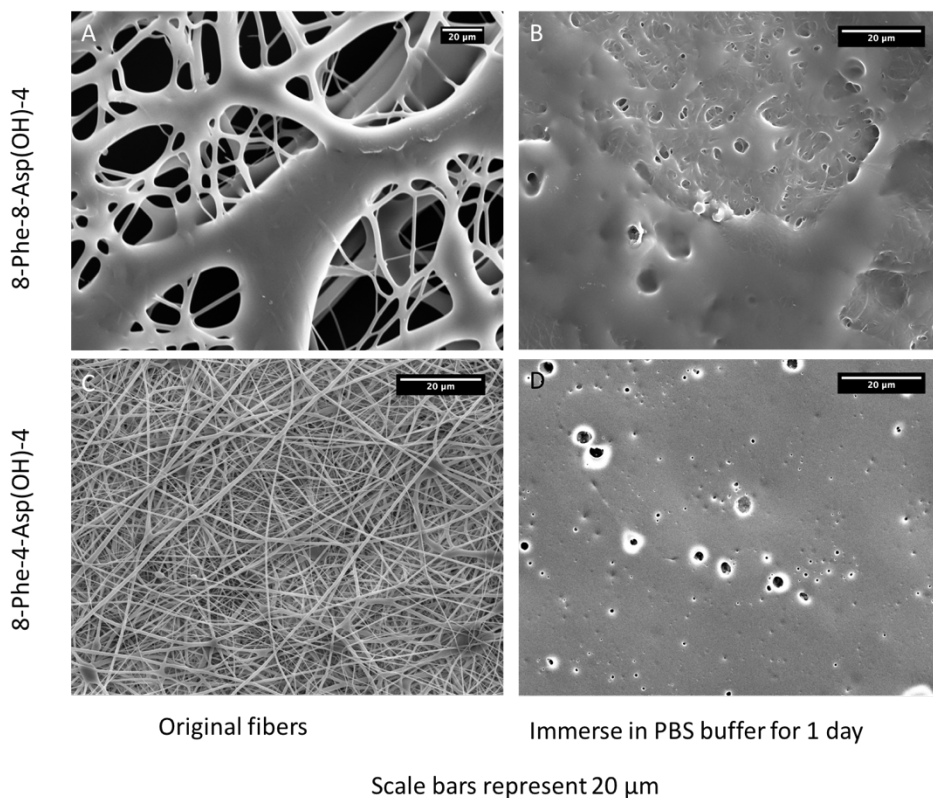
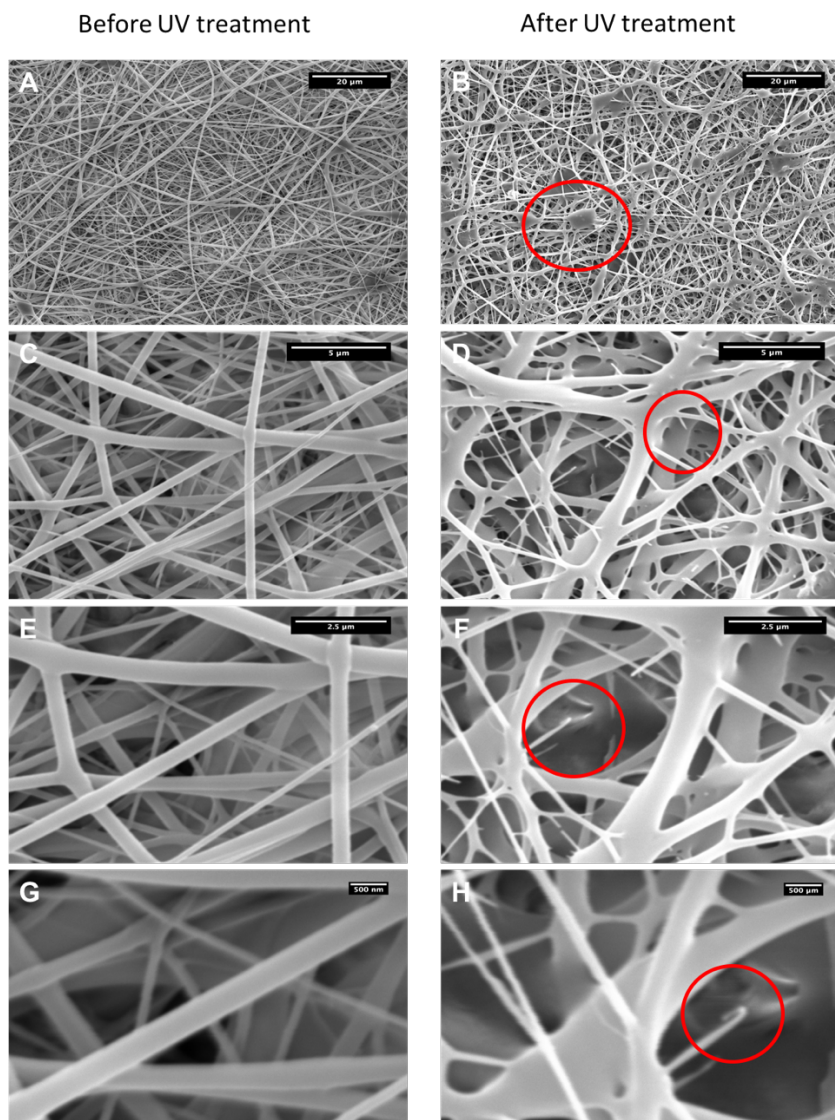


**Figure 4.10: Electrospun mats: (A) original 8-Phe-8-Asp(OH)-4 fibers, (B) 8-Phe-8-Asp(OH)-4 fibers after immersion in PBS for 1 day, (C) original 8-Phe-4-Asp(OH)-4 fibers, (B) 8-Phe-4-Asp(OH)-4 fibers after immersion in PBS for 1 day.**

#### **UV cross-linking of Cinnamate-functionalized PEA Scaffolds**

In order to prevent the fusion issue described in former section, cinnamate-functionalized PEAs were subjected to UV treatment to cross-link the alkene groups on the cinnamoyl

moieties in order to produce cross-linked electrospun mats. The UV treatment was performed by placing the samples facing the medium pressure mercury lamp at a distance around 20 cm. The samples were irradiated for 0.5 h, 1 h, and 2 h. Irradiation time under 2 h showed no cross-linking as the samples were completely soluble in CH<sub>2</sub>Cl<sub>2</sub>. The effect of cross-linking was tested by immersing cross-linked mats in PBS, followed by SEM imaging of the morphological change. Figure 4.11 shows the SEM images of cinnamate 8-Phe-4-Asp(OH)-4 electrospun mats before and after UV treatment. Compared to the electrospun mats before UV treatment (Figure 4.11 A, C, E, G), UV-cured electrospun mats (Figure 4.11 B, D, E, H) had chunks of fibers and broken fibers. As shown in Figure 4.11 B, D, E and H. Red circles highlight the damaged fibers. The cinnamoyl moiety absorbs UV light with a wavelength of ~280 nm. It is possible that part of the energy from the UV irradiation generated heat in the samples. Since the T<sub>g</sub>s of both PEAs are relatively low, sample heating could cause morphological change. Furthermore, extensive irradiation with UV light may result in chemical damage such as the cleavage of ester and amide bonds.



Scale bars represent 25  $\mu\text{m}$ , 5  $\mu\text{m}$ , 2.5 $\mu\text{m}$ , 500 nm, respectively

**Figure 4.11: Electrospun cinnamate 8-Phe-4-Asp(OH)-4 functional PEAs, (A, C, E, G) before and (B, D, F, H) after UV treatment. Red circles highlight the damaged fibers after UV treatment.**

Despite the visual damage to the fibers, UV cured electrospun fibrous mats were immersed in PBS to test the effect of the cross-linking. SEM images of cross-linked mats before and after immersion in PBS are shown in Figure 4.12. After immersion in PBS for 1 day (Figure 4.12D), fibers did not fuse as much as the uncross-linked mats. However, photo-cross-linking only helped maintain the fiber morphology to a very limited extent.

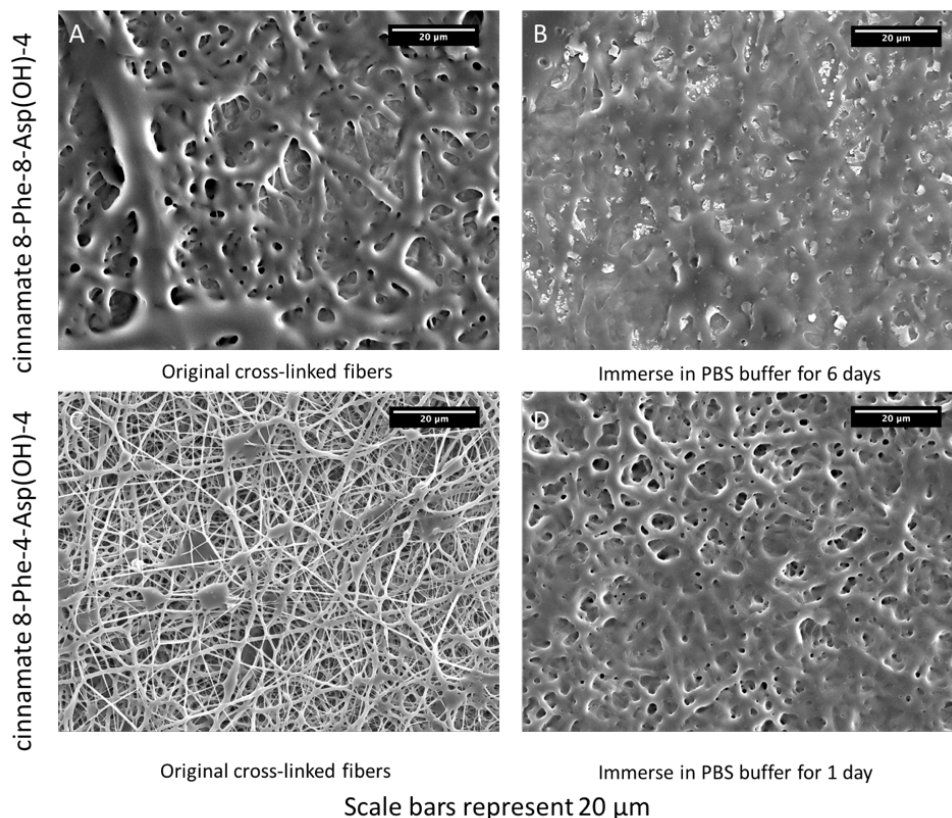


**Figure 4.12: Electrospun mats: (A) original cinnamate-functionalized 8-Phe-8-Asp(OH)-4 cross-linked fibers, (B) cinnamate-functionalized 8-Phe-8-Asp(OH)-4 cross-linked fiber after immersion in PBS for 6 days, (C) original cinnamate-functionalized 8-Phe-4-Asp(OH)-4 cross-linked fibers, (D) cinnamate-functionalized 8-Phe-4-Asp(OH)-4 cross-linked fiber after immersion in PBS for 1 day.**

Analyzing the UV-cross-linking process, two factors influence the cross-linking degree: the intensity of the UV irradiation and the duration of the exposure.<sup>92</sup> The intensity of the UV irradiation decreases with the increase in film thickness. In this case, a gradient of cross-linking was expected. A study showed that films with a thickness of 15 μm presented a cross-linking gradient with both sides of the film exposed.<sup>92</sup> For electrospun tissue engineering scaffolds, the thickness of the mats might be as high as 500 μm. It is

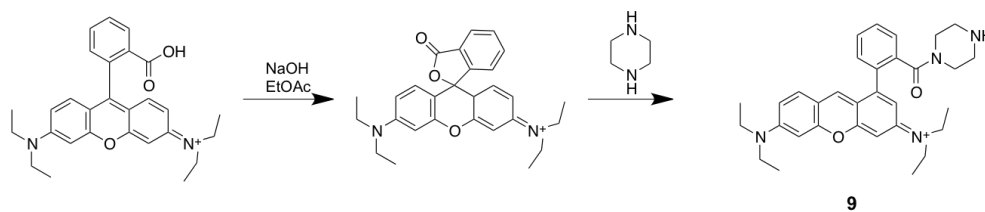
very likely that a cross-linking gradient will result within the structure. In this work, UV irradiation exposure time was also explored. 0.5 h, 1 h, and 2 h were applied. Exposure times under 2 h showed no cross-linking as the fibers were completely soluble in dichloromethane.

When comparing cross-linked electrospun mats of cinnamate-functionalized 8-Phe-8-Asp(OH)-4 and cinnamate-functionalized 8-Phe-4-Asp(OH)-4, it is obvious that cinnamate-functionalized 8-Phe-8-Asp(OH)-4 mats showed better morphological stability after immersion in PBS, as seen in Figures 4.12 B and D. Although the original fibers were not as good as their cinnamate-functionalized 8-Phe-4-Asp(OH)-4 counterparts, the morphological difference before and after PBS immersion is minor. This phenomenon can be explained by considering the mechanism of cinnamoyl photochemistry, the double bonds need to be close to each other in order to be cross-linked. Since the  $T_g$  of 8-Phe-8-Asp(OH)-4 is lower than that of 8-Phe-4-Asp(OH)-4, so that the polymer chain of 8-Phe-8-Asp(OH)-4 has higher mobility, leading to a higher possibility reaction between two vinyl groups.

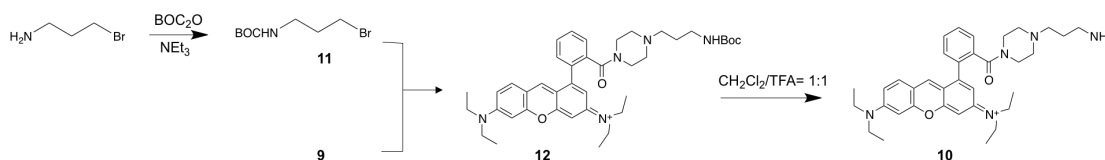
#### **4.4 Model Compound conjugation**

##### **4.4.1 Rhodamine Dye Derivative Synthesis**

Due to their excellent photostability and photophysical properties, rhodamine dyes are widely used as fluorescent probes. Rhodamine piperazine amine (**16**) was synthesized as previously reported (Scheme 4.8).<sup>101</sup> Rhodamine with a reactive primary amine was then synthesized from rhodamine piperazine amide and 3-bromopropan-1-amine. The amino group was kept protected by a BOC group during the process and was deprotected in the last step by treatment with TFA/CH<sub>2</sub>Cl<sub>2</sub>. (Scheme 4.9)



**Scheme 4.8: Syntheses of rhodamine B piperazine amine**



**Scheme 4.9: Syntheses of rhodamine B primary amine**

#### 4.4.2 Rhodamine Dye as Model Compound

Rhodamine B derivatives rhodamine piperazine amine and rhodamine primary amine, were used as model compounds for small bioactive molecules and also to test the reactivity of free carboxyl groups on PEAs.

Firstly, rhodamine B piperazine amine **9** and rhodamine primary amine **10** were reacted with the free carboxylic groups on the PEAs by a dehydrative coupling using EDC/DMAP, to test their suitability for serving as model compound. The crude product was purified by dialysis to remove the unreacted dyes. The dialysate was then measured by UV-visible spectroscopy to measure the concentration of uncoupled rhodamine and thus by deduction the amount of rhodamine coupled to the polymer. Standard curves correlating known concentrations of rhodamine piperazine amine **9** and rhodamine primary amine **10** versus the absorbance at 565 nm were generated in order to determine the concentrations of rhodamine in solution (Figure 4.13). The extinction coefficients ( $\epsilon$ ) for **9** and **10** were found to be  $1.22 \times 10^5 \text{ L} \cdot \text{mol}^{-1} \cdot \text{cm}^{-1}$  and  $4.24 \times 10^4 \text{ L} \cdot \text{mol}^{-1} \cdot \text{cm}^{-1}$  respectively.

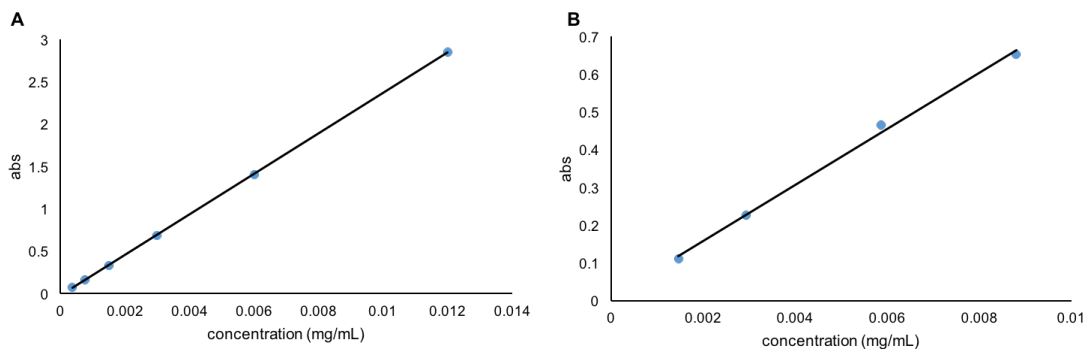
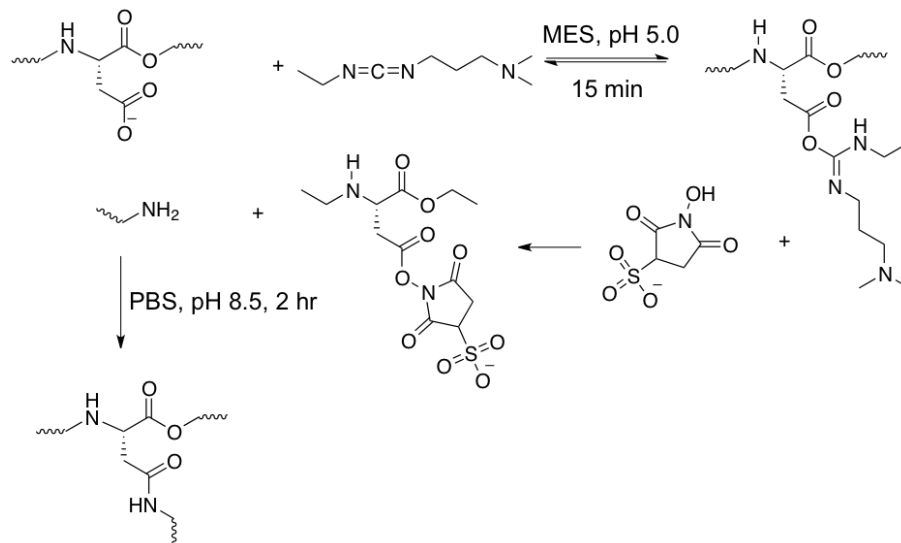


**Figure 4.13: Calibration curves for (A) rhodamine piperazine amine, 9, at 565 nm; (B) rhodamine primary amine, 10, at 564.5 nm.**

For the rhodamine B piperazine amine, conjugation results showed that the conjugation rate was 33 times less than theoretical value, suggesting the reaction with free carboxylic groups did not take place appreciably. The reactivity of secondary amine might be too low. In the case of the rhodamine B primary amine, the amount of conjugated rhodamine was the same as the theoretical value, suggesting that the primary amine groups reacted efficiently with the free carboxylic groups on PEAs. Therefore, compound **10** was chosen as model compound for conjugation on electrospun mats.

The rhodamine primary amine **10** was conjugated to cinnamate-functionalized 8-Phe-8-Asp(OH)-4 electrospun mats via a EDC/sulfo-NHS activation procedure. To demonstrate that coupling rather than simple adsorption of the dye had occurred, control experiments were performed involving immersion of an electrospun mat with the dye under the same conditions but in the absence of the coupling agents EDC/sulfo-NHS. EDC/sulfo-NHS was chosen to activate the free carboxylic groups instead of EDC alone is because the addition of sulfo-NHS has been demonstrated to increase the conjugation yield.<sup>102</sup> EDC catalyzes the formation of amide bonds by forming an intermediate with carboxylic groups. However, when the reaction take place in an aqueous environment, the intermediate is subject to hydrolysis, limiting the overall yields. The advantage of

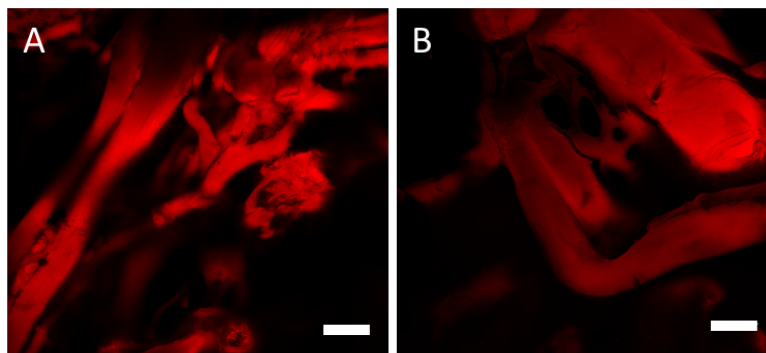
adding sulfo-HNS is that the intermediate ester formed by sulfo-NHS and carboxylic groups has increased stability.<sup>102</sup>



**Scheme 4.10: Conjugation of model compound to 8-Phe-8-Asp(OH)-4 using EDC/sulfo-NHS peptide coupling.**

Confocal microscopy was used to demonstrate the fluorescence of the scaffold samples. Figure 4.14 shows the confocal images of model compound conjugated and adsorbed samples. No obvious differences were observed between the conjugated mats (Figure 4.14A) and the adsorbed control (Figure 4.14B), suggesting the intermolecular forces between compound **10** and electrospun mats were too strong to wash off the adsorbed dyes.





Rhodamine dye conjugated

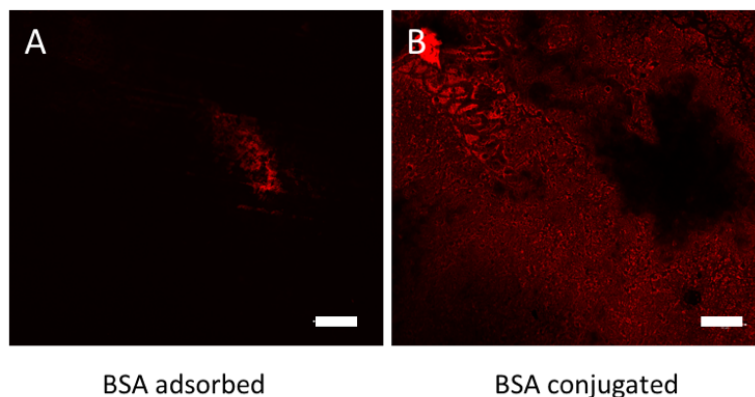
Rhodamine day adsorbed

Scale bars represent 50  $\mu\text{m}$

**Figure 4.14: Confocal microscopy images of (A) Rhodamine primary amide conjugated PEA electrospun mats, (B) rhodamine adsorbed PEA electrospun mats**

#### **4.4.3 BSA Tetramethylrhodamine conjugate as Model Compound**

It was proposed that less adsorption might be observed with a larger molecule, that would be less capable of penetrating the fibers. Thus, bovine serum albumin tetramethylrhodamine conjugate was used as a model compound for large molecules such as growth factors. The conjugation process was conducted by EDC/sulfo-NHS activation of an electrospun mat of cinnamate-functionalized 8-Phe-8-Asp(OH)-4 in the presence of 1.5 mg/mL protein (Scheme 4.9). Again, a control experiment involving the same conditions but the absence of coupling agent was conducted to account for possible adsorption. The covalently conjugated surface exhibited higher fluorescence than the adsorbed surface, suggesting the existence and the use of free carboxylic groups in the PEAs.



Scale bars represent 50  $\mu\text{m}$

**Figure 4.15: Fluorescence images of 8-Phe-8-Asp(OH)-4 electrospun mats. (A) BSA tetramethylrhodamine conjugate conjugated to the surface of 8-Phe-8-Asp(OH)-4. (B) and BSA tetramethylrhodamine conjugate adsorbed to surface of 8-Phe-8-Asp(OH)-4**

#### **4.5 Design of a Thermally Cross-linkable Methacrylate-functionalized PEA**

As morphologically stable fibers were not obtained by electrospinning, the fibers has serious fusion problem when immersed in PBS, SCPL was considered as an alternative method to fabricate 3-D scaffolds from PEAs. Figure 4.17 shows the solvent casting apparatus. The upper chamber was connected to air and the lower chamber was connected to vacuum. The polymer solution was pushed into the mold under a pressure difference to form a polymer solution-porogen construct.

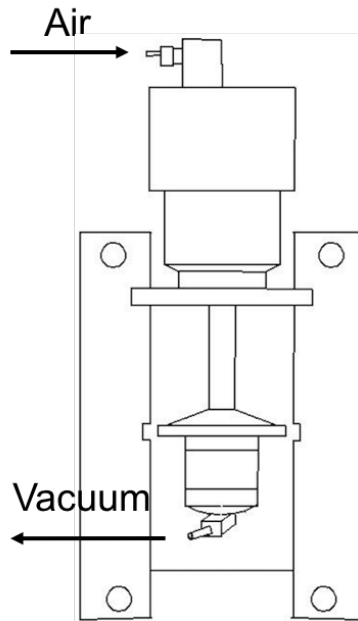
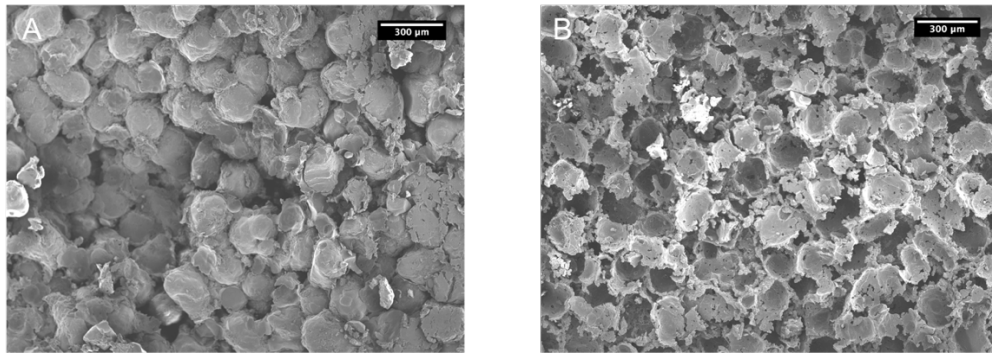


**Figure 4.16: Solvent casting apparatus**

After the solvent was evaporated, the polymer-porogen construct was pushed out of the mold followed by salt leaching in DI water. However, since 8-Phe-8-Asp(OH)-4 electrospun fibers showed morphological instability when immersed in aqueous media, it is reasonable to assume that the solvent casting scaffold morphology will collapse during the salt leaching process. Figure 4.18 shows the SEM images of SCPL scaffolds before and after immersion in PBS. Before the porogens were leached out, the salt-polymer construct maintained intact with  $\text{NH}_4\text{Cl}$  inside the pores (Figure 4.18 A). After it was soaked in water overnight to leach out the salt, the scaffold collapsed. (Figure 4.18 B)

The scaffold was further immersed in PBS for 5 days to investigate the reason of morphological change. No significant weight loss was observed during the period of time, which means the scaffold morphological change was not caused by material degradation.



Before leach out salt

After leach out salt

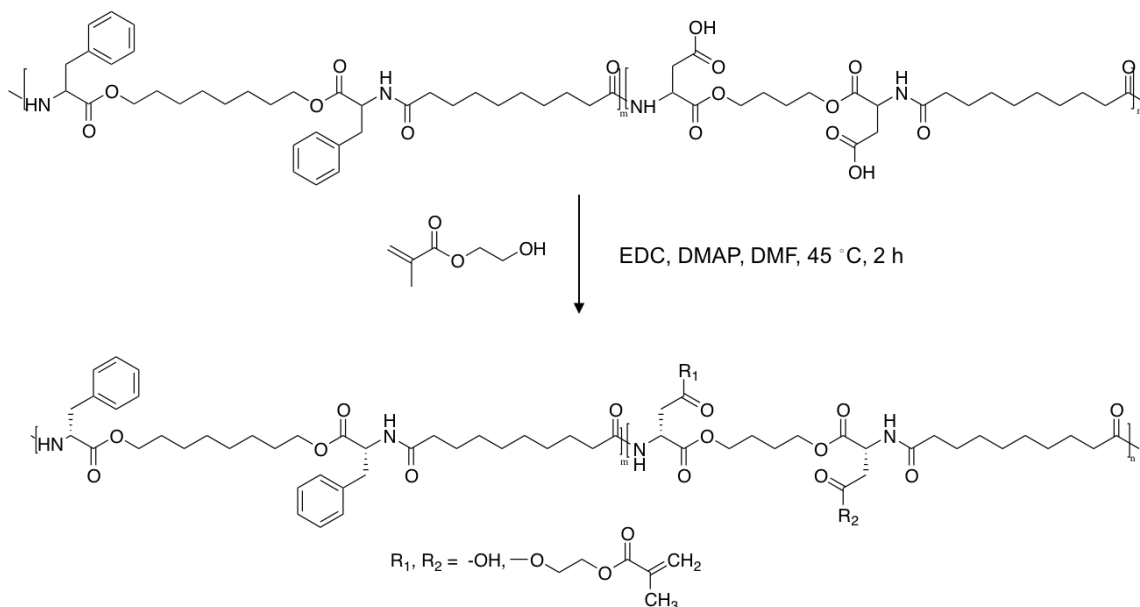
Scale bar represents 300 µm

**Figure 4.17: Uncross-linked 8-Phe-8-Asp(OH)-4 scaffold fabricated by SCPL (A) before salt is leached out (B) after salt is leached out.**

The advantage of SCPL over electrospinning is that the scaffold morphology remains intact in the mold before leaching out the salt. Therefore, the objective of cross-linking in this case is to stabilize the scaffold morphology during the salt leaching process. This requires that the cross-linking takes place before salt leaching, which leads to the design of *in situ* thermal cross-linking with SCPL. Thermal cross-linking was chosen instead of photo-cross-linking to combine with SCPL for scaffold fabrication, because the solvent casting mold is a cylinder with a 4 mm diameter. It is not possible for UV irradiation to penetrate through the thick scaffold and cross-link the material through the entire cross-section, while heat is able to penetrate the scaffold and ensure a uniform temperature over the scaffold. Thermal cross-linking can be performed using conventional polymerizable groups such as methacrylates and acrylates combined with thermal initiators such as benzoyl peroxide and AIBN.<sup>103–105</sup> Methacrylates were selected due to their rapid rate of cross-linking.

#### 4.5.1 Methacrylate-functionalized PEA Synthesis and Characterization

2-Hydroxyethyl methacrylate (HEMA) was chosen to react with pendant carboxylic groups on PEA backbone, using a dehydrative coupling by EDC/DMAP, to incorporate methacrylate groups and make thermally cross-linkable PEAs. HEMA has been used as a monomer and polymerized into poly (2-hydroxyethyl methacrylate) (pHEMA) or polymerized with other monomers, such as *p*-vinyl-benzyl-poly(ethylene oxide) and itaconic acid, to form copolymers. These polymers are used as hydrogels, implant materials and tissue engineering scaffolds.<sup>106–109</sup> HEMA has also been used to introduce vinyl groups on PVA to make photo-cross-linkable and degradable tissue engineering scaffold.<sup>110</sup> The expected low toxicity and good biocompatibility make HEMA suitable for biomedical application. A 20% molar ratio of HEMA was used at first to test the feasibility of *in situ* thermal cross-linking, and all the carboxylic groups were reacted with HEMA. Next, 6% HEMA was incorporated to find an optimal ratio for thermal cross-linking while at the same time leaving some carboxylic acids available for subsequent functionalization. The synthesis procedure is shown in Scheme 4.



**Scheme 4.11: Synthesis of methacrylate-functionalized PEAs**

$^1\text{H}$  NMR spectroscopy was used to confirm the structure of methacrylate 8-Phe-8-Asp(OH)-4 with 6 mol% functionalization (Figure 4.18). The peaks at 5.97 ppm, 5.62 ppm corresponds to the protons on the C=C double bond. The peak at 1.81 ppm corresponds to the protons of the methyl group on methacrylate groups (labeled as **16** and **17** in Figure 4.19, respectively). In this batch, according to the integration of peaks **17** versus **18**, approximately half of the carboxyl groups were reacted with hydroxyethyl methacrylate in this batch of polymer. Only 6 mol% of hydroxyethyl methacrylate relative to backbone monomer was incorporated onto PEA backbone, thus peaks representing other protons on the methacrylate moiety might not be obvious.

GPC was performed on 5 mol% methacrylate 8-Phe-8-Asp(OH)-4. Figure 4.20 showed the overlaid GPC (RI detection) traces of methacrylate 8-Phe-8-Asp(OH)-4 and 8-Phe-8-Asp(OH)-4. After dialysis with molecular weight cutoff of 25 kDa, methacrylate 8-Phe-8-Asp(OH)-4 had lower molecular weight  $M_n = 17.9$  kg/mol,  $M_w = 38.6$  kg/mol, but similar  $D = 2.14$  as 8-Phe-8-Asp(OH)-4. The decreased molecular weight can likely be attributed to residual carboxylic acids present on the polymer that result in undesired interactions with the column packing materials.

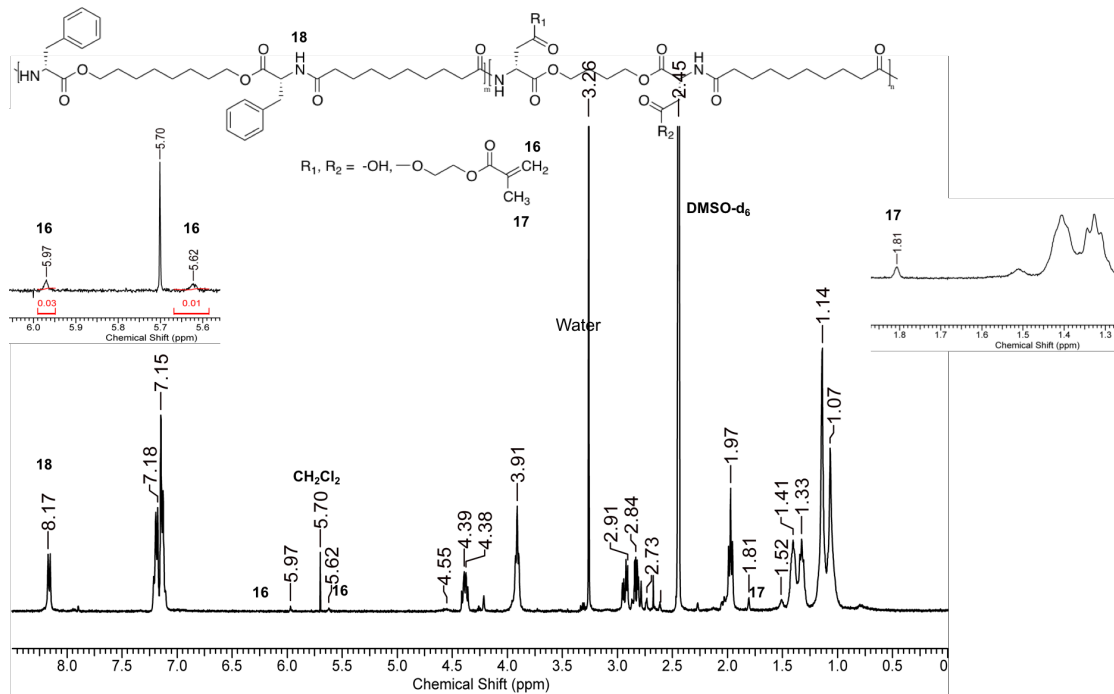


**Figure 4.18:**  $^1\text{H}$  NMR spectrum of methacrylate 8-Phe-8-Asp(OH)-4 functional PEAs, (600 MHz,  $\text{DMSO-d}_6$ )

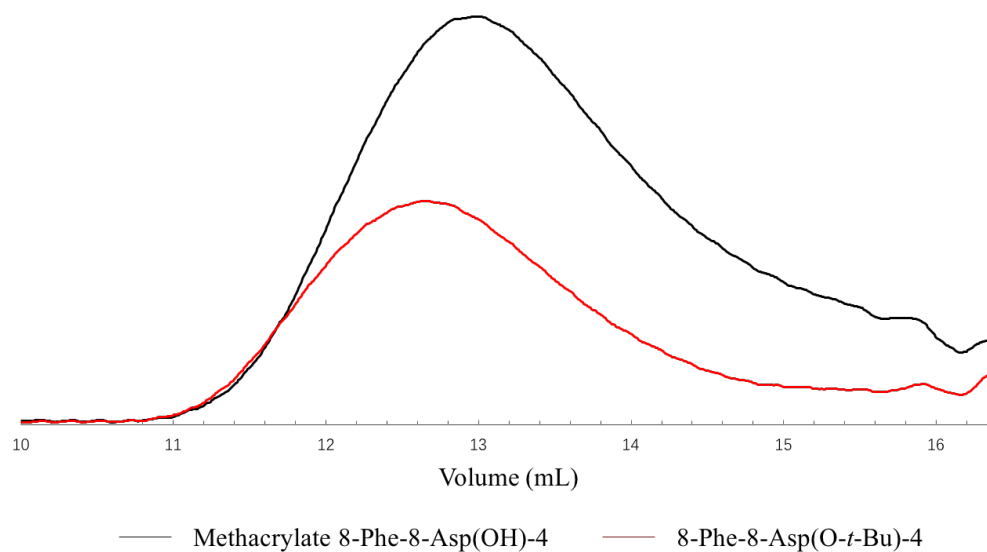
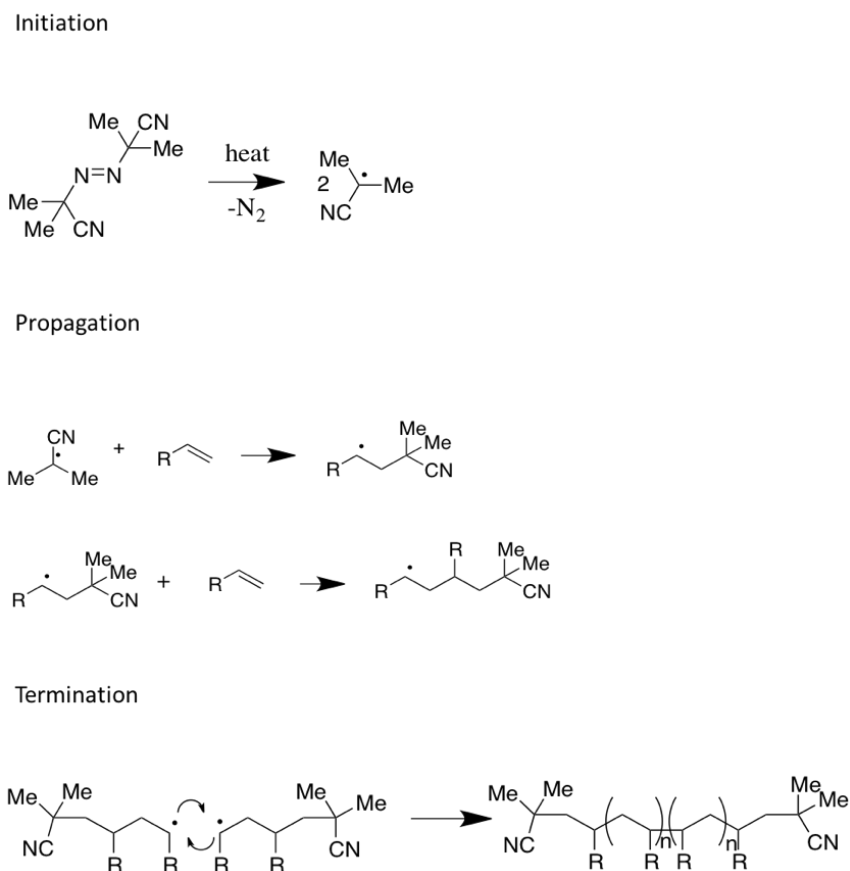


**Figure 4.19:** Overlaid GPC (RI detection) traces of Methacrylate 8-Phe-8-Asp(OH)-4 and 8-Phe-8-Asp(OH)-4.

### 4.5.2 *In Situ* Thermal Cross-linking

Azobisisobutyronitrile (AIBN) was used as the radical initiator. It was dissolved in DMF, together with polymer. The mechanism of free radical generation of AIBN is shown in Scheme 4.11. Under heating condition (around 70 °C), AIBN decomposes, generating two radicals with elimination of one molecule of N<sub>2</sub> gas. These radicals can initiate free radical polymerization or other radical-induced reactions.

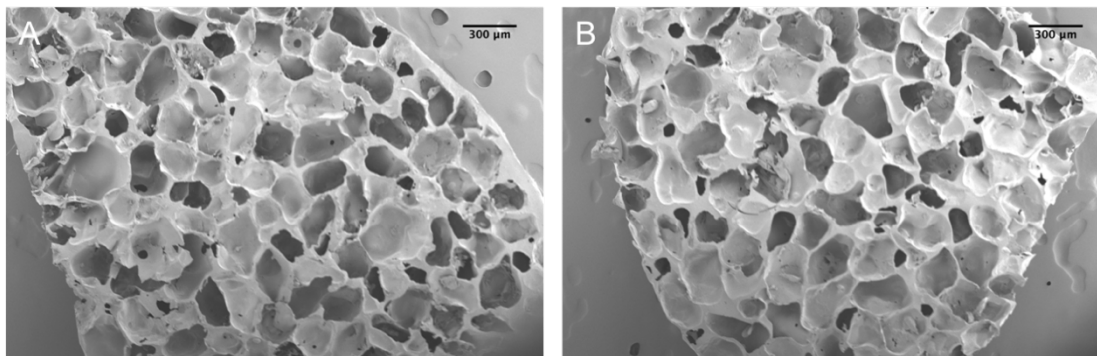


**Scheme 4.12: Free radical polymerization mechanism.**

The polymer-porogen construct prepared from the 20 mol% polymer was prepared and heated to 75 °C to cross-link the material before DMF was evaporated. Toluene was used to extract residual AIBN after the scaffold was cross-linked. The porogens were then leached out by deionized water and the resulting 3-D scaffold was immersed in PBS for 5 days. Figure 4.21 shows the SEM images of cross-linked scaffolds before and after



immersion in PBS. Comparing Figure 4.21 A and B, there is no significant difference between the scaffold morphology, suggesting thermal cross-linking took place and improved scaffold morphological stability. The gel content was calculated to be 86%. The cross-linking of the methacrylate groups was also confirmed by comparing the FTIR spectra of the methacrylate PEAs and of the cross-linked scaffold (Figure 4.22). The sharp peak at  $1735\text{ cm}^{-1}$  represents the C=O ester stretch. Strong absorption around  $1640\text{ cm}^{-1}$  represents C=O stretching on amide bond. Methacrylate PEAs showed a band around  $800\text{ cm}^{-1}$ , representing C-H out of plane bending of the methacrylate group, which is not present in the FTIR spectrum of the cross-linked scaffold. The 1,1-disubstituted C=C stretch should absorb around  $1650\text{ cm}^{-1}$  but may overlap with C=O in this spectrum. The ability of PEAs to be cross-linked with a lower methacrylate group ratio (i.e. 6%) was tested to optimize the thermal cross-linking condition. The PEAs alone showed no cross-linking. Cross-linking agent poly(ethylene glycol) dimethacrylate (PEGDMA) was added. With the increase of PEGDMA ratio: 20 wt%, 25 wt%, 33 wt%, 50 wt%, gel content increased at the same time. However, the  $^1\text{H}$  NMR spectrum of the soluble portion showed a large amount of PEAs that were not cross-linked. This suggested the ratio of methacrylate groups on the PEA is too low. In order to have thermally cross-linkable PEAs and still have enough free pendant carboxylic groups for bioactive conjugation, increased ratios of L-aspartic acid could be incorporated onto PEA backbone. Thus, thermal cross-linking is promising but further optimization will still be required.



Original scaffold

Immerse in PBS buffer after 5 days

**Figure 4.20: Cross-linked 8-Phe-8-Asp(OH)-4 solvent casting scaffold (A) scaffold before immersion in PBS and (B) scaffold after immersion in PBS for 5 days.**

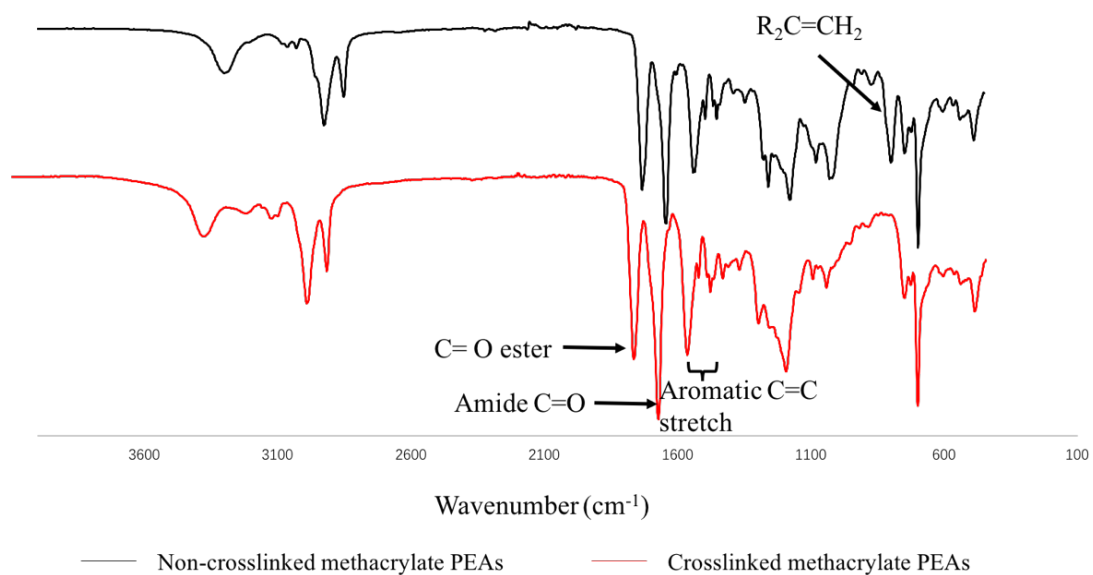


**Figure 4.21: Overlaid FTIR of cross-linked methacrylate 8-Phe-8-Asp(OH)-4 solvent casting scaffold and uncross-linked methacrylate 8-Phe-8-Asp(OH)-4**

## Chapter 5

### 5 Conclusions and Future Directions

#### 5.1 Conclusions

In this study, attempts to meet the objectives that were outlined in Chapter 1 have been partially filled. L-aspartic acid and L-phenylalanine based PEAs were successfully synthesized by interfacial polymerization as previously reported. Based on L-aspartic acid functionalized PEAs, novel cinnamate-functionalized and methacrylate-functionalized PEAs were synthesized by reacting pendant carboxyl groups with hydroxyethyl cinnamate and hydroxyethyl methacrylate to produce photo-cross-linkable and thermally-cross-linkable PEAs, respectively. Polymers were characterized by  $^1\text{H}$  NMR spectroscopy, FTIR spectroscopy and GPC. Photo-cross-linkable PEAs were subjected to electrospinning, followed by UV treatment, to produce cross-linked 3-D scaffolds. Thermally cross-linkable PEAs were subjected to *in situ* cross-linking with solvent casting/particulate leaching to fabricate cross-linked scaffolds. The degree of cross-linking was demonstrated by comparing the morphological change of cross-linked scaffolds before and after immersing in PBS. As demonstrated by SEM imaging, the morphological stability of photo-cross-linked scaffolds improved but still not enough to prevent scaffold collapse in buffer and UV irradiation caused damage to the fibers. Model compounds were conjugated onto the 3-D scaffolds. Confocal fluorescence images suggested the existence and use of free carboxyl groups on the scaffolds. On the other hand, *in situ* thermal cross-linked scaffolds showed good morphological stability, but an optimal ratio of cross-linkable groups and remaining carboxylic acids for further functionalization of the scaffolds has not yet been achieved.

## 5.2 Future Directions

Considering the work presented here, the future work should include:

- Optimizing SCPL parameters, e.g. polymer solution concentration, solution to porogen volume ratio, to get scaffolds with proper inner structure (e.g. interconnectivity, porosity)
- Optimizing methacrylate ratio on 8-Phe-8-Asp(OH)-4 backbone, ensuring effective cross-linking but still have enough carboxyl groups for bioactive molecule conjugation
- Performing *in vitro* cell test on cross-linked 3-D scaffolds, e.g. MTT test for assessing cell metabolic activity. For future vascular tissue engineering application, human smooth muscle cell can be used for further proliferation and differentiation test

## References

1. Naderi, H., Matin, M. M. & Bahrami, a. R. Review paper: Critical Issues in Tissue Engineering: Biomaterials, Cell Sources, Angiogenesis, and Drug Delivery Systems. *J. Biomater. Appl.* **26**, 383–417 (2011).
2. Chan, G. & Mooney, D. J. New materials for tissue engineering: towards greater control over the biological response. *Trends Biotechnol.* **26**, 382–392 (2008).
3. Kuo, C. K. & Ma, P. X. Ionically crosslinked alginate hydrogels as scaffolds for tissue engineering: Part 1. Structure, gelation rate and mechanical properties. *Biomaterials* **22**, 511–521 (2001).
4. Nettles, D. L., Elder, S. H. & Gilbert, J. a. Potential use of chitosan as a cell scaffold material for cartilage tissue engineering. *Tissue Eng.* **8**, 1009–1016 (2002).
5. Boland, E. D. *et al.* Electrospinning Collagen and Elastin: Preliminary Vascular Tissue Engineering. *Front. Biosci.* **9**, 1422–1432 (2004).
6. Sell, S. a *et al.* Cross-linking methods of electrospun fibrinogen scaffolds for tissue engineering applications. *Biomed. Mater.* **3**, 45001 (2008).
7. Zhang, Y. Z., Venugopal, J., Huang, Z. M., Lim, C. T. & Ramakrishna, S. Crosslinking of the electrospun gelatin nanofibers. *Polymer (Guildf)*. **47**, 2911–2917 (2006).
8. Gunatillake, P. A., Adhikari, R. & Gadegaard, N. Biodegradable synthetic polymers for tissue engineering. *Eur. Cells Mater.* **5**, 1–16 (2003).
9. Tang, C., Saquing, C. D., Harding, J. R. & Khan, S. A. In situ cross-linking of electrospun poly(vinyl alcohol) nanofibers. *Macromolecules* **43**, 630–637 (2010).
10. Bigi, A., Cojazzi, G., Panzavolta, S., Roveri, N. & Rubini, K. Stabilization of gelatin films by crosslinking with genipin. *Biomaterials* **23**, 4827–4832 (2002).
11. Atkins, K. M., Lopez, D., Knight, D. K., Gilles, E. R. & Mequanint, K. A Versatile Approach for the Syntheses of Poly(ester amide)s with Pendant Functional Groups.

- J. Polym. Sci. Part A Polym. Chem.* **47**, 3757–3772. (2009).
12. Knight, D. K., Gillies, E. R. & Mequanint, K. Biomimetic l-aspartic acid-derived functional poly(ester amide)s for vascular tissue engineering. *Acta Biomater.* **10**, 3484–3496 (2014).
  13. Ma, L. *et al.* Collagen/chitosan porous scaffolds with improved biostability for skin tissue engineering. *Biomaterials* **24**, 4833–4841 (2003).
  14. Mistry, A. S. & Mikos, A. G. Tissue engineering strategies for bone regeneration. *Regen. Med. Li Clin. Preclin. Appl.* **94**, 1–22 (2005).
  15. Freier, T., Montenegro, R., Koh, H. S. & Shoichet, M. S. Chitin-based tubes for tissue engineering in the nervous system. *Biomaterials* **26**, 4624–4632 (2005).
  16. Ohashi, K. *et al.* Liver tissue engineering at extrahepatic sites in mice as a potential new therapy for genetic liver diseases. *Hepatology* **41**, 132–140 (2005).
  17. Nerem, R. M., Ph, D., Sambanis, A. & Ph, D. Tissue Engineering : From Biology to Biological Substitutes. *Tissue Eng.* **1**, (1995).
  18. Dhandayuthapani, B., Yoshida, Y., Maekawa, T. & Kumar, D. S. Review Article Polymeric Scaffolds in Tissue Engineering Application : A Review. *Int. J. Polym. Sci.* **2011**, (2011).
  19. Cen, L., Liu, W. E. I., Cui, L. E. I., Zhang, W. & Cao, Y. Collagen Tissue Engineering : Development of Novel Biomaterials and Applications. **63**, 492–496 (2008).
  20. Legate, K. R., Nakchbandi, I. & Asz, A. What Mouse Mutants Teach Us About Extracellular Matrix Function. *Annu. Rev. Cell Dev. Biol.* **22**, 591–621 (2006).
  21. Hutmacher, D. W. Scaffolds in tissue engineering bone and cartilage. *Biomaterials* **21**, 2529–2543 (2000).
  22. E, S. & J.T., C. Making tissue engineering scaffolds work. Review on the application of solid freeform fabrication technology to the production of tissue engineering scaffolds. *Eur. Cells Mater.* **5**, 29–40 (2003).

23. Leong, K. F., Cheah, C. M. & Chua, C. K. Solid freeform fabrication of three-dimensional scaffolds for engineering replacement tissues and organs. *Biomaterials* **24**, 2363–2378 (2003).
24. Hollister, S. J. Porous scaffold design for tissue engineering. **4**, (2005).
25. Xiong, Z., Yan, Y., Wang, S., Zhang, R. & Zhang, C. Fabrication of porous scaffolds for bone tissue engineering via low-temperature deposition. *Scr. Mater.* **46**, 771–776 (2002).
26. Malafaya, P. B., Silva, G. A. & Reis, R. L. Natural-origin polymers as carriers and scaffolds for biomolecules and cell delivery in tissue engineering applications. *Adv. Drug Deliv. Rev.* **59**, 207–233 (2007).
27. Parenteau-Bareil, R., Gauvin, R. & Berthod, F. Collagen-based biomaterials for tissue engineering applications. *Materials (Basel)*. **3**, 1863–1887 (2010).
28. K., H., T., K., K., D., Y., T. & Y., A. Development of new drug delivery system for implant bone augmentation using a basic fibroblast growth factor-gelatin hydrogel complex. *Dental materials journal* **26**, 170–177 (2007).
29. Park, H., Temenoff, J. S., Holland, T. a, Tabata, Y. & Mikos, A. G. Delivery of TGF-beta1 and chondrocytes via injectable, biodegradable hydrogels for cartilage tissue engineering applications. *Biomaterials* **26**, 7095–103 (2005).
30. Iwasaki, N. *et al.* Feasibility of polysaccharide hybrid materials for scaffolds in cartilage tissue engineering: Evaluation of chondrocyte adhesion to polyion complex fibers prepared from alginate and chitosan. *Biomacromolecules* **5**, 828–833 (2004).
31. Han, F. *et al.* Preparation, characteristics and assessment of a novel gelatin-chitosan sponge scaffold as skin tissue engineering material. *Int. J. Pharm.* **476**, 124–133 (2014).
32. Li, Z., Ramay, H. R., Hauch, K. D., Xiao, D. & Zhang, M. Chitosan-alginate hybrid scaffolds for bone tissue engineering. *Biomaterials* **26**, 3919–3928 (2005).

33. De Souza Costa, E., Pereira, M. M. & Mansur, H. S. Properties and biocompatibility of chitosan films modified by blending with PVA and chemically crosslinked. *J. Mater. Sci. Mater. Med.* **20**, 553–561 (2009).
34. Elvira, C., Mano, J. F., San Román, J. & Reis, R. L. Starch-based biodegradable hydrogels with potential biomedical applications as drug delivery systems. *Biomaterials* **23**, 1955–1966 (2002).
35. Place, E. S., George, J. H., Williams, K., Stevens, M. M. & George, J. H. Synthetic polymer scaffolds for tissue engineering. *Chem. Soc. Rev.* 1139–1151 (2008). doi:10.1039/b811392k
36. Han, D. K., Park, K. D., Hubbell, J. A. & Kim, Y. H. Surface characteristics and biocompatibility of lactide-based poly(ethylene glycol) scaffolds for tissue engineering. *J. Biomater. Sci. Polym. Ed.* **9**, 667–680 (1998).
37. Kumar, N., Langer, R. S. & Domb, A. J. Polyamides: An overview. *Adv. Drug Deliv. Rev.* **54**, 889–910 (2002).
38. Deitzel, J. ., Kleinmeyer, J., Harris, D. & Beck Tan, N. . The effect of processing variables on the morphology of electrospun nanofibers and textiles. *Polymer (Guildf)*. **42**, 261–272 (2001).
39. Zong, X. *et al.* Structure and process relationship of electrospun bioabsorbable nanofiber membranes. *Polymer (Guildf)*. **43**, 4403–4412 (2002).
40. Gupta, P., Elkins, C., Long, T. E. & Wilkes, G. L. Electrospinning of linear homopolymers of poly(methyl methacrylate): Exploring relationships between fiber formation, viscosity, molecular weight and concentration in a good solvent. *Polymer (Guildf)*. **46**, 4799–4810 (2005).
41. Koski, A., Yim, K. & Shivkumar, S. Effect of molecular weight on fibrous PVA produced by electrospinning. *Mater. Lett.* **58**, 493–497 (2004).
42. Luo, C. J., Stride, E. & Edirisinghe, M. Mapping the influence of solubility and dielectric constant on electrospinning polycaprolactone solutions. *Macromolecules*



- 45**, 4669–4680 (2012).
43. Zhao, Z. *et al.* Preparation and properties of electrospun poly(vinylidene fluoride) membranes. *J. Appl. Polym. Sci.* **97**, 466–474 (2005).
  44. Yuan, X. Y., Zhang, Y. Y., Dong, C. & Sheng, J. Morphology of ultrafine polysulfone fibers prepared by electrospinning. *Polym. Int.* **53**, 1704–1710 (2004).
  45. Ki, C. S. *et al.* Characterization of gelatin nanofiber prepared from gelatin-formic acid solution. *Polymer (Guildf)*. **46**, 5094–5102 (2005).
  46. Geng, X., Kwon, O. H. & Jang, J. Electrospinning of chitosan dissolved in concentrated acetic acid solution. *Biomaterials* **26**, 5427–5432 (2005).
  47. Huang, R., Zhu, X., Tu, H. & Wan, A. The crystallization behavior of porous poly(lactic acid) prepared by modified solvent casting/particulate leaching technique for potential use of tissue engineering scaffold. *Mater. Lett.* **136**, 126–129 (2014).
  48. Sin, D. *et al.* Polyurethane (PU) scaffolds prepared by solvent casting/particulate leaching (SCPL) combined with centrifugation. *Mater. Sci. Eng. C* **30**, 78–85 (2010).
  49. Stevens, B., Yang, Y., Mohandas, A., Stucker, B. & Nguyen, K. T. A review of materials, fabrication methods, and strategies used to enhance bone regeneration in engineered bone tissues. *J. Biomed. Mater. Res. - Part B Appl. Biomater.* **85**, 573–582 (2008).
  50. Murphy, W. L., Dennis, R. G., Kileny, J. L. & Mooney, D. J. Salt fusion: an approach to improve pore interconnectivity within tissue engineering scaffolds. *Tissue Eng.* **8**, 43–52 (2002).
  51. Nam, Y. S., Yoon, J. J. & Park, T. G. A novel fabrication method of macroporous biodegradable polymer scaffolds using gas foaming salt as a porogen additive. *J. Biomed. Mater. Res.* **53**, 1–7 (2000).
  52. Liao, C. J. *et al.* Fabrication of porous biodegradable polymer scaffolds using a

- solvent merging/particulate leaching method. *J. Biomed. Mater. Res.* **59**, 676–681 (2002).
53. Chen, G., Ushida, T. & Tateishi, T. Scaffold design for tissue engineering. *Macromol. Biosci.* **2**, 67–77 (2002).
  54. Armentano, I., Dottori, M., Fortunati, E., Mattioli, S. & Kenny, J. M. Biodegradable polymer matrix nanocomposites for tissue engineering : A review. *Polym. Degrad. Stab.* **95**, 2126–2146 (2010).
  55. Floren, M., Spilimbergo, S., Motta, A. & Migliaresi, C. Porous poly(D, L -lactic acid) foams with tunable structure and mechanical anisotropy prepared by supercritical carbon dioxide. *J. Biomed. Mater. Res. - Part B Appl. Biomater.* **99 B**, 338–349 (2011).
  56. O'Brien, F. J., Harley, B. A., Yannas, I. V. & Gibson, L. Influence of freezing rate on pore structure in freeze-dried collagen-GAG scaffolds. *Biomaterials* **25**, 1077–1086 (2004).
  57. O'Brien, F. J., Harley, B. A., Yannas, I. V. & Gibson, L. J. The effect of pore size on cell adhesion in collagen-GAG scaffolds. *Biomaterials* **26**, 433–441 (2005).
  58. Madhally, S. V. & Matthew, H. W. T. Porous chitosan scaffolds for tissue engineering. *Biomaterials* **20**, 1133–1142 (1999).
  59. Ding, B. *et al.* Preparation and characterization of a nanoscale poly(vinyl alcohol) fiber aggregate produced by an electrospinning method. *J. Polym. Sci. Part B Polym. Phys.* **40**, 1261–1268 (2002).
  60. Panzavolta, S. *et al.* Electrospun gelatin nanofibers: Optimization of genipin cross-linking to preserve fiber morphology after exposure to water. *Acta Biomater.* **7**, 1702–1709 (2011).
  61. Ratanavaraporn, J., Rangkupan, R., Jeeratawatchai, H., Kanokpanont, S. & Damrongsakkul, S. Influences of physical and chemical crosslinking techniques on electrospun type A and B gelatin fiber mats. *Int. J. Biol. Macromol.* **47**, 431–438

- (2010).
62. Rault, I., Frei, V., Herbage, D., Abdul-Malak, N. & Huc, A. Evaluation of different chemical methods for cross-linking collagen gel, films and sponges. *J. Mater. Sci. Mater. Med.* 215–221 (1996).
  63. Englert, C. *et al.* Bonding of articular cartilage using a combination of biochemical degradation and surface cross-linking. *Arthritis Res. Ther.* **9**, R47 (2007).
  64. Gupta, P., Trenor, S. R., Long, T. E. & Wilkes, G. L. In situ photo-cross-linking of cinnamate functionalized poly(methyl methacrylate-co-2-hydroxyethyl acrylate) fibers during electrospinning. *Macromolecules* **37**, 9211–9218 (2004).
  65. Kim, S. H., Kim, S. H., Nair, S. & Moore, E. Reactive electrospinning of cross-linked poly(2-hydroxyethyl methacrylate) nanofibers and elastic properties of individual hydrogel nanofibers in aqueous solutions. *Macromolecules* **38**, 3719–3723 (2005).
  66. Karimi, P., Rizkalla, A. S. & Mequanint, K. Versatile biodegradable poly(ester amide)s derived from  $\alpha$ -Amino acids for vascular tissue engineering. *Materials (Basel)*. **3**, 2346–2368 (2010).
  67. Rodriguez-Galan, A., Franco, L. & Puiggali, J. Degradable poly(ester amide)s for biomedical applications. *Polymers (Basel)*. **3**, 65–99 (2011).
  68. Deng, M., Wu, J., Reinhart-King, C. A. & Chu, C. C. Biodegradable functional poly(ester amide)s with pendant hydroxyl functional groups: Synthesis, characterization, fabrication and in vitro cellular response. *Acta Biomater.* **7**, 1504–1515 (2011).
  69. Guo, K., Chu, C. C., Chkhaidze, E. & Katsarava, R. Synthesis and characterization of novel biodegradable unsaturated poly(ester amide)s. *J. Polym. Sci. Part A Polym. Chem.* **43**, 1463–1477 (2005).
  70. Deng, M., Wu, J., Reinhart-king, C. A. & Chu, C. Synthesis and Characterization of Biodegradable Poly(ester amide)s with Pendant Amine Functional Groups and

- In Vitro Cellular Response. *Biomacromolecules* **10**, 3037–3047 (2009).
71. Pang, X. & Chu, C. C. Synthesis, characterization and biodegradation of functionalized amino acid-based poly(ester amide)s. *Biomaterials* **31**, 3745–3754 (2010).
  72. Katsarava, R. *et al.* Amino Acid-Based Bioanalogous Polymers. Synthesis and Study of Regular Poly(ester amide)s Based on Bis ( -amino acid , -Alkylene Diesters , and Aliphatic Dicarboxylic Acids. *J. Polym. Sci. Part A Polym. Chem.* **37**, 391–407 (1998).
  73. Knight, D. K., Gillies, E. R. & Mequanint, K. Strategies in functional poly(ester amide) syntheses to study human coronary artery smooth muscle cell interactions. *Biomacromolecules* **12**, 2475–2487 (2011).
  74. Soleimani, A., Borecki, A. & Gillies, E. R. Photodegradable poly(ester amide)s for indirect light-triggered release of paclitaxel. *Polym. Chem.* **5**, 7062–7071 (2014).
  75. Yamanouchi, D. *et al.* Biodegradable arginine-based poly(ester-amide)s as non-viral gene delivery reagents. *Biomaterials* **29**, 3269–3277 (2008).
  76. Fonseca, A. C., Gil, M. H. & Simões, P. N. Biodegradable poly(ester amide)s - A remarkable opportunity for the biomedical area: Review on the synthesis, characterization and applications. *Prog. Polym. Sci.* **39**, 1291–1311 (2014).
  77. Guo, K. & Chu, C. C. Controlled release of paclitaxel from biodegradable unsaturated poly(ester amide)s/poly(ethylene glycol) diacrylate hydrogels. *J. Biomater. Sci. Polym. Ed.* **18**, 489–504 (2007).
  78. Zilinskas, G. J., Soleimani, A. & Gillies, E. R. Poly(ester amide)-poly(ethylene oxide) graft copolymers: Towards micellar drug delivery vehicles. *Int. J. Polym. Sci.* **2012**, (2012).
  79. Ouchi, T., Nozaki, T., Okamoto, Y., Shiratani, M. & Ohya, Y. Synthesis and enzymatic hydrolysis of polydepsipeptides with functionalized pendant groups. *Macromol. Chem. Phys.* **197**, 1823–1833 (1996).

80. Tsitlanadze, G. *et al.* Biodegradation of amino-acid-based poly(ester amide)s: in vitro weight loss and preliminary in vivo studies. *J. Biomater. Sci. Polym. Ed.* **15**, 1–24 (2004).
81. Fan, Y., Kobayashi, M. & Kise, H. Synthesis and biodegradation of Poly (ester amide)s containing amino acid residues: The effect of the stereoisomeric composition of L- and D-Phenylalanines on the enzymatic degradation of the polymers. *J. Polym. Sci. Part A Polym. Chem.* **40**, 385–392 (2002).
82. Tsitlanadze, G., Kviria, T. & Katsarava, R. In vitro enzymatic biodegradation of amino acid based poly ( ester amide ) s biomaterials. *J. Mater. Sci. Mater. Med.* **15**, 185–190 (2004).
83. Said, S. S., Pickering, J. G. & Mequanint, K. Controlled delivery of fibroblast growth factor-9 from biodegradable poly(ester amide) fibers for building functional neovasculature. *Pharm. Res.* **31**, 3335–3347 (2014).
84. Horwitz, J. A. *et al.* Biological performance of biodegradable amino acid-based poly(ester amide)s: Endothelial cell adhesion and inflammation in vitro. *J. Biomed. Mater. Res. - Part A* **95 A**, 371–380 (2010).
85. Jokhadze, G., Machaidze, M., Panosyan, H., Chu, C. C. & Katsarava, R. Synthesis and characterization of functional elastomeric poly(ester amide) co-polymers. *J. Biomater. Sci. Polym. Ed.* **18**, 411–438 (2007).
86. Schmedlen, R. H., Masters, K. S. & West, J. L. Photocrosslinkable polyvinyl alcohol hydrogels that can be modified with cell adhesion peptides for use in tissue engineering. *Biomaterials* **23**, 4325–4332 (2002).
87. Yang, E., Qin, X. & Wang, S. Electrospun crosslinked polyvinyl alcohol membrane. *Mater. Lett.* **62**, 3555–3557 (2008).
88. Yasukawa, T., Miyamura, H. & Kobayashi, S. Rate-acceleration in gold-nanocluster-catalyzed aerobic oxidative esterification using 1,2- and 1,3-diols and their derivatives. *Chem. - An Asian J.* **6**, 621–627 (2011).

89. Wu, W., Karamdoust, S., Turowec, B. A. & Gillies, E. R. Synthesis and application of cinnamate-functionalized rubber for the preparation of UV-curable films. *Eur. Polym. J.* **49**, 4238–4248 (2013).
90. Roy, S., Eastman, A. & Gribble, G. W. Synthesis of bisindolymaleimides related to GF109203x and their efficient conversion to the bioactive indolocarbazoles. *Org. Biomol. Chem.* **62**, 7838–7845 (2006).
91. Wittbecker, E. L. & Morgan, P. W. Interfacial Polycondensation. I. \*. **XL**, 521–529 (1996).
92. McCaig, M. S. & Paul, D. R. Effect of UV crosslinking and physical aging on the gas permeability of thin glassy polyarylate films. *Polymer (Guildf)*. **40**, 7209–7225 (1999).
93. Shi, D., Matsusaki, M. & Akashi, M. Photo-tunable protein release from biodegradable nanoparticles composed of cinnamic acid derivatives. *J. Control. Release* **149**, 182–189 (2011).
94. Matsusaki, M., Tran, H. T., Kaneko, T. & Akashi, M. Enhanced effects of lithocholic acid incorporation into liquid-crystalline biopolymer poly(coumaric acid) on structural ordering and cell adhesion. *Biomaterials* **26**, 6263–6270 (2005).
95. Thi, T. H., Matsusaki, M., Shi, D., Kaneko, T. & Akashi, M. Synthesis and properties of coumaric acid derivative homo-polymers. *J. Biomater. Sci. Polym. Ed.* **19**, 75–85 (2008).
96. Liu, L., Hudgins, W. R., Shack, S., Yin, M. Q. & Samid, D. Cinnamic acid: a natural product with potential use in cancer intervention. *Int. J. Cancer* **62**, 345–50 (1995).
97. Tsakos, M., Schaffert, E. S., Clement, L. L., Villadsen, N. L. & Poulsen, T. B. Ester coupling reactions – an enduring challenge in the chemical synthesis of bioactive natural products. *Nat. Prod. Rep.* 605–632 (2015). doi:10.1039/C4NP00106K

98. Chae, B., Lee, S. W., Ree, M., Jung, Y. M. & Kim, S. Bin. Photoreaction and molecular reorientation in a nanoscaled film of poly(methyl 4-(methacryloyloxy)cinnamate) studied by two-dimensional FTIR and UV correlation spectroscopy. *Langmuir* **19**, 687–695 (2003).
99. Hsu, C. M. & Shivkumar, S. N,N-dimethylformamide additions to the solution for the electrospinning of poly(ε-caprolactone) nanofibers. *Macromol. Mater. Eng.* **289**, 334–340 (2004).
100. Choi, S. S., Hong, J. P., Seo, Y. S., Chung, S. M. & Nah, C. Fabrication and characterization of electrospun polybutadiene fibers crosslinked by UV irradiation. *J. Appl. Polym. Sci.* **101**, 2333–2337 (2006).
101. Nguyen, T. & Francis, M. B. Practical synthetic route to functionalized rhodamine dyes. *Org. Lett.* **5**, 3245–3248 (2003).
102. Staros, J. V., Wright, R. W. & Swingle, D. M. Enhancement by N-hydroxysulfosuccinimide of water-soluble carbodiimide-mediated coupling reactions. *Anal. Biochem.* **156**, 220–222 (1986).
103. Peppas, N. a, Moynihan, H. J. & Lucht, L. M. The structure of highly crosslinked poly(2-hydroxyethyl methacrylate) hydrogels. *J. Biomed. Mater. Res.* **19**, 397–411 (1985).
104. Oprea, S., Vlad, S. & Stanciu, A. Poly(urethane-methacrylate)s. Synthesis and characterization. *Polymer (Guildf)*. **42**, 7257–7266 (2001).
105. Decker, C., Masson, F. & Schwalm, R. Dual-curing of waterborne urethane-acrylate coatings by UV and thermal processing. *Macromol. Mater. Eng.* **288**, 17–28 (2003).
106. Arica, M. Y. *et al.* Novel hydrogel membrane based on copoly(hydroxyethyl methacrylate/p- vinylbenzyl-poly(ethylene oxide)) for biomedical applications: Properties and drug release characteristics. *Macromol. Biosci.* **5**, 983–992 (2005).
107. Chirila, T. V *et al.* Poly(2-hydroxyethyl methacrylate) sponges as implant

- materials :in vivo and in vitro evaluation of cellular invasion. *Biomaterials* **14**, 26–38 (1993).
108. Jeyanthi, R. & Panduranga Rao, K. In vivo biocompatibility of collagenpoly(hydroxyethyl methacrylate) hydrogels. *Biomaterials* **11**, 238–243 (1990).
  109. Tomic, S. L., Micic, M. M., Dobic, S. N., Filipovic, J. M. & Suljovrujic, E. H. Smart poly(2-hydroxyethyl methacrylate/itaconic acid) hydrogels for biomedical application. *Radiat. Phys. Chem.* **79**, 643–649 (2010).
  110. Nuttelman, C. R., Henry, S. M. & Anseth, K. S. Synthesis and characterization of photocrosslinkable, degradable poly (vinyl alcohol)-based tissue engineering scaffolds. *Biomaterials* **23**, 3617–3626 (2002).



## Appendices Permission to Reuse Copyrighted Material

Copyright Clearance Center **RightsLink**<sup>®</sup> Home Account Info Help Live Chat



**Title:** Biomimetic l-aspartic acid-derived functional poly(ester amide)s for vascular tissue engineering

**Author:** Darryl K. Knight, Elizabeth R. Gillies, Kibret Mequanint

**Publication:** Acta Biomaterialia


**Publisher:** Elsevier

**Date:** August 2014

Copyright © 2014 Acta Materialia Inc.  
Published by Elsevier Ltd. All rights reserved.

Logged in as:  
Shuyu Liu  
Account #: 3001051334  
[LOGOUT](#)

Copyright Clearance Center **RightsLink**<sup>®</sup> Home Account Info Help Live Chat



**Title:** Polyurethane (PU) scaffolds prepared by solvent casting/particulate leaching (SCPL) combined with centrifugation

**Author:** DongChoon Sin, Xigeng Miao, Gang Liu, Fan Wei, Gary Chadwick, Cheng Yan, Thor Friis

**Publication:** Materials Science and Engineering: C

**Publisher:** Elsevier

**Date:** 1 January 2010

Copyright © 2009 Elsevier B.V. All rights reserved.

Logged in as:  
Shuyu Liu  
Account #: 3001051334  
[LOGOUT](#)

Copyright Clearance Center **RightsLink**<sup>®</sup> Home Account Info Help Live Chat



**Title:** Porous poly(D,L-lactic acid) foams with tunable structure and mechanical anisotropy prepared by supercritical carbon dioxide

**Author:** Michael Floren, Sara Spilimbergo, Antonella Motta, Claudio Migliaresi

**Publication:** Journal of Biomedical Materials Research

**Publisher:** John Wiley and Sons

**Date:** Sep 27, 2011

Copyright © 2011 Wiley Periodicals, Inc.

Logged in as:  
Shuyu Liu  
Account #: 3001051334  
[LOGOUT](#)



**Title:** Porous chitosan scaffolds for tissue engineering  
**Author:** Sundararajan V. Madihally, Howard W.T. Matthew  
**Publication:** Biomaterials  
**Publisher:** Elsevier  
**Date:** June 1999  
Copyright © 1999 Elsevier Science Ltd. All rights reserved.

Logged in as:  
Shuyu Liu  
Account #:  
3001051334

LOGOUT

**Title:** In Situ Photo-Cross-Linking of Cinnamate Functionalized Poly(methyl methacrylate-co-2-hydroxyethyl acrylate) Fibers during Electrospinning  
**Author:** Pankaj Gupta, Scott R. Trenor, Timothy E. Long, et al  
**Publication:** Macromolecules  
**Publisher:** American Chemical Society  
**Date:** Nov 1, 2004  
Copyright © 2004, American Chemical Society

Logged in as:  
Shuyu Liu  
Account #:  
3001051334

LOGOUT

## Curriculum Vitae

Shuyu Liu

### EDUCATION

Sept. 2014–  
Aug 2016                      Master's of Engineering Science  
Graduate Program in Chemical Engineering  
The University of Western Ontario, London, Ontario, Canada  
*Supervisors:* Drs. Kibret Mequanint and Elizabeth Gillies

Sept. 2010 –  
Jun. 2014                      Bachelor of Engineering  
Pharmaceutical Engineering  
Tianjin University, Tianjin, China

### RELEVANT WORK EXPERIENCE

Jan. 2015 –  
Apr. 2016                      **Graduate Teaching Assistant**  
The University of Western Ontario, London, Ontario, Canada